UNIVERSITY OF SOUTHAMPTON

FACULTY OF SCIENCE

DEPARTMENT OF PHYSICS

MODE LOCKING OF A TITANIUM SAPPHIRE LASER

by

Robert Leonard Culley

A Thesis submitted for the Degree of Master of Philosophy

June 1991

CONTENTS

UNIVERSITY OF SOUTHAMPTON

ABSTRACT

FACULTY OF SCIENCE

PHYSICS

Master of Philosophy

MODE LOCKING OF A TITANIUM SAPPHIRE LASER

by Robert Leonard Culley

This thesis describes work which was undertaken to investigate the mode locking behaviour of a titanium-doped sapphire laser. Initially, an intracavity acousto-optic mode locker was used and pulses of 12ps duration were obtained. The behaviour of the laser was investigated as the modulation frequency was detuned from the intermode beat frequency.

Mode locking by second harmonic generation was attempted using a crystal of potassium niobate in a coupled cavity, but mode locking was not obtained either as a self starting process or as an enhancement of the mode locking process when the laser was actively mode locked.

Injection seeding of the titanium sapphire laser was investigated using an injected laser diode signal. The bandwidth of the laser output narrowed under the influence of the injected signal and showed modulation at the laser intermode beat frequency.

The second part of this thesis describes a study of a possible method for assessing the dopant concentration in the cores of rare earth doped fibres. This involved measuring the absorption coefficient and the saturation intensity for the fibres. The method investigated for measuring the absorption coefficient was unsuccessful and the saturation intensity measurements consistently suggested lower than expected dopant concentrations. A concentration related phenomenon appears to be involved and if this could be identified then the method might be acceptable for measuring the dopant concentrations.

ACKNOWLEDGEMENTS

I would like to thank my supervisors, Dr. J.R.M. Barr and Dr. A.C. Tropper for the help they have given me during my research at Southampton. I would also like to thank those technical staff, particularly Mr. E. Roskowiak and Mr. R. Garment who have assisted me in the course of this work.

CHAPTER 1

INTRODUCTION AND Ti:Al_2O_3 LASER CHARACTERISTICS

1.1 Outline of Work Covered

The work covered in this thesis describes several different methods for attempting to obtain mode locked operation from a Ti:Al_2O_3 laser and the experimental results obtained. A possible technique for measuring the dopant concentration in the cores of rare earth doped fibres is also studied and the results obtained from it are presented.

Chapter 1 describes the characteristics of Ti:Al_2O_3 as a laser material and briefly describes the history of the development of Ti:Al_2O_3 lasers and the performance obtained from them. The fabrication process used for crystal manufacture is described followed by considerations to be taken into account when designing a Ti:Al_2O_3 laser system. In particular, the compensation of astigmatism in the laser cavity is considered and an expression is derived for the folding angle required in a folded cavity to compensate for the astigmatism introduced by a Brewster angled laser rod.

Chapter 2 starts with a brief discussion of the theory of mode locking and a theory of the active mode locking of a homogeneously broadened laser using an intracavity modulator is then presented. The operation of an acousto-optic modulator is described and the characteristics of the modulator used in this work are given. A non background free autocorrelation technique is described and was used to measure the pulse duration from the mode locked laser. Pulse durations of 12ps were obtained compared to the 1.4ps predicted from the theory presented in the chapter. Possible reasons for the discrepancy are given. The pulses were found to have considerable excess bandwidth with time-bandwidth products in the region of 2.3 instead of the expected value of 0.44. An intracavity etalon was used in order to obtain bandwidth limited pulses, resulting in pulses with

a duration of 30ps and a time bandwidth product of 0.5.

The detuning behaviour of the laser was investigated as the modulation frequency was detuned from the intermode beat frequency of the laser cavity. As expected, the pulse duration increased and the bandwidth narrowed as a result of the detuning, but the observed behaviour was different depending or not the intracavity etalon was present. Without the etalon a detuning of several hundred Hertz was required before the pulse duration and bandwidth were significantly affected, but with the etalon a detuning of 20Hz was sufficient to cause large changes in the laser output.

Passive mode locking of solid state lasers is covered in Chapter 3. A description of the passive mode locking process using saturable absorbers is given and nonlinear passive mode locking techniques are then covered. Mode locking by nonlinear amplitude modulation is described, using a combination of a dichroic mirror and a nonlinear crystal to form a mirror with an intensity dependent reflection coefficient. Such a mirror may be used to form a coupled cavity and the pulse shortening may occur due to the pulses in the laser cavity and the coupled cavity combining additively at the common mirror.

Coupled cavity mode locking was attempted using potassium niobate as the nonlinear crystal but a mode locked output was not obtained. The laser was then acousto-optically mode locked in order to increase the second harmonic conversion efficiency in the potassium niobate crystal. The second harmonic did not enhance the mode locking of the laser and the conversion efficiency in the potassium niobate crystal was found to be low since the available optics did not permit optimum focusing into the crystal.

Injection seeding of the Ti:Al_2O_3 laser is described in Chapter 4. The theory of injection locking of laser oscillators is considered, as is the injection seeding of a laser using a pulsed, non single frequency signal. A laser diode was used to injection seed the Ti:Al_2O_3 laser and the injection seeding behaviour was investigated with both a pulsed and a free running injected signal. The free

running signal would determine the Ti:Al_2O_3 oscillation frequency when the Ti:Al_2O_3 laser was lasing and it reduced the laser's bandwidth. When the current to the laser diode was modulated, the injection seeding effects were only observed when the modulation frequency was closely matched to the Ti:Al_2O_3 laser's intermode beat frequency. Good isolation of the laser diode from the Ti:Al_2O_3 laser was essential since Ti:Al_2O_3 output entering the diode broadened its bandwidth which in turn broadened the Ti:Al_2O_3 bandwidth.

Chapter 5 describes a method for assessing the dopant concentration in the cores of rare earth doped fibres. A value was required for the absorption coefficient of the doped fibre and this involved measuring the sidelight fluorescence intensity from the fibre, which is expected to show an exponential decay with distance along the fibre. No such exponential decay was observed since pump light travelling in the fibre cladding repeatedly crossed the core and gave large fluctuations in the signal. The response of these fluctuations to changes in the experimental conditions was studied and attempts were made to obtain useable results, but without success. An alternative method, the cut back technique, was successfully used to obtain values for the absorption coefficient.

In order to find the dopant concentration, the saturation intensity of the ions in the fibre had to be found. This was calculated from measurements of the fluorescence intensity at a fixed point in the fibre as the pump power used to excite the ions was increased.

Very low values were obtained for the dopant concentrations, compared to the figures given by the fibre manufacturer. Fibres with both low and high dopant concentrations and different core sizes were tested and two different pump wavelengths were used. The concentration values obtained for the same fibre at different pump wavelengths always agreed closely which indicated that effects related to the concentration were responsible for the results. It would be desirable to identify these effects as the method might then prove useful for assessing the characteristics of fibres.

1.2 Introduction

Titanium-doped sapphire (Ti:Al_2O_3) is a tunable solid state laser material which has lased at wavelengths between 660 and 1100nm [1.1]. The laser transition is homogeneously broadened [1.2] and the laser gives an excellent approximation to an ideal four level system. A four level system is advantageous for laser operation since a three level system in which the bottom level of the laser transition is also the ground state requires higher pump powers in order to achieve a population inversion.

Ti:Al_2O_3 is a powerful source of near infra red radiation with commercially available systems giving up to 5W output for 20W pump power. It is therefore a good pump source for lasers which may be pumped at wavelengths within its tuning range.

The following lasers may be pumped by Ti:Al_2O_3

Laser	Peak absorption (nm)
Nd^{3+}(YAG and glass)	800-810
Er^{3+}	950-1000
Yb^{3+}	900-930
Tm^{3+}	790-800
NaF(F_2^+)*	870

Laser operation from Ti:Al_2O_3 was first reported by Moulton in 1982. Pulsed operation was demonstrated using pulsed dye lasers and frequency doubled Nd:YAG lasers as the pump source and quasi CW operation was obtained using an argon ion pump laser. Heating effects in the poor quality crystals necessitated chopping of the pump beam [1.1].

CW operation was demonstrated with improved quality crystals [1.3] and output powers in excess of 1W were obtained [1.2]. Schulz reported single frequency operation with a frequency stability of 2MHz using a free running unidirectional ring laser [1.4] and more recent work has given linewidths of 1kHz from a Ti:Al_2O_3 laser locked to an external cavity [1.5]. The tunability of Ti:Al_2O_3 and its narrow linewidth when in single frequency operation make it an ideal laser for use in high resolution spectroscopy. Ti:Al_2O_3 lasers have been used in Doppler free two photon absorption spectroscopy [1.6] and are also ideal candidates for lidar measurements of water vapour where a stable, narrow linedwidth source is required at 720, 760 and 940nm [1.7].

Mode locked operation of Ti:Al_2O_3 has been the subject of considerable attention since the large bandwidth offers the possibility of femtosecond pulse durations. Active mode locking was reported by Roy et.al. [1.8] in 1987 and Schulz [1.4] with pulse durations of the order of 100 ps and output powers of several hundred mW. Kafka et al obtained 6ps pulses from an acousto-optically mode locked laser in which the modulation frequency was detuned from the cavity length [1.9]. More recently, Kafka and co-workers have obtained pulses with a duration of 1.3ps and an average output power of 2W by incorporating a Gires Tournois Interferometer into the cavity in order to compensate for dispersion [1.10]. These are the shortest pulses and highest output powers obtained from an actively mode locked Ti:Al_2O_3 laser.

In recent work, nonlinear techniques have been used to mode lock Ti:Al_2O_3 lasers. Coupled cavity mode locking schemes using nonlinear processes in fibres have yielded subpicosecond pulses [1.11], [1.12] and Ti:Al_2O_3 lasers have also been self mode locked by misaligning the cavity mirrors slightly. Spence et.al. reported a self mode locked laser with an intracavity prism pair to compensate for dispersion

[1.13]. An output of 50fs pulses with an average power of 450mW was obtained. Likforman and co-workers [1.14] have reported 100fs pulses with a power of 2W from an identical experimental arrangement and a fibre-prism pulse compressor outside the cavity reduced the pulse duration to 27fs.

The high powers available from Ti:Al_2O_3 lasers offer the possibility of extending its tuning range into the violet end of the visible spectrum by frequency doubling. Adams and Ferguson have demonstrated a single frequency Ti:Al_2O_3 laser whose frequency was doubled by a $LiIO_3$ crystal in an enhancement cavity [1.15]. An output of up to 40mW was achieved over a tuning range from 355 to 435nm. Such a tunable source is of particular interest for spectroscopic applications since frequency doubled infra red dye lasers offer lower output powers and larger linewidths.

The availability of high power laser diodes has stimulated interest in all solid state tunable laser systems whose compactness is of particular interest for airborne and spaceborne applications. A Q-switched neodymium laser may be pumped by laser diode arrays to give output pulses sufficiently powerful to pump a Ti:Al_2O_3 laser after frequency doubling. Maker and Ferguson [1.16] reported a diode pumped mode locked and Q switched Nd:YLF laser as a frequency doubled pump source for a Ti:Al_2O_3 laser which produced microjoule pulses of 400ns duration. More recent work by Steele et al [1.17] has yielded pulse energies approaching 1mJ with a 7ns duration and a 40Hz repetition rate.

Ti:Al_2O_3 has a broad absorption band between 400 and 600nm and may therefore be pumped with an argon ion laser or, for pulsed operation, a frequency doubled Nd:YAG laser. The broad absorption and emission bands arise from the vibronic nature of the electronic transitions in Ti:Al_2O_3.

The Ti^{3+} ion has a single d electron outside a closed shell argon atom structure. The ion substitutes for an Al^{3+} ion in the sapphire crystal and occupies a site with a slightly distorted octahedral symmetry. The electron interacts strongly with the predominantly cubic crystal field which splits the 3d level into a ^2E_g excited level and a ^2E_g ground state. A smaller trigonal component of the crystal field further splits the $^2T_{2g}$ level and further splittings occur due to spin-orbit coupling [1.18].

After excitation to the ^2E_g level, rapid phonon emission brings the ion to the lowest energy level of the excited state, from where it undergoes radiative decay to the $^2T_{2g}$ level. Further phonon emission occurs, returning the ion to its ground state. The phonon emission associated with the transitions of the Ti^{3+} ion accounts for the broad emission and absorption bands.

The $Ti:Al_2O_3$ laser is free of excited state absorption as the higher energy levels of the Ti^{3+} ion can only be reached by ultra-violet absorption. At room temperature the lifetime of the decay is 3.1μs, but it tends to a value of 3.8μs at lower temperatures. Multiphonon non radiative decay is responsible for the reduced lifetime at higher temperatures [1.1]. The sapphire crystal has a high thermal conductivity which minimises thermal problems.

There is a parasitic absorption of the $Ti:Al_2O_3$ fluorescence due to Ti^{3+} - Ti^{4+} pairs in the crystal. This is minimised by growing the crystals in an oxygen free atmosphere and by post growth annealing to reduce Ti^{4+} ions to Ti^{3+} ions. [1.19, 1.20 and Section 1.2].

The main alternative to $Ti:Al_2O_3$ as a tunable laser source in the near infra red is provided by dye lasers. Several dyes are required to cover the tuning range of the $Ti:Al_2O_3$ laser and the dye laser also has the disadvantage of a poisonous gain medium which may spill or leak and which picks up contaminants from the surrounding environment.

The tightly focused beam in the dye jet gives a high optical intensity which gives rise to photodegradation - dye molecules in a triplet state may attack contaminants in the dye solution or break apart and the quality of the dye is gradually reduced.

For single frequency operation a solid state laser is preferable to a dye laser since the laser rod will remain constant in length whereas a dye jet suffers variations in thickness which cause variations in the output frequency.

The objective of this work is to mode lock a Ti:Al_2O_3 laser. The Rutherford Appleton Laboratory requires a laser which will give stable, reproducible short pulses at a wavelength around 250nm in order to injection lock a KrF excimer laser. This may be accomplished by frequency tripling the output of a mode locked Ti:Al_2O_3 laser operating at 750nm. Short, stable pulses with a duration of 50fs and amplitude fluctuations of less than 1% have been obtained from a Ti:Al_2O_3 laser [1.10]. This system used an intracavity acousto-optic mode locker with a Gires-Tournois Interferometer to compensate for dispersion and produced 1.3ps pulses. These were compressed to 50fs using a fibre-prism pulse compressor.

The final chapter of this thesis describes a study of a method for calculating the concentration of the dopant ions in the cores of rare earth doped fibres. The lasers which are formed from such fibres cover a wide range of wavelengths in the visible part of the spectrum and the near infra red. They are of particular interest for telecommunications purposes as laser action is available at frequencies where the absorption of silica is minimised, thus allowing the transmission of signals over long distances.

It is desirable to know the dopant concentration in fibres in order to characterise them and a method for calculating this value is described and investigated in Chapter 5.

1.3 Crystal Growth and Crystal Characteristics

In order to optimise laser performance, the Ti:sapphire laser rod must be cut so that its c-axis is parallel to the plane of polarisation of the pump beam. The reason for this is that the absorption cross section of the Ti^{3+} ions is 2.3 times larger for light polarised parallel to the c-axis than for light polarised perpendicular to it. A Brewster angled rod requires π polarised light i.e. light which is polarised parallel to the major axis of the elliptical rod ends. The crystal must therefore be cut so that the c-axis is in the same plane as the major axes of the Brewster surfaces. A second reason for cutting the rod in this manner is that the parasitic absorption of the Ti:sapphire fluorescence is minimised when the laser output is polarised parallel to the c-axis [1.21].

Ti:Al_2O_3 crystals have been grown by three different techniques. Union Carbide Corporation grow crystals commercially using the Czochralski method and Strauss et.al. [1.22] have used a gradient freeze technique. Initial stages of this work were conducted using a laser rod grown by Crystal Systems Incorporated using the Heat Exchanger Method (HEM) [1.19].

The HEM method utilises an electrically heated furnace containing a crucible at the bottom of which is a Ti:Al_2O_3 seed crystal placed on a heat exchanger. The crucible is filled with a mixture of fragmented sapphire and Ti_2O_3. Once melted, the temperature gradient in the liquid is determined by the furnace temperature and the temperature gradient in the solid in the lower part of the crucible is determined by the temperature of the heat exchanger. Helium gas is passed through the heat exchanger in order to control its temperature and this, in conjunction with changes in the furnace temperature, controls the movement of the solid-liquid interface up through the liquid. Independent control of the temperature gradients in the solid and in the liquid improves the uniformity of the crystal growth and improves

the quality of the resultant crystal.

After crystal growth the heat exchanger temperature can be raised and the furnace temperature lowered to anneal the crystal in situ before cooling it down. This reduces stresses caused by solidification. The parasitic infra red absorption in the crystal is minimised by filling the chamber with a reducing atmosphere in order to prevent the formation of Ti^{4+} ions. The final result of the HEM process described in [1.19] is a cylindrical crystal approximately 10cm in diameter and 10cm in length.

The concentration of titanium ions in the crystal is not uniform. It is found to vary along the length of the crystal, being greater at the top end and lower at the bottom end which was in contact with the heat exchanger. In order to obtain laser rods in which the dopant concentration is uniform, the rods are cut so that the rod axis is perpendicular to the growth axis as well as to the crystal c-axis.

An important characteristic of $Ti:Al_2O_3$ crystals is the Figure of Merit (FOM). This is the ratio of the absorption coefficient at 514nm to the absorption coefficient at 800nm. High quality crystals are currently obtainable with FOM > 200.

The FOM is an important factor in the design of a $Ti:Al_2O_3$ laser [1.23]. In modelling the performance of a Ti:sapphire laser, the laser is optimised by maximising the output power while varying the absorption coefficients at 514nm and 800nm, the laser rod length, the pump and cavity beam waists and the output coupler transmission.

$Ti:Al_2O_3$ crystals are generally produced with dopant concentrations of between 0.01 and 0.1% by weight. Increasing the titanium concentration causes the unwanted absorption of the fluorescence to increase more rapidly than the absorption at the pump wavelength ie. the FOM decreases at higher dopant concentrations. In the absence of the parasitic absorption a higher dopant concentration

giving greater absorption of the pump beam would optimise the efficiency of the laser, but in practice lower dopant concentrations are required to reduce the parasitic absorption. This also reduces thermal problems in the rod. At these dopant concentrations, laser rod lengths of a couple of cm are used to give adequate pump absorption. Generally, between half and two thirds of the pump power is absorbed in the laser rod.

It is found [1.23] that optimum output is obtained if the product $\alpha_p L$ has a value between 1.5 and 2.0, where α_p is the absorption coefficient of the crystal in units of cm^{-1} and L is the rod length in cm. For example, a rod length of 2cm will give optimum output for values of α_p between $0.75cm^{-1}$ and $1cm^{-1}$. These absorption coefficient values correspond to dopant concentrations of between 0.035 and 0.05 per cent titanium by weight. Having optimised $\alpha_p L$, the FOM will determine the laser's performance and should be as high as possible while keeping α_p within its required range of values.

1.4 Cavity Design

Ti:Al_2O_3 is high threshold laser medium due to the large linewidth of the transition and in order to minimise the threshold it is necessary to focus the pump beam down to a narrow waist in the laser rod [1.23]. For the same reason it is desirable to minimise losses due to reflections from the rod ends, which may be done either by anti reflection coating or by Brewster angling them. A tightly focused beam is liable to damage the anti reflection coatings so the rod ends are Brewster angled. A Brewster angled surface also has the advantage of minimising the losses at both the pump and the laser output wavelengths. An anti reflection coating is not capable of covering such a large wavelength range.

A Brewster angled rod introduces astigmatism into the cavity

which may be compensated for by using a folded cavity. A folded cavity also allows the unabsorbed beam from the pump laser to be separated from the laser output. The off axis mirrors introduce astigmatism into the cavity and by designing the cavity correctly it is possible to have the astigmatism due to the mirrors and the astigmatism due to the laser rod cancelling each other out [1.24].

Active mode locking was investigated using a laser with a four mirror folded cavity [Fig. 1.1].

M_1 and M_2 have identical radii of curvature of 15cm and the Ti:sapphire crystal is positioned between them at the centre of curvature of M_1 and the focal point of M_2. The beam in the remaining two arms of the cavity is therefore collimated and the output beam is taken from the output coupler M_4. The cavity mirrors are highly reflecting around 800nm but are relatively transparent at the argon ion pump wavelength. The pump beam is focused into the crystal through M_1 by a 20cm focal length lens positioned just outside the cavity. Most of the unabsorbed pump beam then passes out of the cavity through M_2.

The path difference traversed by rays in the crystal differs for tangential and sagittal rays. With reference to Fig. 1.2 we write expressions for the effective distances which the rays traverse in the Brewster angled crystal [1.24].

$$L^s_{eff} = t\sqrt{n^2+1} \;/\; n^2 \qquad (1.1)$$

$$L^T_{eff} = t\sqrt{n^2+1} \;/\; n^4$$

Fig.1.1 A schematic diagram of the actively mode locked laser.

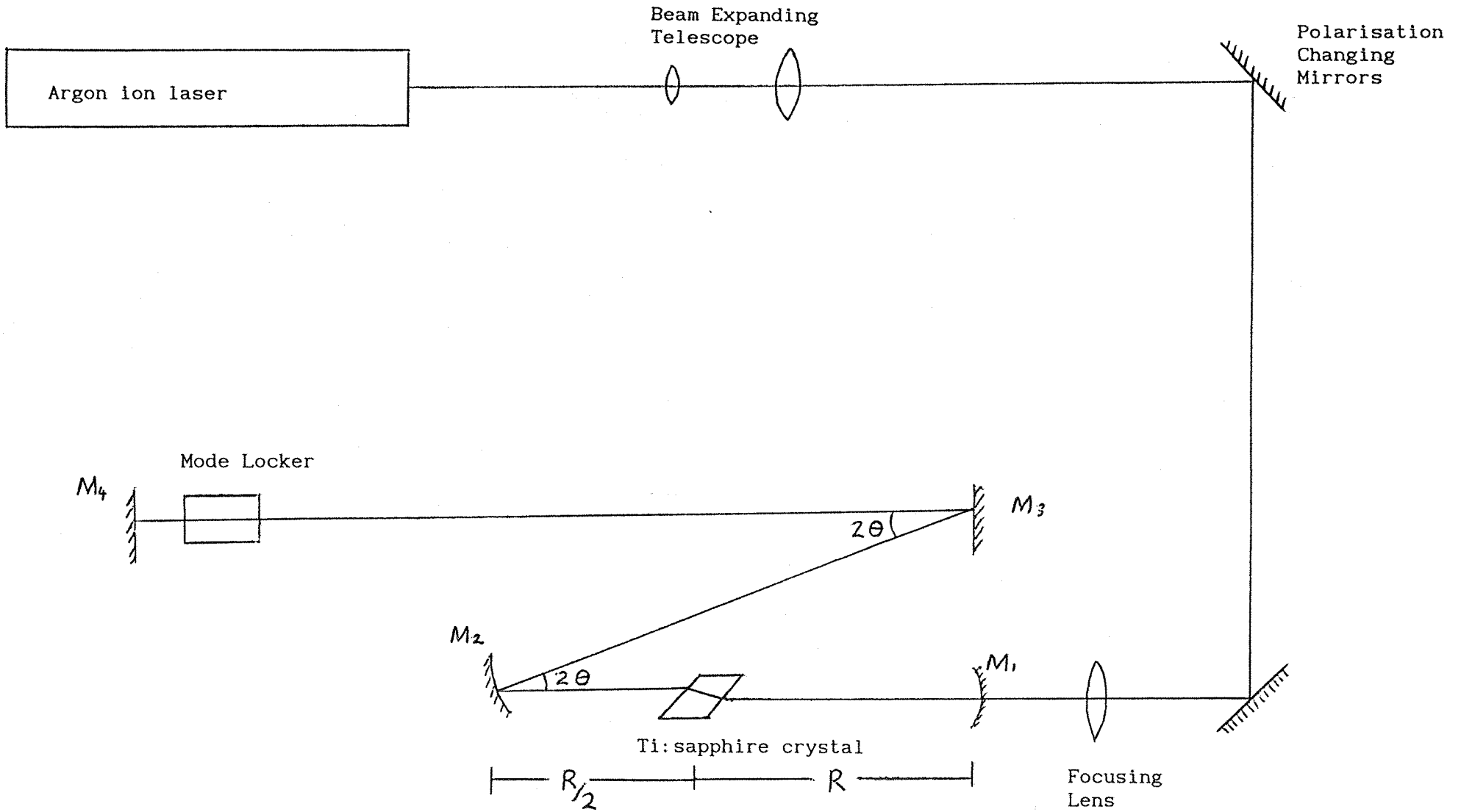

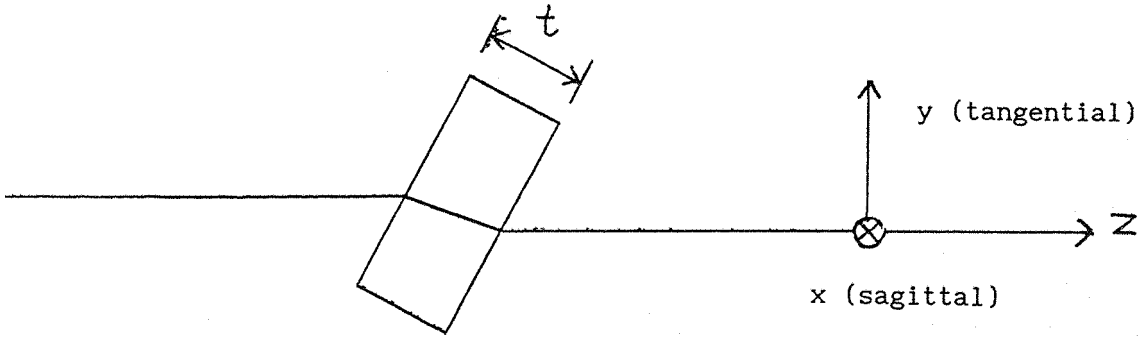

Fig. 1.2 Sagittal and tangential rays in an angled crystal.

where $L^s eff$ is the distance traversed by a sagittal ray, $L^T eff$ is the distance traversed by a tangential ray and n is the crystal refractive index.

The astigmatism of the off axis mirror M_2 results in different effective focal lengths in the sagittal (xz) and tangential (yz) planes. These focal lengths are related to the actual focal length f as follows [1.25]

$$f_x = \frac{f}{\cos\theta}$$

$$f_y = f\cos\theta \qquad (1.2)$$

With reference to Fig. 1.3, ray matrices may be derived for a sagittal ray in the cavity and for a tangential ray in the cavity. The following ray matrices are required.

Matrix for a distance d in free space

$$\begin{pmatrix} 1 & d \\ 0 & 1 \end{pmatrix}$$

Brewster angled crystal of thickness t

Tangential plane

$$\begin{pmatrix} 1 & L^T eff \\ 0 & 1 \end{pmatrix}$$

Sagittal plane

$$\begin{pmatrix} 1 & L^s eff \\ 0 & 1 \end{pmatrix}$$

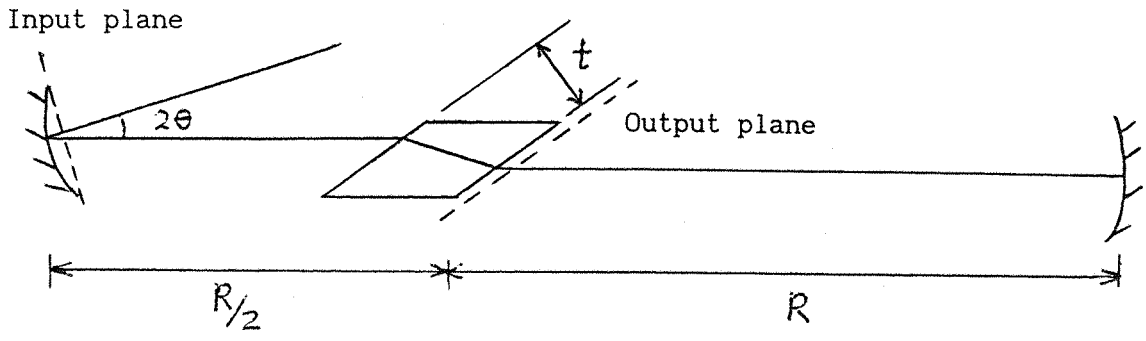

Fig. 1.3 The situation to be analysed in finding the condition for astigmatism compensation.

Mirror of radius of curvature R at an angle θ to the incident beam

Tangential plane

$$\begin{pmatrix} 1 & 0 \\ -\frac{2}{R\cos\theta} & 1 \end{pmatrix}$$

Sagittal plane

$$\begin{pmatrix} 1 & 0 \\ -\frac{2\cos\theta}{R} & 1 \end{pmatrix}$$

The ray transfer matrices are derived for a beam which travels from an input plane just before it is incident on the off axis mirror to an output plane just after it has passed through the Brewster angled rod.

The tangential matrix is

$$\begin{pmatrix} 1 & L^{T}eff \\ 0 & 1 \end{pmatrix} \begin{pmatrix} 1 & R/2 \\ 0 & 1 \end{pmatrix} \begin{pmatrix} 1 & 0 \\ -\frac{2}{R\cos\theta} & 1 \end{pmatrix}$$

$$= \begin{pmatrix} 1 - \frac{1}{\cos\theta} - \frac{2L^{T}eff}{R\cos\theta} & R/2 + L^{T}eff \\ -\frac{2}{\cos\theta} & 1 \end{pmatrix}$$

The sagittal matrix is

$$\begin{pmatrix} 1 & L^{s}eff \\ 0 & 1 \end{pmatrix} \begin{pmatrix} 1 & R/2 \\ 0 & 1 \end{pmatrix} \begin{pmatrix} 1 & 0 \\ -\frac{2\cos\theta}{R} & 1 \end{pmatrix}$$

$$= \begin{pmatrix} 1 - \cos\theta - \frac{2L^{s}effcos\theta}{R} & R/2 + L^{s}eff \\ -\frac{2\cos\theta}{R} & 1 \end{pmatrix}$$

The complex beam parameter, q, of a Gaussian beam is defined as

$$\frac{1}{q} = \frac{1}{R} - \frac{j\lambda}{\pi W^2} \tag{1.3}$$

Where R is the radius of curvature of the wavefront and W is the spot size. Let q_1 be the complex beam parameter at the input plane and q_2 be the complex beam parameter at the output plane. q_1 transforms to q_2 according to the ABCD law

$$q_2 = \frac{Aq_1+B}{Cq_1+D} \tag{1.4}$$

where $\begin{pmatrix} A & B \\ C & D \end{pmatrix}$ is the ray transfer matrix from the input plane to the output plane.

q_1 is the same in the sagittal and tangential planes as the beam is collimated and q_2 is the same in the sagittal and the tangential planes when the astigmatism in the cavity is compensated. This is because the astigmatism introduced by the off axis mirror is compensated for by the astigmatism in the rod, leaving a stigmatic beam to propagate from the rod to the on axis mirror.

For a compensated cavity we may therefore use the ABCD law to relate the sagittal and tangential ray matrices for the system shown in Fig. 1.3.

$$q_2 = \frac{Aq_1+B}{Cq_1+D} \text{ (sagittal)} = \frac{Aq_1+B}{Cq_1+D} \text{ (tangential)} \tag{1.5}$$

Equating the two matrices we have

$$\frac{\left(1 - \frac{1}{\cos\theta} - \frac{2L^{T}eff}{R\cos\theta}\right)q + \frac{R}{2} + L^{T}eff}{-\frac{2}{R\cos\theta}q + 1} = \frac{\left(1 - \cos\theta - \frac{2L^{s}effcos\theta}{R}\right)q + \frac{R}{2} + L^{s}eff}{-\frac{2cos\theta}{R}q + 1} \qquad (1.6)$$

Crossmultiplying, we obtain

$$-\frac{2}{R\cos\theta}\left(1 - \cos\theta - \frac{2L^{s}effcos\theta}{R}\right)q^{2} - \frac{2}{R\cos\theta}\left(\frac{R}{2} + L^{s}eff\right)q$$

$$+\left(1 - \cos\theta - \frac{2L^{s}effcos\theta}{R}\right)q + \frac{R}{2} + L^{s}eff$$

$$= -\frac{2cos\theta}{R}\left(1 - \frac{1}{\cos\theta} - \frac{2L^{T}eff}{R\cos\theta}\right)q^{2} - \frac{2cos\theta}{R}\left(\frac{R}{2} + L^{T}eff\right)q$$

$$+\left(1 - \frac{1}{\cos\theta} - \frac{2L^{T}eff}{R\cos\theta}\right)q + \frac{R}{2} + L^{T}eff \qquad (1.7)$$

Equating the terms in q^{2}

$$-\frac{2}{R\cos\theta}\left(1 - \cos\theta - \frac{2L^{s}effcos\theta}{R}\right) = -\frac{2cos\theta}{R}\left(1 - \frac{1}{\cos\theta} - \frac{2L^{T}eff}{R\cos\theta}\right) \qquad (1.8)$$

$$\frac{1}{\cos\theta} - \cos\theta = \frac{2L^{s}eff}{R} - \frac{2L^{T}eff}{R} \qquad (1.9)$$

$$\frac{R}{2} \sin\theta \tan\theta = L^{s}eff - L^{T}eff \qquad (1.10)$$

Using (1.1) and (1.10)

$$R\sin\theta \tan\theta = 2t\ (n^2-1)\sqrt{n^2+1}/n^4 \qquad (1.11)$$

which may be written as

$$f\sin\theta \tan\theta = t(n^2-1)\sqrt{n^2+1}/n^4 \qquad (1.12)$$

Equation (1.12) is the expression derived for a compensated cavity by Kogelnik et al in [1.13].

For this laser the crystal thickness t was 0.5cm and the focal length f of the folding mirror was 7.5cm. The refractive index n of $Ti:Al_2O_3$ is 1.76. These values when substituted into Equation (1.12) give a folding angle θ of 10°.

A Spectra-Physics Model 3900 Ti:sapphire laser was also used in this work. Its cavity is as shown in Fig.1.4.

The crystal is equidistant from M_2 and M_3, whose radii of curvature are equal. It is at the focal point of each mirror so that the beams between M_1 and M_2 and between M_3 and M_4 are collimated. One of these is the output coupler and the other is a high reflector.

This cavity has an off axis mirror on either side of the crystal and the astigmatism due to both mirrors must be eliminated in order to give an output beam free of astigmatism. In this situation Equation (1.12) becomes

Fig. 1.4 The Spectra-Physics Ti:sapphire laser cavity.

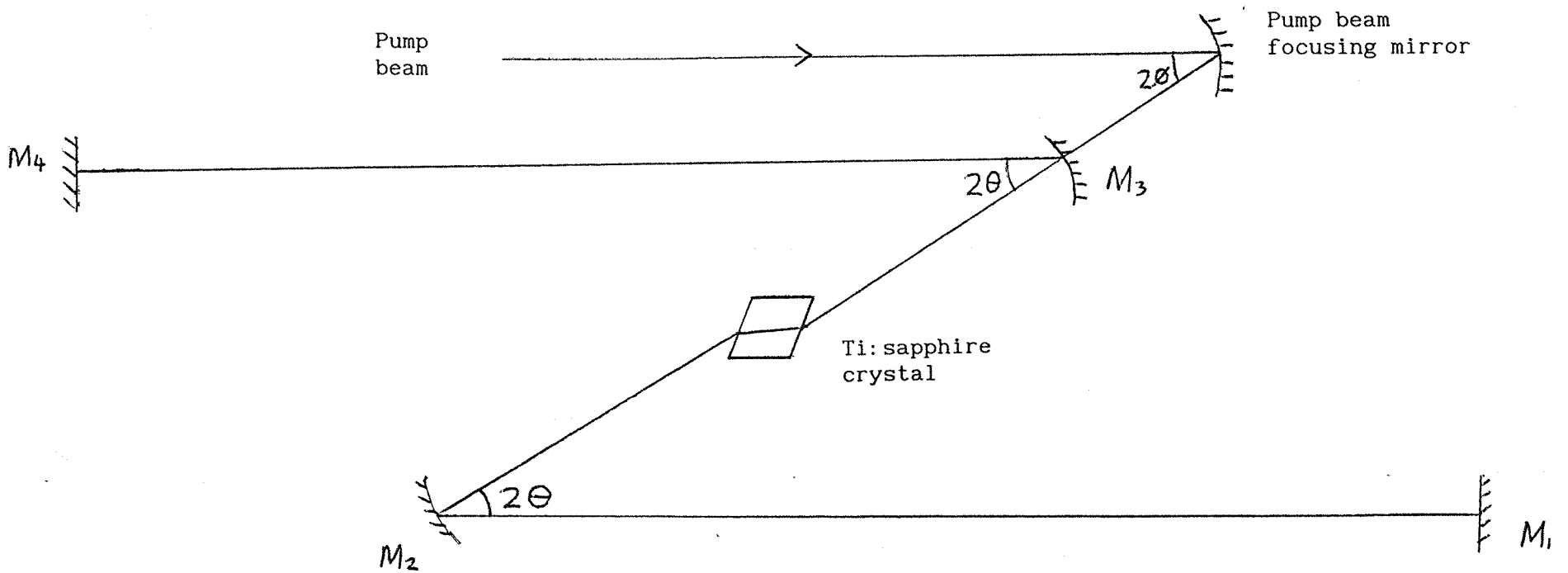

$$2f\sin\theta\tan\theta = t(n^2-1)\sqrt{n^2+1}\ /n^4 \qquad (1.13)$$

For this laser the crystal thickness was 2.0cm and the focal length of the mirrors was 5cm. The refractive index is 1.76 and these values give a folding angle θ of 17°.

Although the astigmatism in the output beam is eliminated, there is still astigmatism present in the beam between M_2 and M_3. The waists in the tangential and sagittal planes differ in size and location so in order to maximise the overlap between the pump and cavity beams and thus maximise the efficiency, astigmatism is introduced into the pump beam by focusing it into the crystal using an off axis mirror (Fig.1.4). The pump focusing mirror is therefore at an angle ϕ to the pump beam where ϕ is chosen to give a close match between the pump and cavity beams.

The degree of accuracy with which the folding angle θ must be chosen can be calculated by considering the change in the stability ranges in the tangential and sagittal planes caused by a change in θ. There is a range of values for the distance between M_1 and M_2 over which the cavity is stable and the range for stability in the sagittal plane will differ from the range for stability in the tangential plane if the astigmatism is not compensated. For optimum compensation the stability ranges overlap and the laser may be adjusted so that it is operating in the centre of the stability range in each plane. As the folding angle is varied from this value the overlap between the stability ranges is reduced until a certain value of θ is reached at which the laser is always unstable in either the sagittal or tangential plane.

It can be shown [1.24] that the cavity is stable over a range of spacings between M_1 and M_2 given by

$$2S = \frac{f^2}{d_2} \qquad (1.14)$$

where f is the focal length of M_2 and d_2 is the length of the collimated beam in the cavity between M_2 and M_4. It can also be shown that the spot size does not vary much over the central part of the stability range, but falls rapidly to zero at its limits. For the laser used in the active mode locking work the length of the collimated beam in the cavity was approximately 1m, giving a stability range 2S of 5.6mm.

If the centre of each stability region is 2.8mm away from the optimum location, the two regions will not overlap and the laser will always be unstable in either the tangential or the sagittal plane. For a variation of 0.7mm from the optimum position, the laser will still be in the central twenty five per cent of the stability range in each plane and the spot sizes will be within 10% of their values at the optimum folding angle.

For f = 5cm and $\theta = 10^\circ$, the change in θ required to give a change in f_x or f_y of 0.7mm is 4°, a degree of accuracy in θ which is easily achieved when setting up the laser.

1.5 References

1.1 P.F. Moulton, J. Opt. Soc. Am. B. 3 p.125 (1986).

1.2 A Sanchez, R.E. Fahey, A.J. Strauss and R.L. Aggarwal, Tunable Solid State Lasers II. Springer Verlag: Berlin (1986).

1.3 P. Albers, E. Stark and G. Huber, J. Opt. Soc. Am. B. 3 p.134 (1986).

1.4 P.A. Schulz, IEEE J. Quantum Electron. QE24 p.1039 (1988).

1.5 W. Vassen, C. Zimmerman, R. Kallenbach and T.W. Händsch, Opt. Commun. 75 p.435 (1990).

1.6 C.S. Adams and A.I. Ferguson, Opt. Commun. 75 p.419 (1990).

1.7 P. Brockman, C.H. Bair, J.C. Barnes, R.V. Hess and E.V. Browell, Opt.Lett. 11 p.712 (1986).

1.8 R. Roy, P.A. Schulz and A. Walther, Opt.Lett. 12 p.672 (1987).

1.9 J.D. Kafka, A.J. Alfrey and T. Baer, Ultrafast Phenomena VI. Springer Verlag: Berlin (1988).

1.10 J.D. Kafka, M.L. Watts, D.J. Roach, M.S. Keirstead, H.W. Schaaf and T. Baer, Ultrafast Phenomena VII. Springer Verlag: Berlin (1990).

1.11 J. Goodberlet, J. Wang and J.G. Fujimoto, Opt.Lett. 14 p.1125 (1989).

1.12 P.M.W. French, J.A.R. Williams and J.R. Taylor, Opt.Lett. 14 p.686 (1989).

1.13 D.E. Spence, P.N. Kean and W. Sibbett, Opt.Lett. 16 p.42 (1991).

1.14 J.P. Likforman, G. Grillon, M. Joffre, C. Le Blanc, A. Migus and A. Antonetti, Appl. Phys. Lett. 58 p.2061 (1991).

1.15 C.S. Adams and A.I. Ferguson, Opt. Commun. 79, p.219 (1990).

1.16 G.T. Maker and A.I. Ferguson, Opt. Lett. 15 p.375 (1990).

1.17 T.R. Steele, D.C. Gerstenberger, A. Drobshoff and R.W. Wallace, Opt. Lett. 16 p.399 (1991).

1.18 C.E. Byvik and A.M. Buoncristiani, IEEE J. Quantum. Electron. 21 p.1619 (1985).

1.19 C.F. Khattak and A.N. Scoville, SPIE vol.681 Laser and Nonlinear Optical Materials (1986) p.58.

1.20 M.R. Kokta, Tunable Solid State Lasers II. Springer Verlag: Berlin (1986).

1.21 W.R. Rapoport and C.P. Khattak. Tunable Solid State Lasers II. Springer Series in Optical Sciences Vol.52, p.212. Springer, New York.

1.22 A.J. Strauss, R.E. Fahey, A. Sanchez and R.L. Aggarwal, SPIE Vol.681. Laser and Nonlinear Optical Materials. p.62 (1986).

1.23 A.J. Alfrey, IEEE J. Quantum Electron. QE25 p.760 (1989).

1.24 H.W. Kogelnik, E.P. Ippen, A. Dienes and C.V. Shank, IEEE J. Quantum Electron QE8 p.373 (1972).

1.25 G.S. Monk, Light: Principles and Experiments. McGraw-Hill, New York (1937).

CHAPTER TWO

ACTIVE MODE LOCKING OF THE Ti:Al_2O_3 LASER

2.1 Theory of Active Mode Locking

In a free running laser, many longitudinal modes oscillate simultaneously with no relationship between their amplitudes and phases. The laser output therefore fluctuates rapidly on a time scale given by the coherence time of the laser i.e. the inverse of its bandwidth.

If the modes are forced to adopt a fixed phase relationship to each other, the laser output will vary with time in a well defined manner. With the modes locked together such that there is a point in the laser cavity where all the modes have the same phase, the intensity distribution in the cavity will consist of a short, intense pulse at this one point. There will be essentially no intensity at all other points in the cavity. The pulse will oscillate back and forth in the resonator and the laser output will consist of a train of short pules separated by the round trip time of the resonator with no laser output in between the pulses.

Mode locked operation of a laser may be obtained by placing an amplitude modulator in the cavity. In an actively mode locked laser this is a device to which a radio frequency electrical signal is applied in order to vary its optical transmission. The frequency is chosen so that maximum transmission through the modulator occurs at intervals separated by the round trip time of the laser cavity. Viewed in the time domain, this ensures that the part of the intracavity signal which passes through the modulator at one maximum transmission point always returns to the modulator when its transmission is at a maximum. It is thus favoured over signals which reach the modulator at any other time and a circulating pulse develops

in the cavity. This pulse undergoes broadening in the gain medium and when the mode locked laser reaches its steady state the pulse broadening in the active medium is balanced by the pulse narrowing in the modulator.

The action of the modulator may also be considered in the frequency domain. The modulation frequency is equal to the longitudinal mode spacing of the cavity which is given by $C/2L$ where L is the cavity length and C is the velocity of light. The modulator may be regarded as imposing sidebands at frequencies $\nu_n \pm C/2L$ on any cavity mode of frequency ν_n. Since these sidebands are the adjacent longitudinal modes to the frequency ν_n, these adjacent modes grow more readily if their phases are the same as the phases of the generated sidebands. If the phases differ, destructive interference will occur. The longitudinal modes therefore become locked together in a particular phase relationship.

A theory of active mode locking has been developed by Kuizenga and Siegman [2.1] to predict the behaviour of homogeneously broadened laser systems. It requires both the pulse profile and the line shape to be Gaussian so it assumes an ideal amplitude modulator whose transmission characteristic is such that it can be approximated to a Gaussian transmission around the peak transmission. Such a transmission characteristic is given by Equation (2.1).

$$T = \exp\ (-2\delta_1\ \sin^2\ \omega_m t) \qquad (2.1)$$

Where $2\delta_1$ is the peak-to-peak variation in the transmitted signal and ω_m is the angular frequency of the modulation.

Consider a Gaussian pulse of the form

$$E(t) = \frac{1}{2}\ Eo\ \exp(-\alpha t^2)\ \exp[j(\omega_p t + \beta t^2)] \qquad (2.2)$$

α determines the Gaussian envelope of the pulse and β is a linear frequency shift or chirp during the pulse. Using a complex constant γ defined as

$$\gamma = \alpha - j\beta \tag{2.3}$$

(2.2) may be rewritten as

$$E(t) = \frac{1}{2} Eo \exp(-\gamma t^2) \exp(j\omega_p t) \tag{2.4}$$

The Fourier transform of this is

$$E(\omega) = \frac{E_o}{2}\sqrt{\frac{\pi}{\gamma}} \exp[-(\omega-\omega_p)^2/4\gamma] \tag{2.5}$$

The Full Width at Half Maximum of the pulse is

$$\tau = \sqrt{2\ln 2/\alpha} \tag{2.6}$$

and the bandwidth is

$$\Delta f = \frac{1}{\pi}\sqrt{2\ln 2(\alpha^2+\beta^2)/\alpha} \tag{2.7}$$

In the steady state situation the circulating pulse will be unchanged after making one complete round trip in the cavity. Fig. 2.1 shows the situation to be analysed.

The amplitude gain in a homogeneously broadened laser is given by [2.1]

$$g_a(\omega) = \exp g/[1 + 2j(\omega-\omega_a)/\Delta\omega] \tag{2.8}$$

g is the saturated gain at line centre for a double pass through the laser medium. ω_a is the centre frequency for the transition and $\Delta\omega$ is the atomic linewidth. Where the bandwidth of the pulse is much less than the linewidth we may expand the lineshape about its centre as follows:-

$$g_a(\omega) = G \exp\left[-2jg\left(\frac{\omega-\omega_a}{\Delta\omega}\right) - 4g\left(\frac{\omega-\omega_a}{\Delta\omega}\right)^2\right] \tag{2.9}$$

where $G = e^g$

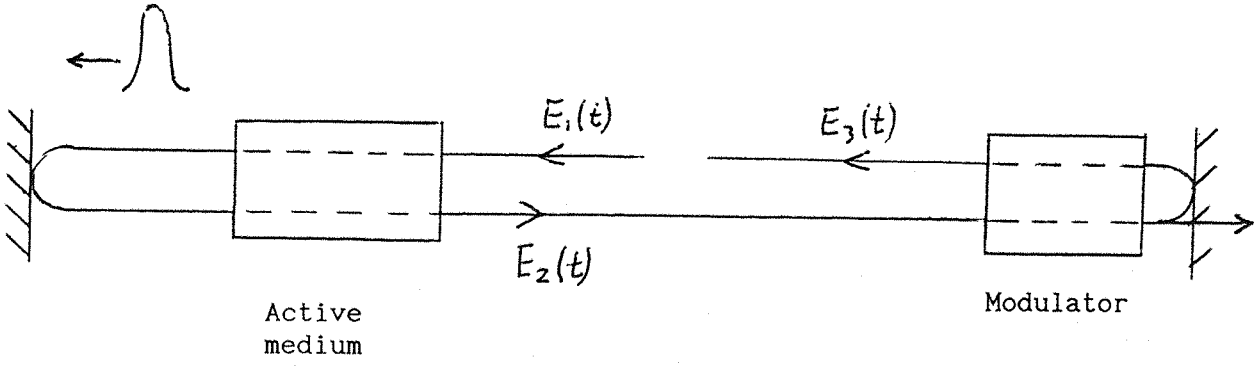

Fig. 2.1 Circulating pulse in the cavity of a mode locked laser.

The lineshape is now Gaussian and a Gaussian pulse passing through an active medium with this lineshape will remain Gaussian.

A pulse $E_1(t)$ enters the active medium and the Fourier transform of the pulse coming out is $E_2(\omega) = g_a(\omega)E_1(\omega)$

$$= \frac{E_o G}{2}\sqrt{\frac{\pi}{\gamma}}\ \exp\left[-2jg\left(\frac{\omega-\omega_a}{\Delta W}\right) - 4g\left(\frac{\omega-\omega_a}{\Delta\omega}\right)^2 - (\omega-\omega_p)^2/4\gamma\right] \qquad (2.10)$$

Where the pulse is on line centre this can be rewritten as

$$E_2(\omega) = \frac{E_o G}{2}\sqrt{\frac{\pi}{\gamma}}\ \exp[-A(\omega-\omega_a)^2]\ \exp\ [-jB(\omega-\omega_a)] \qquad (2.11)$$

$$\text{Where } A = \frac{1}{4\gamma} + 4g/\Delta\omega^2 \qquad (2.12)$$

and

$$B = 2g/\Delta\omega \qquad (2.13)$$

Transforming back to the time domain.

$$E_2(t) = \left(E_o G/4\sqrt{\gamma A}\right)\ \exp[-(t-B)^2/4A]\ \exp(j\omega_a t) \qquad (2.14)$$

For short pulses passing through the modulator at peak transmission, the transmission of the ideal modulator can be approximated to

$$T = \exp\ [-2\delta_1(\omega_m t)^2] \qquad (2.15)$$

The peak of the pulse goes through the modulator at time t = B and so the pulse leaving the modulator is given by

$$E_3(t) = E_2(t)\ \exp\ [-2\delta_1\omega_m^2(t - B)^2] \qquad (2.16)$$

The round trip for the pulse also includes a time delay $2L/C$ where L is the cavity length and C is the velocity of light and an effective mirror reflectivity r which is taken to include all the cavity losses.

Therefore, after a round trip the pulse is given by

$$E_4(t) = rE_3\left[t - \frac{2L}{C}\right] \tag{2.17}$$

The pulse must make one round trip in a time T_m where T_m is the interval between the modulator's maximum transmissions.

So for a self consistent solution

$$E_1(t - T_m)e^{-j\phi} = E_4(t) \tag{2.18}$$

Where the phase angle ϕ allows for a possible phase shift of the optical signal with respect to the pulse envelope.

Using (2.2), (2.14), (2.16) and (2.17), (2.18) may be written as

$$\frac{E_o}{2} \exp\left[-\gamma(t - T_m)^2\right] \exp\left[jW_a(t - T_m)\right] \exp(-j\phi)$$

$$= \frac{rE_oG}{4\sqrt{\gamma A}} \exp\left(-\left[t-B-\left(\frac{2L}{C}\right)\right]^2/4A\right)\exp\left(2\delta_1\ \omega_m^2\left[t-B-\left(\frac{2L}{C}\right)\right]^2\right)$$

$$.\exp\left(j\omega_a\left[t - \frac{2L}{C}\right]\right) \tag{2.19}$$

From which

$$T_m = \frac{2L}{C} + B \tag{2.20}$$

$$\gamma = \frac{1}{4A} + 2\delta_1 \omega_m^2 \qquad (2.21)$$

$$e^{-j\phi} = \left(rG/2\sqrt{\gamma A}\right)\exp(j\omega_a B) \qquad (2.22)$$

From (2.21) and (2.11)

$$\gamma = \delta_1 \omega_m^2 \pm \frac{1}{2}\sqrt{(2\delta_1 \omega_m^2)^2 + \frac{\delta_1 \omega_m \Delta\omega^2}{2g}} \qquad (2.23)$$

For lasers with a large linewidth $\omega_m << \Delta\omega$ and also $\Delta\omega^2/g\omega_m\delta_1 >> 1$ which allows (2.23) to be approximated to

$$\gamma = (\omega_m \Delta\omega/4)\sqrt{\frac{2\delta_1}{g}} \qquad (2.24)$$

The negative sign in (2.24) is ignored since the real part of γ must be positive.

For amplitude modulation $\gamma = \alpha$ since $\beta = 0$.

It follows that the pulsewidth and bandwidth are

$$\tau_p = \frac{\sqrt{\sqrt{2}\ln 2}}{\pi}\left(\frac{g}{\delta_1}\right)^{1/4}\left(\frac{1}{f_m \Delta f}\right)^{1/2} \qquad (2.25)$$

$$\Delta f_p = \sqrt{2\sqrt{2}\ln 2}\left(\frac{\delta_1}{g}\right)^{1/4}(f_m \Delta f)^{1/2} \qquad (2.26)$$

The product of the pulse duration and the bandwidth is

$$\tau_p \Delta f_p = \frac{2\ln 2}{\pi} = 0.44 \qquad (2.27)$$

Major assumptions in this theory are that the lineshape is Gaussian and the pulse profile is Gaussian. The theory may therefore be expected to break down in the case of pulses whose bandwidth is significant compared to the linewidth or whose profile is distorted from a Gaussian profile. The theory also assumes that the mode locked laser has reached its steady state and it neglects any effects due to spontaneous emission.

Published experimental results confirm that pulse durations may differ considerably from those predicted by Kuizenga and Siegman's work. For example, Maker and Ferguson [2.2] obtained 12ps pulses from a mode locked Nd:YAG laser and noted that the parameters of their laser and the Kuizenga and Siegman theory predicted pulse durations of 32ps.

2.2 The Acousto-Optic Modulator

The basic principle underlying the operation of an acousto-optic modulator is the diffraction of light by acoustic waves. A radio frequency electric signal is applied to a piezoelectric transducer bonded to a substrate block. The transducer generates an acoustic signal which passes into the substrate and is reflected back from the opposite surface, creating a standing acoustic wave. The strain due to this standing wave gives refractive index variations in the substrate (the photoelastic effect) which act as a grating whose line spacing is determined by the acoustic wavelength. An optical beam passing through this region perpendicular to the direction of travel of the acoustic signal experiences periodic diffraction. This leads to a periodic variation in the amplitude of the transmitted beam which

for an ideal modulator gives the transmission characteristic given in Equation (2.1).

The diffracted beams are symmetrical about the transmitted beam and are separated from it by angles given by [2.3]

$$\theta_m = \pm \frac{m\lambda}{n\Lambda} \qquad (2.28)$$

where m is an integer, λ is the wavelength in vacuo of the optical signal, n is the refractive index of the medium and Λ is the acoustic wavelength. Each diffracted order is frequency shifted by an amount $\pm m \nu_a$ where ν_a is the acoustic frequency and most of the diffracted power appears in the first order beams.

Efficient modulation requires a standing wave in the substrate and this in turn requires that there are a whole number of half wavelengths between the two faces of the substrate. The radio frequency signal applied to the transducer must therefore be tuned to one of the "resonances" of the modulator - those frequencies at which a standing wave is set up due to repeated reflections between the opposite faces of the substrate, When on a resonance the acoustic power absorbed by the modulator is maximised and the power reflected from the modulator back into the radio frequency amplifier is minimised.

Monitoring the reflected radio frequency power therefore allows the resonant frequencies to be identified.

The standard material for the substrate is fused quartz as this has good optical properties which minimise the optical losses when it is inserted in the laser cavity. However, it is unsuitable for use at modulation frequencies greater than several hundred megahertz because it has a high acoustic attenuation and the attenuation is proportional to the square of the acoustic frequency [2.4]. TeO_2 and lithium niobate are also commonly used as acousto-optic media. Lithium

niobate is a particularly good material for use at high frequencies as it has a low acoustic attention of only $0.2 dBcm^{-1}$ at a frequency of 1GHz. Fused quartz has an attenuation of $3 dBcm^{-1}$ at this frequency and is therefore unsuitable for use in this frequency range.

It can be shown [2.5] that for the diffraction regime in which the mode locker operates the diffraction efficiency is inversely proportional to the optical wavelength. A longer wavelength laser will experience less diffraction in the modulator than a shorter wavelength laser and the mode locked pulses will be longer. However, as shown in Equation (2.25) the dependence of the pulse duration on the diffraction efficiency is quite weak.

The piezoelectric transducer is generally made of $LiNbO_3$ or ZnO and it is bonded to or deposited on the substrate with metallic layers on either side of it to serve as electrodes. The central frequency around which the modulator operates is determined by the thickness of the transducer. The diffraction efficiency of the device falls as the acoustic frequency is moved away from this centre frequency, giving the modulator an effective bandwidth.

The modulator used in this work was designed to operate at frequencies around 60MHz, but in practice it was found to give the highest diffraction efficiency at frequencies around 35MHz. Diffraction efficiencies were measured by placing the modulator in the output beam of the laser and then measuring the incident and transmitted power. At 35MHz, 1.0W of radio frequency power applied to the modulator diffracted 25% of the power in a beam incident on the modulator. At 60 MHz driving frequency, the same RF power gave 10% diffraction.

From Equation 2.25 it is seen that an increase in diffraction efficiency shortens the pulses which are expected from the mode locked laser. However, the pulse duration is also inversely proportional to the square root of the modulation frequency so the pulses will lengthen if the modulation frequency is reduced to take advantage of the greater modulator efficiency.

The pulse duration is more strongly dependent on the modulation frequency than on the diffraction efficiency so driving frequencies around 60MHz were used in this work. Attempts were made to mode lock the laser using a driving frequency of 35MHz. but when the laser cavity was lengthened to match this frequency the laser would not mode lock. Also, the lengthening of the laser cavity caused the output power to drop by about 50%.

The diffraction efficiency of the modulator reached a maximum at drive powers of 1.5 or 2W and showed little improvement when the power was increased beyond this. Drive powers in this region were used when mode locking the laser and gave 15% diffraction at 60MHz.

2.3. Results

Active mode locking was investigated using the arrangement shown in Fig. 1.1. The pump source was the 6W all lines output of an argon ion laser. A horizontally polarised beam was required for the Ti:sapphire laser so the vertically polarised ion laser output was converted to a horizontally polarised beam by a pair of highly reflecting mirrors coated for the argon ion output wavelengths. The vertically polarised beam is incident on the first mirror at an angle of 45° and is reflected vertically downwards with its polarisation horizontal. The second mirror then turns the vertical beam through 90° so that it travels horizontally, still with horizontal polarisation i.e. it travels out of the page as shown in Fig. 2.2.

A beam expanding telescope expanded the beam by a factor of five to give a larger beam incident on the 20cm focal length lens which focused the beam into the crystal. This allows the beam to be focused more tightly into the crystal.

For a Gaussian beam of wavelength λ passing through a lens of focal length f the waist size W_1 of the beam incident on the lens and the waist size W_2 of the beam which has passed through the lens are

Fig.2.2 Use of mirrors to change the plane of polarisation of a beam

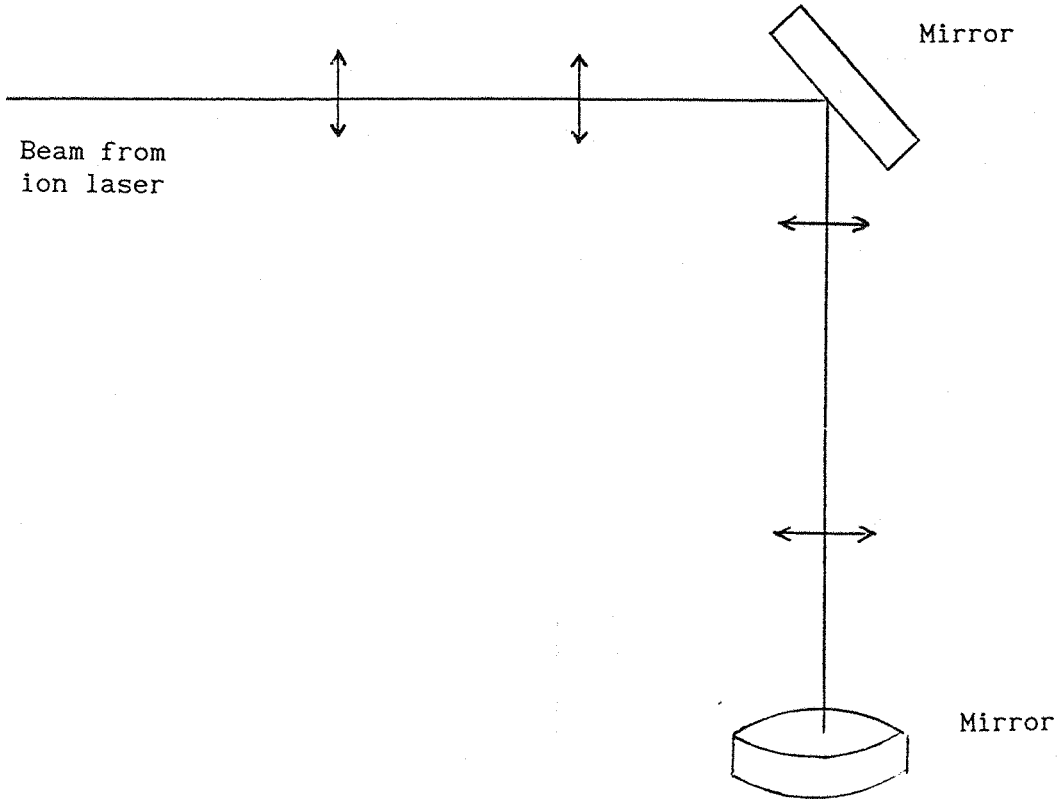

related by the expression

$$\frac{W_2^2}{W_1^2} = \frac{f^2}{(d_1-f)^2+Z_o^2} \qquad (2.29)$$

where d_1 is the distance of the waist W_1 from the lens and $Z_o = \frac{\pi W_1^2}{\lambda}$. For large W_1, Equation (2.29) approximates to

$$W_2 = \frac{\lambda f}{\pi \cdot W_1} \qquad (2.30)$$

The beam incident on the focusing lens is therefore required to have a large diameter in order to give a small value of W_2.

The threshold of the laser was 1.5W pump power with an output coupler whose transmission was 1.6%. The output obtained with 6W pump power was 300mW, corresponding to a slope efficiency of 6.7%. No attempt was made to tune the laser and its output wavelength was 808nm.

Mode locked operation of the laser was obtained using an acousto-optic mode locker placed close to the output coupler (see previous section) and pulse durations were measured using a non background free autocorrelation technique (Fig 2.3). The train of pulses from the mode locked laser is incident upon the first beam splitter which reflects one beam along a path of fixed length and transmits the other along a path of variable length. The moving prism is driven backwards and forwards at a frequency of about 1Hz by an electric motor and the beam reflected from it is recombined with the beam from the fixed prism at the second beam splitter. The combined beam is then focused into a frequency doubling lithium iodate crystal which generates the second harmonic of the laser output. This is detected by a photomultiplier tube after passing through filters which exclude the

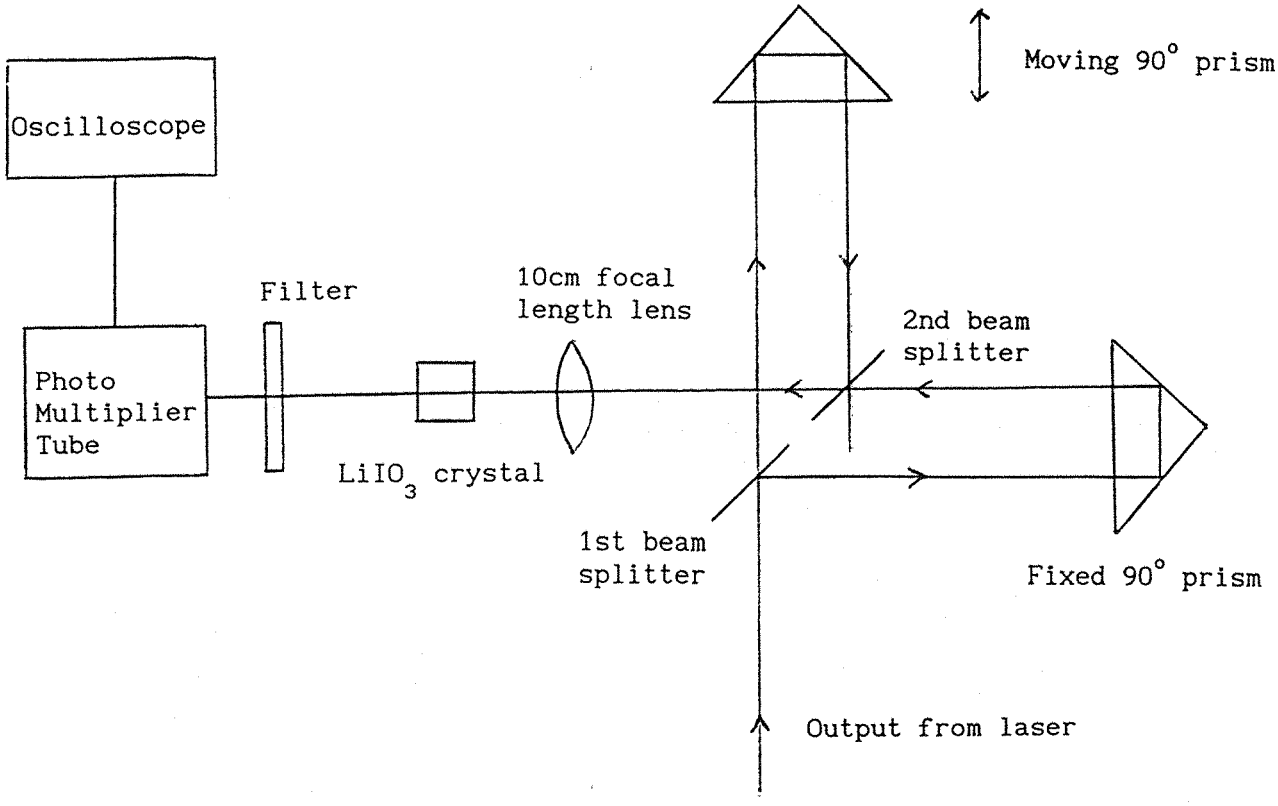

Fig.2.3 A schematic diagram of the autocorrelator.

fundamental frequency.

As the second harmonic intensity is proportional to the square of the incident intensity, a stronger signal is seen when the two path lengths between the prisms and the beam splitters are the same i.e. when the pulses are recombined so that they overlap. The photomultiplier tube therefore detects a varying signal as the moving prism is translated and the width of the peak signed observed on the oscilloscope may be used to deduce the pulse duration. The autocorrelation traces are produced by using the oscilloscope in xy mode with the second harmonic signal giving the y displacement and a potentiometer linked to the movement of the prism giving the x signal.

The second order autocorrelation signal obtained from this non background free technique is given by [2.6]

$$G(\tau) = 1 + 2\frac{\int_{-\infty}^{\infty} I(t)\, I(t+\tau)dt}{\int_{-\infty}^{\infty} I^2(t)dt} \qquad (2.31)$$

where $I(t)$ is the pulse intensity at time t and τ is the delay introduced by the autocorrelator.

An important parameter in non-background free autocorrelation measurements is the peak to background ratio or contrast ratio. This is the ratio of the peak value of the autocorrelation function (at τ = 0) to the background value. From Equation (2.31) it is apparent that this ratio should be 3, but this is only the case if the pulse has a smoothly varying envelope; a pulse with substructure will have a different value for the contrast ratio. The contrast ratio is also of assistance when setting up the autocorrelator so that the two pulse trains overlap properly in the frequency doubling crystal. If the overlap is poor, the observed contrast ratio will be reduced.

I(t) is a time-averaged intensity and all phase information in the pulses is lost. Also, the Full Width at Half Maximum of the autocorrelation function is larger than that of the pulses from which it is derived [2.7]. For example, a Gaussian pulse of the form

$$I(t) = e^{-t^2/T^2} \tag{2.32}$$

has the following autocorrelation function

$$G(\tau) = 1 + 2e^{-\tau^2/2T^2} \tag{2.33}$$

The peak in the autocorrelation function therefore, has an FWHM which is greater than that of the pulses by a factor of $\sqrt{2}$.

The pulse duration expected from the mode locked laser is given by Equation (2.25)

$$\tau_p = \frac{\sqrt{\sqrt{2}\ \ln 2}}{\pi} \left(\frac{g}{\delta_1}\right)^{1/4} \left(\frac{1}{f_m \Delta f}\right)^{1/2} \tag{2.25}$$

The modulation frequency, f_m, was 120MHz and the linewidth Δf of the lasing transition is approximately 1.1×10^{14}Hz. A value for g is calculated using the expression $g = 1/2 \ln 1/R$ where R is an effective power reflectivity of a mirror which is taken to include the output coupler transmission and the losses in the Ti:sapphire rod. For this laser the value of g was 0.015.

δ_1 is half the modulation depth θ_m which can be calculated from the diffraction efficiency ε by using Equation (2.34) [2.8].

$$\varepsilon = \frac{1}{2}\,[1-J_o(2\theta_m)] \qquad (2.34)$$

where $J_o(2\theta_m)$ is the zero-order Bessel function of $2\theta_m$.

For $\varepsilon = 0.15$ a value $\theta_m = 0.4$ is obtained, giving $\delta_1 = 0.2$. These values give an expected pulse duration of 1.4ps.

Previously reported results for actively mode locked Ti:sapphire lasers generally gave pulse durations of 50-100ps [2.9 - 2.11], although 6ps pulses have been reported for a laser whose modulation frequency was slightly detuned from the cavity length [2.12]. More recently, [1.9] 1.3ps pulses have been reported from an actively mode locked Ti:sapphire laser which incorporated a Gires-Tournois Interferometer to compensate for dispersion in the cavity and shorten the pulses.

Pulse durations of 12ps were observed from the mode locked laser, assuming a Gaussian pulse profile and an autocorrelation trace is shown in Fig.2.4. The corresponding bandwidth of the laser output is shown in Fig. 2.5 and has a value of 190 GHz. This gives a time-bandwidth product of 2.3, indicating that the pulses are far from bandwidth limited.

The apparatus used to measure the pulse bandwidths is shown in Fig. 2.6. The laser output was either split by a beam splitter, giving one beam for the autocorrelator and one beam for the bandwidth measurement, or alternatively the laser output through the planar high reflector was used for the bandwidth measurement.

A 2400 lines per mm diffraction grating was placed in the beam at grazing incidence so that the beam was incident on its entire length for optimum resolution. The first order diffracted light was focused onto a linear diode array by a 1m focal length lens and the width of the focused spot at the array is proportional to the bandwidth of the signal.

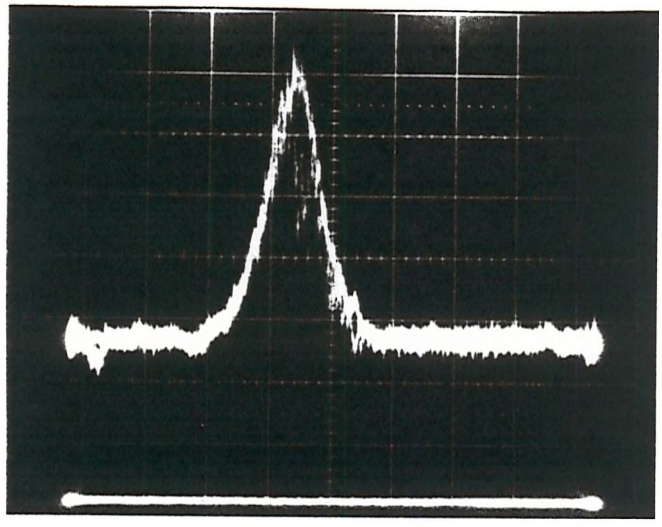

Fig. 2.4 Autocorrelation trace of a train of 12ps pulses.

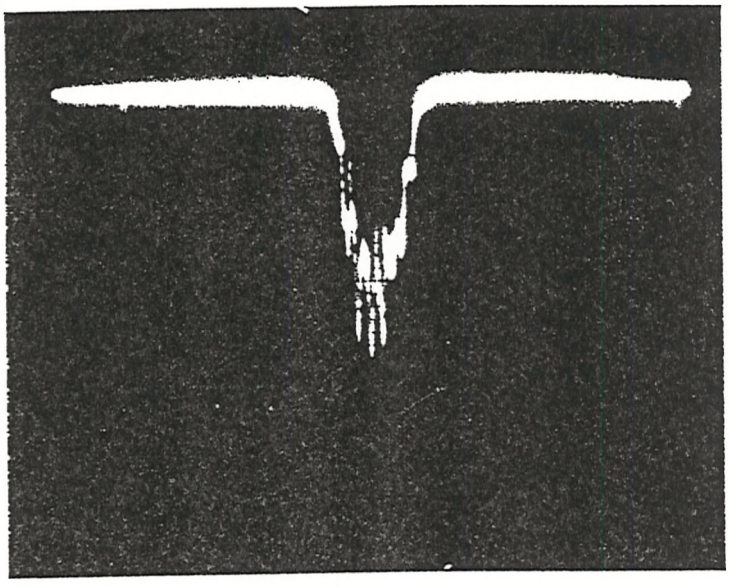

Fig. 2.5 Bandwidth of the pulses shown in Fig. 2.4.
The bandwidth is 190GHz
Horizontal scale 260GHz cm^{-1}

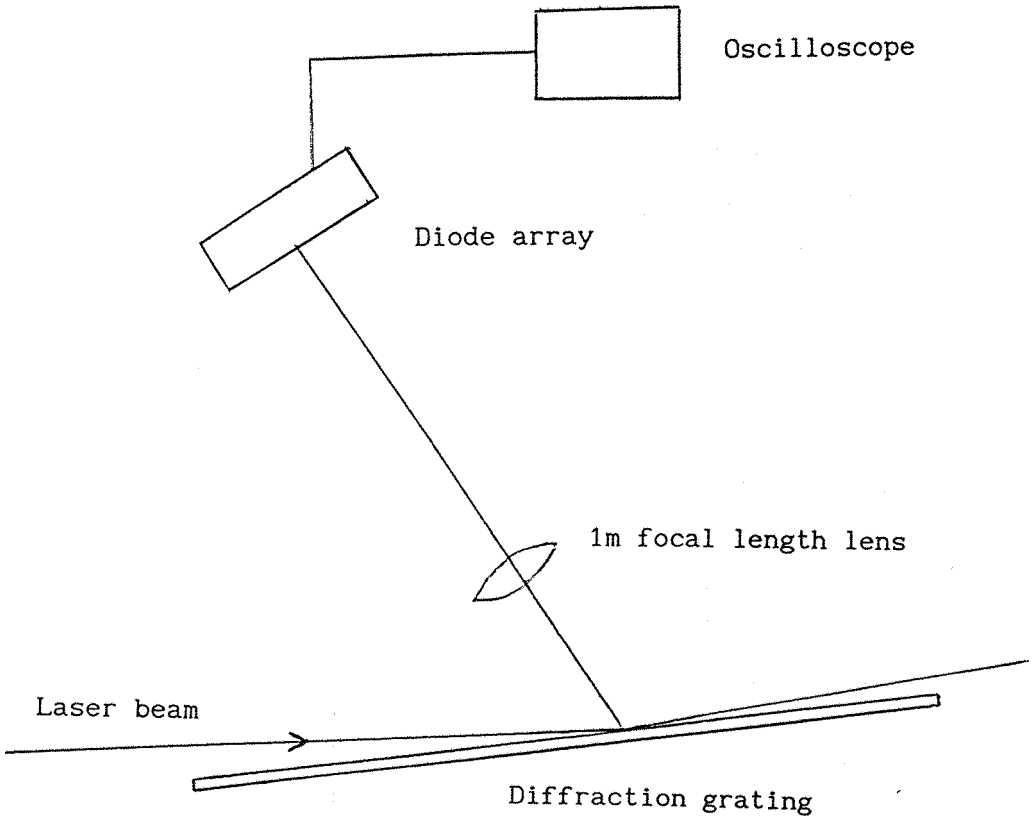

Fig.2.6 Apparatus for measuring the bandwidth of the laser.

The linewidth $\Delta\lambda$ is given by

$$\Delta\lambda = \frac{d\cos\theta r}{f} \Delta x \qquad (2.35)$$

Where d is the line spacing on the grating, θr is the angle between the diffracted beam and the grating normal and f is the focal length of the lens. Δx is the width of the spot at the array.

The resolution of the system was about 3GHz, limited by the resolution of the grating. The output from the array which consisted of 1024 elements spaced over 25mm was observed on an oscilloscope so that the bandwidth could be calculated from the observed signal.

In an attempt to obtain bandwidth limited pulses, a Brewster angled etalon of thickness 125μm was inserted in the laser cavity. The transmission of an etalon varies with the incident frequency and has a value of 100% at maxima which are separated by a frequency difference.

$$\Delta\nu = \frac{C}{2nd\cos\theta} \qquad (2.36)$$

where $\Delta\nu$ is known as the Free Spectral Range of the etalon. C is the velocity of light in vacuo, n is the refractive index of the etalon, d is the thickness of the etalon and θ is the angle between the incident beam and the normal to the etalon. n is 1.5 for glass, giving $\theta = 56^{\circ}$ for the Brewster angled etalon.

As the frequency of the light moves away from a transmission maximum, the transmission falls below 100%. When inserted in the laser cavity this loss will cause the laser to operate with a narrow bandwidth centred on a transmission maximum.

The Free Spectral Range of the etalon used was 1440GHz which was greater than the bandwidth of the pulses previously observed. The pulse bandwidth was reduced to 20GHz and the pulse duration increased

to 26ps. This gave a time-bandwidth product of 0.5 compared to 2.3 for the 12ps pulses obtained without the etalon and a minimum value of 0.44 for a Gaussian pulse profile. The measurement uncertainty introduced by the 3GHz resolution of the grating allows a bandwidth limited pulse to have a measured time-bandwidth product of 0.5.

The shortest pulses are expected when the circulating pulse in the laser cavity always passes through the modulator at the times of minimum loss. When the modulation frequency is detuned from its optimum value of precisely the cavity round trip frequency, the pulses are expected to broaden [2.1].

The effects of detuning the modulator frequency were investigated both with and without an intracavity etalon and it was found that the laser's response differed in each case. Fig. 2.7 shows the response of the pulse duration and bandwidth to a detuning of the modulation frequency without an intracavity etalon. For negative detuning - a modulation frequency below the optimum frequency - the pulse duration and bandwidth remained unchanged until the modulation frequency had been reduced to 200Hz below the optimum frequency. At this point the mode locked operation became intermittent, accompanied by intermittent reductions in the bandwidth. Further reduction in the modulation frequency gave a free running laser output with a narrow bandwidth of 11GHz compared to 160GHz for the pulsed output. The output power of the laser gradually fell as the modulation frequency was reduced further and for a 700Hz detuning the output power was 40% less than when mode locked. A reduction in output power is expected as the pulse is suffering losses in the modulator due to not passing through it at the point of maximum transmission. Increasing the detuning from 200 to 700Hz caused a slight shift in the laser's output wavelength, equivalent to a 50GHz increase in the output frequency.

As indicated in Fig. 2.7 positive detuning - a modulation frequency greater than the optimum frequency - gave a gradual increase in the pulse duration from 12ps to 18ps for a 300Hz detuning, but had no effect on the bandwidth. Increasing the detuning gave a more

Fig. 2.7 Pulse width and bandwidth plotted against detuning with no intracavity etalon.

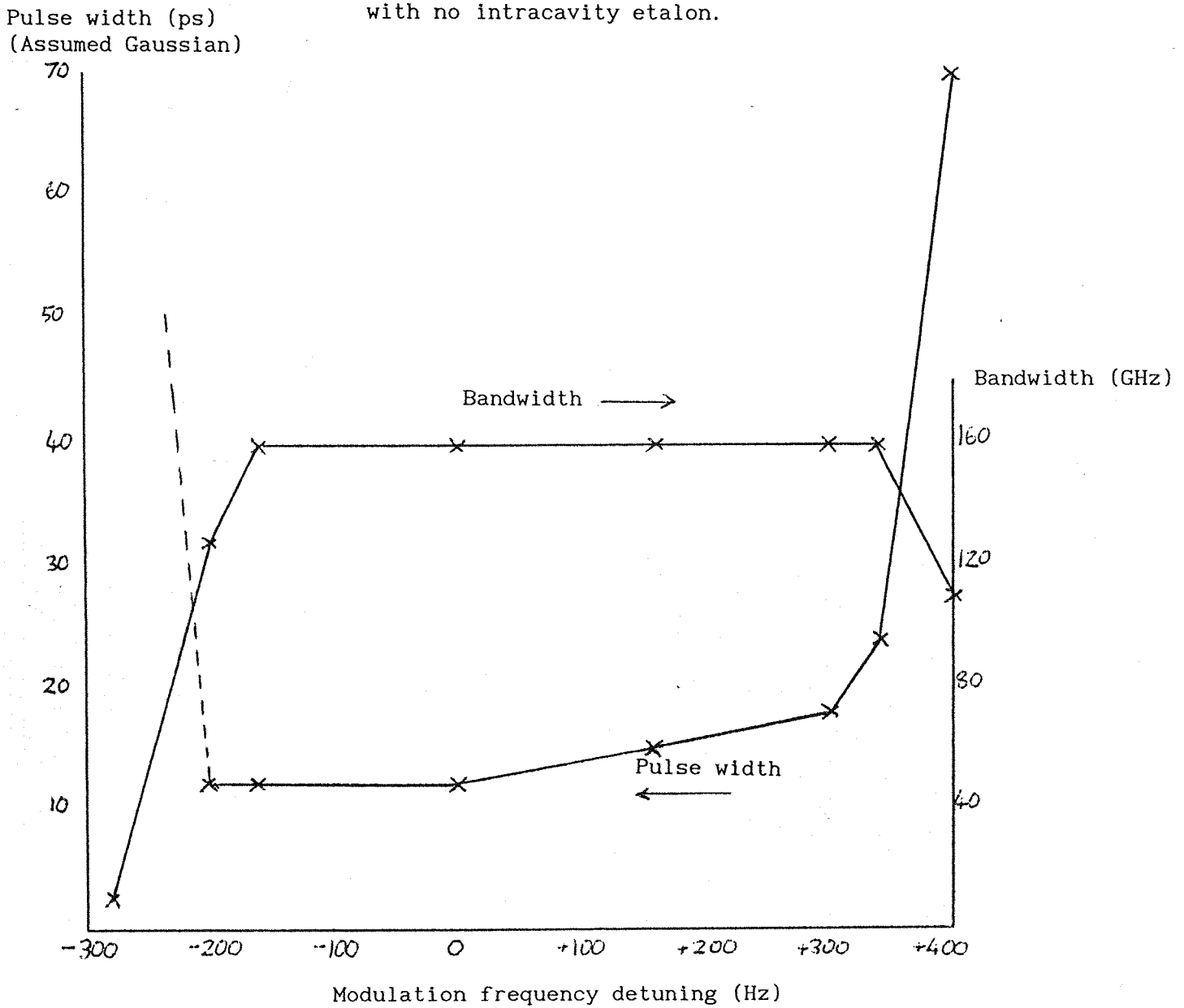

rapid lengthening of the pulses accompanied by a reduction in the bandwidth. Positive detuning of the modulation frequency had no effect on the output power. A detuning of 400Hz was required before pulsed output ceased, compared to approximately 250Hz in the case of negative detuning.

When the power supply to the mode locker was switched off, the free running laser output was found to have a bandwidth of 250GHz compared to 160GHz for mode locked operation with zero detuning.

The behaviour of the laser when the 125μm etalon was used is shown in Fig. 2.8. Unlike the results obtained without the etalon, these show a pronounced maximum in the bandwidth and a minimum in the pulse duration. They occur at modulation frequencies which differ by 40Hz but this difference is believed to be due to the output frequency of the radio frequency generator having changed slightly.

Taking this into account, a detuning as small as 20Hz gives a sharp reduction in the bandwidth and an increase in the pulse duration. For negative detuning, the increase in pulse duration is rapid and the output is no longer pulsed for detunings greater than 80Hz. Positive detuning gives a much more gradual increase in the pulse duration.

Increasing the negative detuning from zero to 300Hz reduced the bandwidth from 47GHz to 9GHz, beyond which it remained unaltered. At a detuning of 760Hz, the laser wavelength jumped from 808nm to 792nm. The output power was unaffected, but the laser started to lase intermittently at 808nm when the detuning was increased to 900Hz. Increasing the detuning increased the tendency of the laser to lase at 808nm until the detuning was 1400Hz, at which point the output was entirely at 808nm.

The output power was unaffected by detuning over this range, but was found to fall as the detuning was increased further. The laser output fell to zero when the detuning was 30kHz. Positive detuning

Fig. 2.8 Pulse width and bandwidth plotted against detuning with a 125μm intracavity etalon.

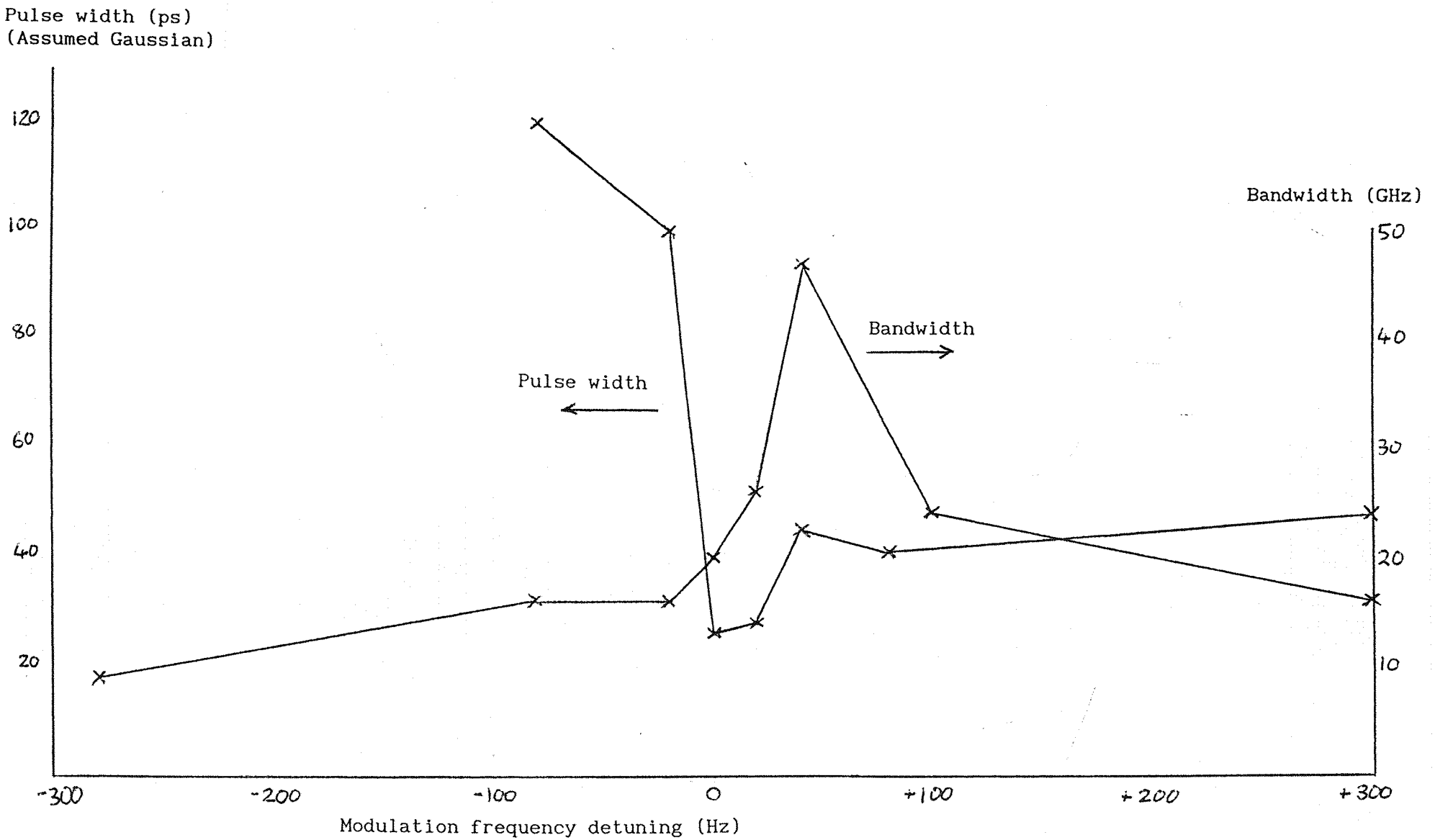

had a similar effect on the output power which fell to zero when the tuning was 90kHz but the wavelength jump was only observed for negative detuning. There was, however, a 30GHz increase in the laser's output frequency for detunings greater than 3kHz. This is similar in magnitude to the 50GHz increase in the laser's frequency which was observed with a 700Hz negative detuning and no etalon.

Including the etalon in the cavity had a major effect on the bandwidth of the free running laser. It was found to be 9GHz compared to 47GHz at optimum mode locking. Without the etalon the free running bandwidth was larger than the mode locked bandwidth.

Acousto-optic mode locking of the Ti:A_2O_3 laser has generated 12ps with considerable excess bandwidth. The analysis of [2.1] predicts a pulse duration of 1.4ps but as in the case of some published results e.g. [2.2] the actual pulse duration differs considerably from the predicted value. Use of a 125μm thick intracavity etalon reduced the time-bandwidth product from 2.3 to an almost transform limited value of 0.5 but gave a longer pulse duration of 30ps.

The behaviour of the mode locked laser as the mode locker modulation frequency was detuned from the intermode beat frequency was investigated. The response of the laser to the detuning was found to be strongly influenced by the intracavity etalon.

Without the etalon present the modulation frequency had to be detuned from the intermode beat frequency by several hundred Hertz before the pulses began to broaden and their bandwidth began to decrease. With no power applied to the mode locker the free running bandwidth of the laser was greater than the mode locked bandwidth with zero detuning.

The detuned laser behaved differently with the etalon in the cavity. A 20Hz detuning, the smallest which the signal generator could apply to the modulator, gave a sharp reduction in the bandwidth of the laser output and an increase in the pulse duration. A

modulation frequency less than the intermode beat frequency caused the laser wavelength to jump from its usual value of 808nm to 792nm for values of detuning between 760 and 1400Hz. The bandwidth of the free running laser was much less than the mode locked bandwidth with zero detuning, in contrast to the situation observed without the etalon.

36a

2.4 References

2.1 D.J.Kuizenga and A.E. Siegman, IEEE J. Quantum Electron. QE6 p.694 (1970).

2.2 G.T.Maker and A.I.Ferguson, Opt. Lett. 14 p.788 (1989).

2.3 E.Young and S.K.Yao, Proc. IEEE 69 p.54 (1981).

2.4 D.A.Pinnow, IEEE J. Quantum Electron. QE6 p.223 (1970).

2.5 C.F. Quate, C.D.W. Wilkinson and D.K. Winslow, Proc. IEEE 53 p.1604 (1965).

2.6 D.M. Rayner, P.A. Hackett and C. Willis, Rev. Sci. Instrum. 53 p.38 (1982).

2.7 K.L. Sala, G.A. Kenney-Wallace and G.E. Hall, IEEE J. Quantum Electron. QE16 p.990 (1980).

2.8 G.T. Maker, S.J. Keen and A.I. Ferguson, Appl. Phys. Lett. 53 p.1675 (1988).

2.9 P.M.W. French, J.A.R. Williams and J.R. Taylor, Opt. Lett 14 p.686 (1989).

2.10 P.A. Schultz, IEEE J. Quantum Electron. QE24 p.1039 (1988).

2.11 R.Roy, P.A. Schulz and A. Walther, Opt. Lett 12 p.672 (1987).

2.12 J.D. Kafka, A.J. Alfrey and T. Baer, Ultrafast Phenomena VI. Springer Verlag: Berlin (1988).

CHAPTER 3

PASSIVE MODE LOCKING OF THE Ti:Al_2O_3 LASER BY SECOND HARMONIC GENERATION

3.1 Introduction

Early work with passively mode locked solid state lasers was accomplished using organic dyes as intracavity saturable absorbers. In 1965 Mocker and Collins [3.1] reported a passively mode locked ruby laser with a pulse duration of 1ns and Clobes and Brienza [3.2] reported a Nd:YAG laser with pulse durations of 25ps. Nd:glass was the subject of considerable attention as its large linewidth offered the possibility of subpicosecond pulses and in 1967 Armstrong reported 4 ps pulses from a mode locked Nd:glass laser [3.3].

A phenomenon commonly observed with the flashlamp pumped Nd: silicate lasers was the deterioration of the quality of the pulses after the beginning of the pulse train. The initial pulses were short and bandwidth limited, but as the pulse intensity increased, self phase modulation in the laser medium broadened the pulse spectrum and the dispersion caused the pulses to fragment. Fragmentation may also result from self-focusing as the pulse intensity increases.

Phosphate glasses have been used as neodymium hosts as they have lower nonlinear refractive indices than silica and therefore suffer less from self phase modulation and self focusing, while retaining the advantage of a large linewidth. Alfano et. al. [3.4] obtained pulses of 2.4ps duration from a Nd:phosphate laser.

As the circulating field in the laser cavity begins to grow from the initial spontaneous emission it consists of many longitudinal

modes with random amplitudes and phases, or alternatively it may be regarded as a series of narrow spikes with varying amplitudes and widths. The bandwidth of the spontaneous emission is the width of the gain profile so the shortest spikes in the cavity will have a pulsewidth given by the inverse of this. The signal increases in intensity as it passes repeatedly through the gain medium and spectral narrowing caused by the gain medium broadens the noise spikes.

A point is reached at which one of the noise spikes has sufficient intensity to start saturating the absorber so it undergoes less attenuation than the rest of the intracavity signal and grows faster until it is able to extract the energy stored in the gain medium.

A distinction can be made between the pulse shortening process due to a fast absorber and that due to a slow absorber. If the recovery time for the dye is much shorter than the pulse width then the absorber is saturated by the instantaneous intensity of the pulse. The peak of the pulse therefore saturates the absorber and passes through with less attenuation than is experienced by the wings of the pulse.

A slow absorber has a recovery time which is much greater than the pulse duration and is saturated by the integrated intensity or energy of the pulse. The leading edge of the pulse is attenuated and the peak experiences little attenuation as it saturates the absorption. The trailing edge of the pulse is also not attenuated as the absorption does not recover in time to affect it.

Passive mode locking is the favoured method for the generation of the shortest laser pulses since the radio frequency modulation signal applied to the intracavity modulator in an actively mode locked laser is relatively slowly varying and this leads to pulses of a longer duration. Pulse durations from actively mode locked lasers are generally in the range of tens of picoseconds whereas pulse durations

of tens of femtoseconds may be obtained using passively mode locked systems. [3.5].

The mode locking process induced by a saturable absorber will not give a train of output pulses which is reproducible from one shot to the next in a flashlamp pumped laser. The initial noise distribution in the cavity may not contain one fluctuation which is significantly stronger than the others and this leads to a train of output pulses in which the main pulse is accompanied by weaker satellite pulses. Active mode locking has the advantage of giving a reproducible train of output pulses whose characteristics are more readily controlled.

Combined active-passive mode locking has been investigated in an attempt to combine the pulse shortening characteristics of a saturable absorber with the reproducibility of an actively mode locked system. Kishida and Yamane [3.6] added an acousto-optic modulator to a passively mode locked Nd: glass laser and noted that satellite pulses were eliminated and good shot-to-shot reproducibility was obtained. In such a laser the maximum transmission point in the modulator cycle establishes a window in which a favoured pulse will build up and any pulse outside this window will be suppressed.

3.2 Passive Mode Locking Using Techniques Other Than Saturable Dyes

In recent years, nonlinear processes other than saturable absorption with dyes have been used to mode lock solid state lasers. These processes have been used to shorten the pulse duration of actively mode locked lasers and are also capable of serving as the sole mode locking mechanism.

Such a process was first demonstrated in the soliton laser of Mollenauer and Stolen [3.7] in which a synchronously pumped colour centre laser is coupled to an external cavity containing a length of optical fibre. Pulses from the laser pass into the fibre, are

reflected back by a mirror at the end of the fibre and are reinjected into the laser. The external cavity length is an integral multiple of the laser cavity length so that the pulses reinjected into the laser are coincident with the pulse already in it. The interaction of the fibre index nonlinearity with negative group velocity dispersion causes the pulses to shorten and the shortened pulses reinjected into the laser cause the pulse in the laser cavity to shorten. This continues until the pulses in the fibre become solitons and hence have the same shape after passing through the fibre that they had before entering it.

Blow and Nelson [3.8] later established that soliton formation in the fibre is not essential for operation of the laser. They enhanced the mode locking of a synchronously pumped colour centre laser using a fibre which would not support solitons at the laser's operating wavelength. In this case the mode locking enhancement occurs when the pulse from the fibre is reinjected into the laser with a phase such that self phase modulation in the fibre causes the pulses to interfere more constructively near the peak than in the wings. As the pulse shortening occurs due to the pulses in the laser and external cavities combining additively at the common mirror, this mode locking mechanism is referred to as additive pulse mode locking (APM). French, Williams and Taylor have applied this technique to a Ti:Al_2O_3 laser and have reduced the duration of the pulses from an acousto-optically mode locked laser from 75ps to 770fs [3.9].

Ouelette and Piche have demonstrated a passively mode locked CO_2 laser in which the output coupler consists of a Michelson interferometer with a nonlinear crystal inserted into one arm. [3.10]. The interferometer is adjusted so that the self phase modulation in the crystal causes the interferometer to give an enhanced reflectivity at high intensity. The nonlinear interferometer therefore behaves as a fast saturable absorber and shortens the mode locked pulses. In another experiment the same authors placed the interferometer outside the laser cavity and mode locked the CO_2 laser

using an acousto-optic modulator. The interferometer narrowed the pulses from the actively mode locked laser by a factor of up to 1.6 [3.10].

In more recent work, lasers have been mode locked purely by self phase modulation in the external fibre cavity. Goodberlet et al. [3.11] have demonstrated a passively mode locked Ti:Al_2O_3 laser which produced chirped pulses with a duration of 1.4ps. Dispersive compensation of these pulses reduced the pulse duration to 200fs. Liu and Chee have used the same method to produce 4ps pulses from a passively mode locked Nd:YLF laser with output powers of up to 7W. [3.12].

Nonlinear amplitude modulation may also be used to mode lock lasers. Stankov [3.13] proposed a mirror with an intensity-dependent reflection coefficient consisting of a nonlinear crystal and a dichroic mirror. The fundamental frequency from the laser undergoes partial conversion to its second harmonic in the crystal and is then reflected back from the dichroic mirror. This mirror is chosen to have a high reflectivity at the second harmonic and a lower reflectivity at the fundamental frequency. If the phase relation between the reflected beams is correct, the second harmonic will undergo partial reconversion into fundamental on the second pass through the nonlinear crystal. The required phase difference may be obtained using the dispersion in air by adjusting the spacing between the crystal and the mirror. Increasing the intensity of the fundamental beam increases the intensity of the second harmonic and hence the intensity of the reflected fundamental due to the reconverted second harmonic. The reflectivity of the crystal and mirror combination therefore increases at higher intensities.

Stankov has reported 45ps pulses from a Nd:YAG laser mode locked using a KTP crystal as the nonlinear element [3.14] and suggested that the pulse duration is limited by the time available for the mode locked pulse to build up in the flashlamp pumped laser. An

intracavity crystal will introduce losses and may also limit the laser bandwidth by acting as an etalon. These latter problems may be avoided by placing the nonlinear crystal in an external cavity.

Coupled cavity mode locking of a Nd:YAG laser has been demonstrated by Barr and Hughes [3.15] and has produced pulse durations in the range 30 - 50ps.

3.3 Theory of Mode Locking by Second Harmonic Generation

A schematic diagram of the experimental arrangement for second harmonic mode locking using a coupled cavity is shown in Fig. 3.1. The second harmonic crystal is contained in an external cavity whose length is matched to that of the laser cavity. The laser output coupler has field amplitude reflection and transmission coefficients r_3 and t_3 at the fundamental wavelength. Barr and Hughes [3.16] have presented an analysis of mode locking by a nonlinear amplitude modulator in a coupled cavity, applicable to a homogeneously broadened laser whose output reaches a steady state. Following this analysis, the fields incident on and reflected from the output coupler are given by $a_1(t)$ and $b_1(t)$ respectively for the fields in the laser cavity. The fields in the external cavity incident on and reflected from the output coupler are given by $a_2(t)$ and $b_2(t)$. The equations relating the fields in the cavities are [3.17].

$$b_1(t) = r_2 a_1(t) + i t_2 a_2(t) \qquad (3.1)$$

$$b_2(t) = i t_2 a_1(t) + r_2 a_2(t)$$

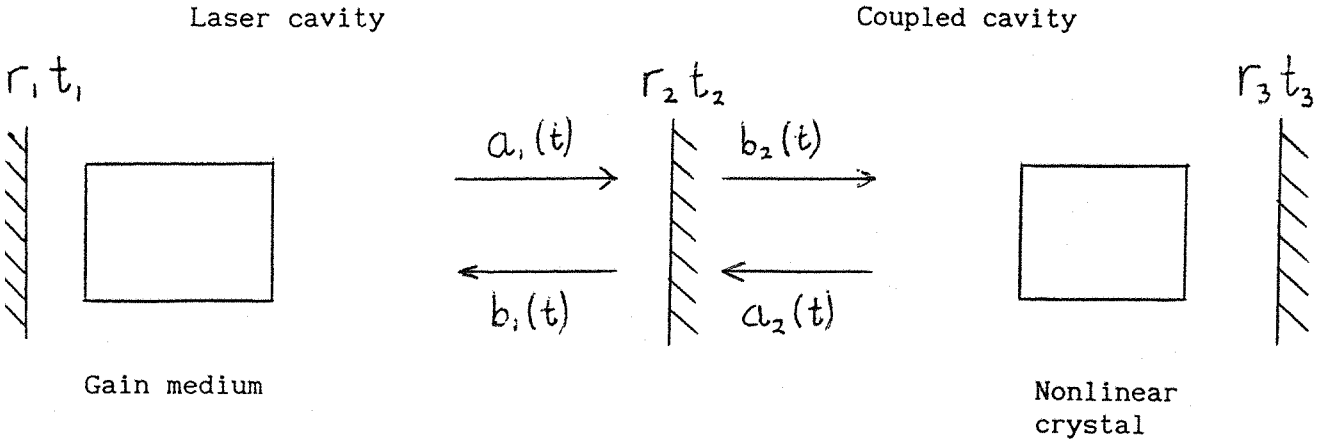

Fig. 3.1 A schematic diagram of the arrangement for coupled cavity mode locking using second harmonic generation.

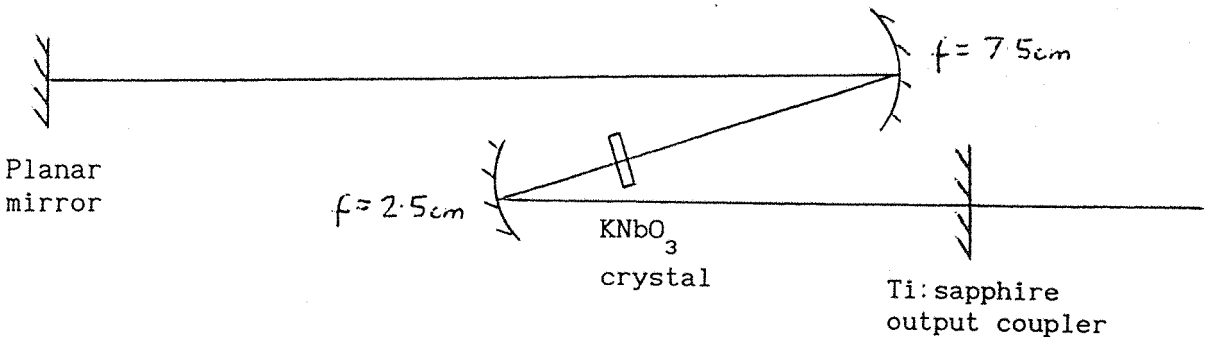

Fig. 3.2 The experimental arrangement for mode locking by second harmonic generation.

After reflection from the nonlinear mirror the field in the external cavity may be written as

$$a_2(t) = b_2(t)m(t)e^{-i\phi} \tag{3.2}$$

where ϕ is the round trip phase change in the external cavity and $m(t)$ is the transmission coefficient for a double pass through the nonlinear crystal. Equation (3.1) may be solved to give the reflection coefficient of the external cavity.

$$r(t) = \frac{b_1(t)}{a_1(t)} - \frac{r_2 - r_3 m(t)\exp(-i\phi)}{1 - r_2 r_3 m(t)\exp(-i\phi)} \tag{3.3}$$

For optimum mode locking it is desirable to have a low value of r_3 [3.18]. When $r_3 << r_2$ the reflection coefficient of the external cavity may be written as

$$r(t) = r_2 - r_3 t_2^2 m(t)\exp(-i\phi) \tag{3.4}$$

The reflection coefficient varies with the phase change in the external cavity and is a minimum for $\phi = 2q\pi$ and a maximum for $\phi = (2q + 1)\pi$ where q is an integer.

An expression is now needed for the modulator transmission $m(t)$. The combination of a nonlinear crystal and a mirror of amplitude reflectivity r_3 has a nonlinear reflectivity r_{nl} which is given approximately by [3.18].

$$r_{nl} = r_3 \exp\left(\frac{\sigma\eta}{2}\right) \tag{3.5}$$

η is the conversion efficiency on the first pass of the fundamental beam through the crystal and σ is a fitting parameter dependent on r_3 and given in [3.16]. The nonlinear mirror may either compress or stretch the pulses, depending on the phase difference between the fundamental and the second harmonic due to reflection from the mirror. For $\sigma > 0$, the nonlinear reflectivity of the crystal and mirror is greater than the linear reflectivity r_3 of the mirror and the nonlinear mirror acts as a pulse compressor. If $\sigma < 0$ the nonlinear mirror has a reflectivity less than the linear reflectivity of the mirror and acts as a pulse stretcher.

The effect of the nonlinear mirror on an incident pulse is found by considering the nonlinear reflectivity given by (3.5) on each part of the pulse profile. For a pulse described by its electric field amplitude $f(t)$ the conversion efficiency is given by

$$\eta(t) = \eta_o \frac{f^2(t)}{f^2(0)} \tag{3.6}$$

η_o is the conversion efficiency at the peak of the pulse $f(0)$. The conversion efficiency is greatest at the peak of the pulse and little second harmonic is generated by the wings. The modulator transmission may now be written as

$$m(t) = \exp\left(\frac{\sigma\eta_o}{2} \frac{f^2(t)}{f^2(0)}\right) \tag{3.7}$$

This indicates that the nonlinear mirror has a much greater effect near the peak of the pulse than it has in the wings. In the wings the ratio of $f^2(t)$ to $f^2(0)$ approaches zero so the modulator transmission approaches unity and the wings are unaffected by it.

An expression may be found for the pulse duration obtained by assuming a Gaussian pulse shape. The pulse shape is expressed as

$$f(t) = f_o \exp(-yt^2)\exp(i\omega_a t) \tag{3.8}$$

where ω_a is the centre frequency of the gain medium. Substituting (3.8) into (3.7) and expanding the exponential allows the modulator transmission to be written as

$$m(t) = \exp\left(\frac{\sigma\eta_o}{2}\right) \exp(-\sigma\eta_o yt^2) \tag{3.9}$$

As in (3.7) the modulator transmission has a value of $\exp(\sigma\eta_o/2)$ at the peak of the pulse and approaches unity with increasing t. Equation (3.9) has the same form as equation (2.15), the expression used for the transmission of an amplitude modulator in the Kuizenga and Siegman analysis of active mode locking. Equation (3.9) may be substituted into (3.4), from which one obtains

$$r(t) = r \exp(\Gamma\sigma\eta_o yt^2) \tag{3.10}$$

where

$$r = r_2 - r_3 t_2^2 \exp\left(\frac{\sigma\eta_o}{2}\right) \exp(-i\phi) \tag{3.11}$$

and

$$\Gamma = \frac{r_3}{r_2} t_2^2 \exp\left(\frac{\sigma\eta_o}{2}\right)\exp(-i\phi) \tag{3.12}$$

This assumes that $r_3 << r_2$ and the exponent in (3.9) has been expanded to the term in t^2. Mode locking by amplitude modulation requires a real value of Γ since an imaginary component of Γ gives rise to phase modulation. The value of $\sigma\Gamma$ must be negative to ensure that the reflection coefficient $r(t)$ of the coupled cavity has a maximum at the peak intensity of the pulse. These conditions are satisfied when $\exp(-i\phi) = 1$, $\phi = 2q\pi$ where q is an integer and $\sigma < 0$. In this case the nonlinear mirror is acting as a pulse stretcher. Alternatively $\exp(-i\phi) = -1$, $\phi = (2q + 1)\pi$ and $\sigma > 0$ which gives mode locking and pulse shortening.

The pulse duration may be calculated assuming a steady state situation. For a standard amplitude modulator, the pulse duration obtained is given by Equation (2.25) which may be written as

$$\tau = \left(\frac{2\ln 2}{\pi}\right)^{1/2} \left(\frac{2g_2(4\pi^2)}{\Delta\omega_m^2}\right)^{1/4} \frac{1}{\sqrt{f_a}} \qquad (3.13)$$

g_2 is the double pass amplitude gain, f_a is the bandwidth of the laser transition, Δ is the modulation depth and ω_m is the modulation frequency. In order to give a transmission function which is Gaussian around its peak, the modulator transmission is approximated to

$$m(t) = \exp\left(\frac{-\Delta\omega_m^2 t^2}{2}\right) \qquad (3.14)$$

This modulator response has the same form as (3.10) which gives the response of the coupled cavity incorporating the nonlinear modulator to the incident pulse. From comparison of (3.14) with (3.10) we find

$$\frac{\Delta\omega_m^2}{2} = -\Gamma\sigma\eta_o y \tag{3.15}$$

The Full Width at Half Maximum, τ, of the pulse intensity is given by Equation (2.6).

$$\tau = \sqrt{\frac{2\ln 2}{y}} \tag{2.6}$$

Equation (3.15) may therefore be expressed in terms of τ as

$$\frac{\Delta\omega_m^2}{2} = \frac{\Gamma(2\ln 2)\sigma\eta_o}{\tau^2} \tag{3.16}$$

It can be seen from (3.16) that the nonlinear amplitude modulator functions as a modulator whose modulation frequency ω_m increases as the pulse duration shortens. This allows the nonlinear modulator to generate shorter pulses than would be the case using a conventional amplitude modulator. The pulse duration τ obtained from the nonlinear modulator is found by substituting (3.16) into (3.13).

$$\tau = \frac{2}{\pi}\left(\frac{2g_2\ln 2}{-\Gamma\sigma\eta_o}\right)^{1/2}\frac{1}{f_a} \tag{3.17}$$

Due to the dependence of ω_m on the pulse duration τ in (3.16), the value of τ is now inversely proportional to f_a instead of being inversely proportional to $f_a^{1/2}$ as is the case with the conventional modulator which operates at a fixed value of ω_m. The nonlinear modulator therefore makes better use of the available bandwidth.

Use of Equation (3.13) in the analysis implies that the approximations used in its derivation also apply to Equation (3.17)

i.e. the laser is homogeneously broadened and its output consists of Gaussian pulses with a bandwidth less than the bandwidth of the transition. Equation (3.17) also assumes that the laser reaches a steady state and that group velocity dispersion in the crystal is insignificant.

A suitable nonlinear crystal for mode locking a $Ti:Al_2O_3$ laser is potassium niobate ($KNbO_3$). This crystal has a high damage threshold and large nonlinear susceptibilities. It may be temperature tuned to give noncritical phase matching for fundamental wavelengths between 840 and 1100nm [3.19] and therefore covers a large part of the $Ti:Al_2O_3$ laser's tuning range.

At room temperature, noncritical phase matching may be obtained in $KNbO_3$ for a wavelength of 860nm and mode locking by second harmonic generation was attempted using a Spectra-Physics Model 3900 $Ti:Al_2O_3$ laser operating at this wavelength. A schematic diagram of the experimental arrangement is shown in Fig. 3.2.

The external cavity consists of four mirrors, of which the first is the output coupler of the $Ti:Al_2O_3$ laser. A mirror of focal length 2.5cm focused the beam from the laser into the $KNbO_3$ crystal and another mirror of focal length 7.5cm recollimated the beam. The fourth mirror was the planar output coupler of the laser used in the active mode locking work. This was mounted on a translation stage so that the length of the external cavity could be adjusted and matched to the length of the main cavity. The folding angles in the cavity were kept as small as possible to minimise astigmatism.

The laser was tuned using a three plate birefringent tuner and gave an output of around 800mW at 860nm when pumped with 5W of all lines argon ion output. The threshold pump power was 1.1W and the output coupler transmission was 3.6%. The slope efficiency of this laser was 20%.

The $KNbO_3$ crystal was five millimetres square and 2mm thick. It was set up for type I noncritical phase matching with the fundamental frequency polarised along the b axis and propagating along the a axis. The second harmonic is then polarised along the c axis.

3.4 Second Harmonic Generation

Nonlinear optical effects such as second harmonic generation (SHG) arise from the nonlinear component of the polarisation in the medium which is induced by the incident electric field. In the case of SHG the fundamental frequency induces a polarisation wave at the fundamental frequency ω_1 and also a polarisation wave at the second harmonic frequency $2\omega_1$. This latter polarisation has a phase velocity and wavelength in the medium which are determined by the refractive index n_1 for the fundamental wave. The second harmnonic polarisation radiates an electromagnetic wave at a frequency $2\omega_1$ which propagates with a phase velocity and wavelength which are determined by the refractive index n_2 at the second harmonic frequency. The polarisation wave and the electromagnetic wave which it radiates will therefore become out of step as they propagate through the medium and a point will be reached when the radiation being emitted starts to interfere destructively with that emitted previously. This distance, known as the coherence length, sets an upper limit on the thickness of the crystal which may be used for SHG.

The phase mismatch between the polarisation and electromagnetic waves is expressed as the difference in their wave numbers and is written as

$$\Delta k = \frac{4\pi}{\lambda_1} (n_1 - n_2) \qquad (3.18)$$

The conversion efficiency η for SHG, neglecting depletion of the fundamental frequency is given by [3.19]

$$\eta = \frac{P(2\omega)}{P(\omega)} = \frac{2\omega_1^2 d^2 l^2}{\pi W^2 \varepsilon_o C^3 n_1^2 n^2} P(W) \frac{\sin^2(\Delta k l/2)}{(\Delta k l/2)^2} \qquad (3.19)$$

where $P(\omega)$ is the power in the fundamental signal, $P(2\omega)$ is the power in the second harmonic signal, d is the nonlinear susceptibility, W is the radius of the fundamental beam and l is the length of the nonlinear medium.

It is evident from (3.19) that a long interaction length l will maximise the second harmonic power, but only if the phase mismatch is zero. For $\Delta k \neq$ zero the second harmonic power rises and falls periodically with a period given by $\frac{\Delta k l}{2} = \pi$. The coherence length is the distance from the input crystal face to the first maximum in the second harmonic power and is given by $\Delta k l = \pi$. It is desirable to maximise this length by reducing Δk, ideally to zero.

This condition may be achieved in a birefringent crystal by phase matching. The direction of propagation and the polarisation of the fundamental and second harmonics are chosen so that the birefringence of the crystal cancels out the dispersion. For most values of θ, the angle between the direction of propagation and the optic axis of the crystal, the conversion efficiency is found to be highly sensitive to the exact direction of propagation. A divergence of $\delta\theta$ from the phase matched value of θ may adversely affect the conversion efficiency for values of $\delta\theta$ as small as 1mrad. Under these conditions the phase matching is known as critical phase matching.

The phase mismatch resulting from a deviation $\delta\theta$ is found to be linear in $\delta\theta$ and proportional to sin 2θ [3.20]. Therefore, if the phase matching angle is 90° the linear dependence of Δk on $\delta\theta$ is eliminated leaving a much smaller dependence on $(\delta\theta)^2$. The phase matching is less sensitive to deviation from θ and is known as noncritical phase matching. If the dispersion and birefringence give

values of n_1 and n_2 which are sufficiently close, noncritical phase matching may be achieved over a range of fundamental wavelengths by temperature tuning the crystal.

Noncritical phase matching is also advantageous as it eliminates the walk-off between the fundamental and second harmonic beams which occurs as they propagate through the crystal. The angle of walk-off is proportional to $\sin 2\theta$ [3.20] so the walk-off does not occur in the case of non-critical phase matching.

3.5 Experimental Results

The intracavity power of the $Ti:Al_2O_3$ laser was monitored through the planar high reflector and feedback from the external cavity was indicated by a fluctuation in the intracavity power when the external cavity was disturbed by tapping the mirror holders. The second harmonic signal showed large fluctuations when the external cavity was disturbed which indicated a change in the reflectivity of the external cavity.

The external cavity caused the $Ti:Al_2O_3$ laser to give a sinusoidally modulated output whose modulation frequency was equal to the intermode beat frequency of the laser. The amplitude of the modulation was 30% of the magnitude of the d.c. component of the laser output. Misalignment of the external cavity eliminated the feedback and also eliminated the modulation on the laser output. Tapping the mirror holders caused a temporary increase in the amplitude of the sinusoidal modulation but had no effect on the d.c. component of the output. This was observed whether or not the output wavelength was properly tuned for SHG so the second harmonic was having no effect on the laser's behaviour.

A 350mW output from the free running laser generated 35μW of second harmonic, giving a conversion efficiency of 0.01%. The

conversion efficiency was too low for the second harmonic to influence the laser's behaviour so the laser was mode locked using an acousto-optic mode locker in order to give a high peak intensity in the $KNbO_3$ crystal. The mode locker was designed to operate at driving frequencies around 120MHz and hence its modulation frequency was 240MHz which matched the intermode beat frequency of the laser.

The output of the mode locked laser consisted of pulses of 30ps duration as measured with the autocorrelator and assuming a Gaussian profile. The bandwidth of the laser output was 30GHz, giving a time-bandwidth product of 0.9. No bandwidth limiting etalon was used and this time-bandwidth product was considerably less than the value of 2.3 which was obtained in the earlier mode locking work with no etalon present in the cavity.

440mW of laser output was now sufficient to generate 4.4mW of second harmonic, a conversion efficiency of 1%. Tapping the mirror mounts in the external cavity no longer caused significant fluctuations in the second harmonic power: it now only varied by about 10% compared to temporary increases of a factor of five which were observed when the laser was free running.

Blocking the external cavity just in front of its output coupler or misaligning the cavity to prevent feedback into the laser caused a doubling of the second harmonic signal, indicating that the coupled cavity was having an adverse effect on the mode locking. The output coupler in the external cavity had a low transmission of only 2% at 860nm and an argon ion laser mirror was substituted for it in an attempt to remedy this. Its transmission at 860nm was 63% and the increase in the second harmonic signal resulting from misaligning or blocking the cavity was reduced to 25%.

The length of the external cavity was varied by moving its output coupler which was mounted on a translation stage in order to find a point at which the cavity lengths were matched. At this point the SHG

should influence the mode locking and a variation in the second harmonic power should be observed. It was not possible to find a point at which this happened.

The conversion efficiency expected for the second harmonic generation may be calculated from Equation (3.19). A value for W_1 the beam radius in the crystal may be calculated using Equation (2.29) and is found to be 10μm, taking the radius of the beam incident on the 2.5cm focal length mirror to be 0.5mm, the figure for the beam radius given by Spectra- Physics. The value of d_{32}, the required nonlinear coefficient for the $KNbO_3$ crystal is -20.5 pm V^{-1} and the value for n_1 and n_2 is 2.28. Assuming a fundamental power of 350mW and perfect phase matching, the conversion efficiency is found to be 0.33% for the free running laser. The experimental value was 0.01% for the free running laser.

Several possibilities might account for the low experimental value for the conversion efficiency. If the bandwidth of the fundamental signal is too large, then it will not all be phase matched and the conversion efficiency will be reduced. The bandwidth over which phase matching occurs is given in [3.19] and is inversely proportional to the crystal length. For a 2mm $KNbO_3$ crystal and a wavelength of 860nm, the phase matched bandwidth is 110GHz. The bandwidth of the laser was 20GHz when free running and 30GHz when mode locked so the phase matching bandwidth of the crystal does not account for the difference between the measured and experimental values for the second harmonic power.

The acceptance angle $\delta\theta$ might also limit the conversion efficiency. This is the maximum deviation from the phase matching angle θm which is allowed before the phase matching is lost. For noncritical phase matching the acceptance angle is given in [3.19].

$$\delta\theta = \left[\frac{1.39\lambda}{\pi l(n_o^{2\omega} - n_e^{2\omega})}\right]^{1/2} \cdot n_o^{\omega} \qquad (3.20)$$

where λ is the fundamental wavelength, l is the crystal length and n_o^{ω} is the refractive index for the fundamental wave. $n_o^{2\omega} - n_e^{2\omega}$ is the birefringence at the second harmonic wavelength. Taking $n_o^{\omega} = n_e^{2\omega} = 2.28$ and $n_o^{2\omega} = 2.50$, $\delta\theta$ is found to be 67m rad or 3.8°. The divergence angle for a focused Gaussian beam is given by

$$\delta\theta = \frac{\lambda}{\pi W_o} \qquad (3.21)$$

where W_o is the beam waist. For a 10μm waist and a wavelength of 860nm the divergence angle is 1.6° so the conversion efficiency is not affected by beam divergence.

Equation (3.19) assumes that the fundamental beam is collimated and therefore has the same peak intensity along the length of the crystal. This assumption is only valid if the confocal parameter of the beam is much larger than the crystal length.

The confocal parameter Z_o of the beam is given by

$$Z_o = \frac{2\pi W_o^2}{\lambda} \qquad (3.22)$$

and for the 10μm beam waist in the crystal the value of Z_o is 0.73mm. The crystal length is 2mm so the beam intensity is less at the faces of the crystal than it is at the centre, giving a loss of conversion efficiency.

From (3.19) the conversion efficiency is inversely proportional to the square of the beam radius and the beam radius W at a distance z from the waist is found from Equation (3.23)

$$W(z) = W_o\left[1 + \left(\frac{\lambda z}{\pi W_o^2}\right)^2\right]^{1/2} \qquad (3.23)$$

For a 10μm waist at the centre of a 2mm thick crystal the beam radius at the crystal faces is larger than the waist by a factor of three, thus reducing the conversion efficiency at the crystal faces by a factor of nine compared to the conversion efficiency obtained at the waist. It would be beneficial to use a mirror of longer focal length selected to give a confocal parameter equal to the crystal length as this would optimise the conversion efficiency.

Mode locking of the laser by nonlinear amplitude modulation was attempted using second harmonic generation in a crystal of potassium niobate. At room temperature noncritical phase matching is obtained at a wavelength of 860nm so mode locking was attempted at this wavelength using a coupled cavity mode locking scheme with the potassium niobate crystal placed in an external cavity.

Feedback from the external cavity was indicated by fluctuations in the intracavity power when the external cavity was disturbed and the feedback also caused the laser to give a sinusoidally modulated output modulated at the intermode beat frequency. These effects were observed whether or not the output wavelength was tuned for second harmonic generation so the second harmonic was having no effect on the laser. The conversion efficiency of 0.01% in the crystal was too low for the second harmonic to affect the laser so the conversion efficiency was increased to 1% by mode locking the laser using an acousto-optic modulator. The coupled cavity had an adverse effect on the mode locking, as indicated by an increase in the second harmonic power when the feedback into the laser was blocked. This effect was reduced by replacing the output coupler of the external cavity with an

argon ion laser output coupler which had a much higher transmission at the laser wavelength.

With the two cavity lengths equal it should be possible to observe a change in the second harmonic power due to the effect of the second harmonic on the mode locking, but no such effects were observed.

The calculated value of the conversion efficiency for the free running laser is 0.33% compared to an observed value of 0.01%. It was found that the beam was too tightly focused in the crystal, giving much larger spot sizes at the faces of the potassium niobate crystal than at the waist within the crystal and hence reducing the conversion efficiency. In future work it would thus be beneficial to focus the beam into the crystal using a mirror whose focal length gives the focused beam a confocal parameter equal to the crystal length in order to optimise the conversion efficiency.

3.6 References

3.1 H.W. Mocker and R.J. Collins, Appl. Phys. Lett 7 p.270 (1965).

3.2 A.R. Clobes and M.J. Brienza, Appl. Phys. Lett. 14 p.287 (1969).

3.3 J.A. Armstrong, Appl. Phys. Lett. 10 p.16 (1987).

3.4 R.R. Alfano, N.H. Schiller and G.A. Reynolds, IEEE J. Quantum Electron. QE17 p.290 (1981).

3.5 J. A. Valdmanis, R.L. Fork and J.P. Gordon, Opt. Lett. 10 p.131 (1985).

3.6 S. Kishida and T. Yamane, Opt. Commun. 18 p.19 (1976).

3.7 L.F. Mollenauer and R.H. Stolen, Opt. Let. 9 p.13 (1984).

3.8 K.J. Blow and B.P. Nelson, Opt. Lett. 13 p.26 (1988).

3.9 P.M.W. French, J.A.R. Williams and J.R. Taylor, Opt. Lett. 14 p.686 (1989).

3.10 F. Ouelette and M. Piche, Opt. Commun. 60 p.99 (1986).

3.11 J. Goodberlet, J. Wang and J.G. Fujimoto, Opt. Lett. 14 p.686 (1989).

3.12 J.M. Liu and J.K. Chee, Opt. Lett. 15 p.685 (1990).

3.13 K. Stankov. Appl. Phys. B. 45 p.191 (1988).

3.14 K. Stankov, Opt. Lett. 14 p.361 (1989).

3.15 J.R.M. Barr and D.W. Hughes, Appl. Phys. B. 49 p.323 (1989).

3.16 J.R.M Barr and D.W. Hughes, J. Mod. Opt. 37 p.447 (1990).

3.17 K.J. Blow and D. Wood, J. Opt. Soc. Am. B 5 p.269 (1988).

3.18 J.R.M. Barr, Opt. Commun. 70 p.229 (1989).

3.19 J.C. Baumert, J. Hoffnagle and P. Gunter, SPIE vol. 492 ECOOSA 1984 p.374.

3.20 W. Koechner, "Solid State Laser Engineering," Springer Verlag (Berlin).

CHAPTER 4

INJECTION SEEDING OF THE Ti:Al_2O_3 LASER

4.1. Introduction and Theory of Injection Locking

If a weak monochromatic signal is injected into the cavity of a laser and if its frequency is sufficiently close to the free running output frequency of the laser, it can control the output characteristics of the laser. The output frequency and bandwidth of the laser are those of the injected signal. This process is referred to as injection locking and similar effects may be obtained in electronic and mechanical oscillators as well as in laser oscillators. When used with lasers it allows one to combine the controlled stable output characteristics of a low power laser with the high output power of a laser which would otherwise be noisy and difficult to control.

Injection locking of one laser by another was first demonstrated by Stover and Steier [4.1] using two single frequency helium-neon lasers. Part of the output of one laser was injected into the other and the injected frequency was varied over a range of several tens of MHz by changing the cavity length. Part of the output of each laser was directed onto a photodetector so that the beat signal between the two lasers could be observed on an oscilloscope. When the injected frequency was sufficiently close to the free running frequency of the second laser, the beat signal was observed to disappear since the frequencies were identical.

The maximum difference between the free running frequency ω_o of the laser and the injected frequency ω_1 at which injection locking can still occur may be calculated by regarding the laser as a regeneratively amplifying interferometer cavity with partially reflecting mirrors. The amplitude gain for a signal injected into

such a cavity is given by [4.2]

$$g(\omega) = \frac{1-R}{1-G_{rt}(\omega)} \tag{4.1}$$

where R is the reflectivity of the input/output mirror. $G_{rt}(\omega)$ is the complex round trip gain inside the laser cavity and may be written as

$$G_{rt}(\omega) = G(\omega)\exp\left(-j\phi(\omega)\right) \tag{4.2}$$

$G(\omega)$ is the round trip gain taking into account gain in the laser medium, internal losses and the mirror transmission. $\phi(\omega)$ is the round trip phase change. Equation (4.1) can therefore be rewritten as

$$g(\omega) = \frac{1-R}{1-G(\omega)\cos\phi(\omega)+jG(\omega)\sin\phi(\omega)} \tag{4.3}$$

As the cavity approaches threshold, $G(\omega)$ approaches unity and for frequencies close to a longitudinal mode frequency ω_o the round trip phase change $\phi(\omega)$ approaches a multiple of 2π. Therefore $\cos\phi(\omega) \rightarrow 1$ and $\sin\phi(\omega) \rightarrow \phi(\omega)$ where $\phi(\omega) = T(\omega-\omega_o)$ and T is the cavity round trip time. Equation (4.3) therefore simplifies to

$$g(\omega) = \frac{1-R}{1-G+jGT(\omega-\omega_o)} \tag{4.4}$$

Threshold is reached when the value of G reaches exactly unity at ω_o and G remains clamped at this value for steady state oscillation above threshold. Threshold is therefore the point at which the regenerative gain $g(\omega)$ goes to infinity for a signal at the oscillation frequency ω_o of the laser.

G is clamped at a value of unity for a frequency ω_o so the regenerative gain at any other frequency remains finite. From Equation (4.4) the power amplification for an injected signal of frequency ω when the laser is oscillating at a frequency ω_o is approximately

$$|g(\omega)|^2 = \frac{\gamma_e^2}{(\omega-\omega_o)^2} \tag{4.5}$$

where γ_e is the energy decay rate of the cavity due to the output coupling, which for large R is given by

$$\gamma_e = \frac{1-R}{T} \tag{4.6}$$

Consider a weak signal of intensity I_1 and frequency ω_1 which is injected into a laser which is lasing at frequency ω_o with an output intensity I_o. As ω_1 is moved closer to ω_o the power $|g(\omega_1)|^2 I_1$ in the regeneratively amplified signal will rise until it approaches the laser output intensity I_o. The amplified signal saturates the gain enough to turn off the laser output at ω_o, leaving only the amplified injected signal at ω_1. Moving ω_1 closer to ω_o has no further effect on the amplified intensity $|g(\omega_1)|^2 I_1$ since all the power available from the gain medium is going into the amplified signal. The amplified output intensity is limited to the laser output intensity I_o.

At the frequencies where the power of the amplified injected signal becomes equal to the free running output power we may make the following approximation.

$$|g(\omega_1)|^2 I_1 = \frac{\gamma_e^2 I_1}{(\omega_1-\omega_o)^2} \simeq I_o \tag{4.7}$$

The signal at frequency ω_1 will therefore take over from the free running laser output when it lies within the approximate range of frequencies given by

$$|\omega_1 - \omega_o| \simeq \gamma_e \sqrt{\frac{I_1}{I_o}} \tag{4.8}$$

The complete injection locking range $\Delta\omega_{lock}$ for the laser is twice this value i.e.

$$\Delta\omega_{lock} \simeq 2\gamma_e \sqrt{\frac{I_1}{I_o}} \tag{4.9}$$

4.2 Injection Seeding of Pulsed Lasers

An injected signal from a second laser may be used to control the operation of mode locked lasers as well as free running lasers. Moses et. al. [4.3] first proposed injecting a mode locked signal from one laser into another laser in order to mode lock it and they demonstrated such a system using Rhodamine 6G dye lasers. An R6G laser was synchronously pumped by an argon ion laser and gave an output consisting of 15ps pulses. The output of this low power master laser was injected into a flashlamp pumped R6G cavity which generated a train of 20ps pulses with a peak power which was greater than that of the injected pulses by a factor of 3×10^4.

Injection of a mode locked signal has also proved successful as a method of mode locking excimer lasers. The short duration of the laser action - a few tens of nanoseconds - is not sufficient for the pulse shortening processes resulting from intracavity saturable absorbers or modulators to generate picosecond pulses. Reksten et. al. [4.4] injection mode locked an XeCl laser using a frequency

doubled Rhodamine 6G dye laser as the source of injected pulses. Pulses of 7 ps duration were obtained from the XeCl laser in the first demonstration of subnanosecond pulses from a mode locked excimer laser.

In the case of injection mode locking the injected signal consists of many longitudinal modes as does the output of the slave laser. Many modes of the slave laser are therefore locked to modes of the master laser instead of a single mode injected signal giving rise to a signal mode slave laser output. In a laser where the injected signal is too weak or too far from a longitudinal mode frequency to lock the slave laser it is more appropriate to regard the injected signal as setting up initial conditions for the growth of the signal in the slave laser. The signal then grows without being under the control of the injected signal and the situation may be described more accurately as the injection seeding of the slave laser.

A $Ti:Al_2O_3$ laser injection seeded by a pulsed dye laser has been reported by Brockman et. al. [4.5]. A frequency doubled Nd:YAG laser was used to pump both the $Ti:Al_2O_3$ laser and the LDS-750 dye laser which produced an output pulse with a bandwidth of 1.4GHz and a duration of several nanoseconds. The injection seeded $Ti:Al_2O_3$ laser gave an output pulse with the same bandwidth and a duration of approximately 50ns.

4.3 Laser Diode Injection Seeding of the $Ti:Al_2O_3$ Laser

a. Experimental Method

Laser diodes provide a compact and cheap source of laser output in the near infra red and a pulsed output may be obtained from them by modulating the driving current. Single frequency operation is also readily obtained from them as the short laser cavity results in widely separated longitudinal modes so lasing is easily suppressed on modes

other than the one closest to the gain peak.

Injection seeding of the $Ti:Al_2O_3$ laser was investigated using both a pulsed and a free running laser diode output as the source of the injected signal. The Sharp LT016 GaAlAs single frequency laser diode operated at a wavelength of 803nm and was designed to have a maximum allowed output of 40mW. It was modulated using the circuit shown in Figure 4.1.

The diode and transformer were mounted in a die cast box in order to prevent radio frequency pickup on other equipment. The capacitor was used to prevent the RF signal from passing back to the diode driver whose maximum current output of 90mA gave an output from the diode of 20mW. The RF modulation signal was generated using a synthesiser and amplifier and applied to the diode driving current through the transformer.

A schematic diagram of the experimental arrangement for injection seeding is shown in Fig.4.2. The collimated diode beam was passed through an optical isolator to prevent the light from the $Ti:Al_2O_3$ laser and the diode light reflected from the high reflector from entering the diode. Two planar mirrors were used to steer the beam into the $Ti:Al_2O_3$ laser in order to facilitate alignment of the diode beam with the beam in the $Ti:Al_2O_3$ cavity. Alignment was achieved by matching the $Ti:Al_2O_3$ beam passing through the high reflector with the diode beam, both at the isolator and at the high reflector.

Proper alignment was confirmed by the observation of injection seeding effects, initially using an unmodulated diode beam. A beam splitter was placed in the diode beam so that part of the laser diode output could be combined with part of the $Ti:Al_2O_3$ output to enable observation of the combined beams using a CCD camera connected to a monitor. With the $Ti:Al_2O_3$ frequency identical to the diode frequency one would expect to observe interference fringes. Initially, no sign of any interaction between the two lasers was

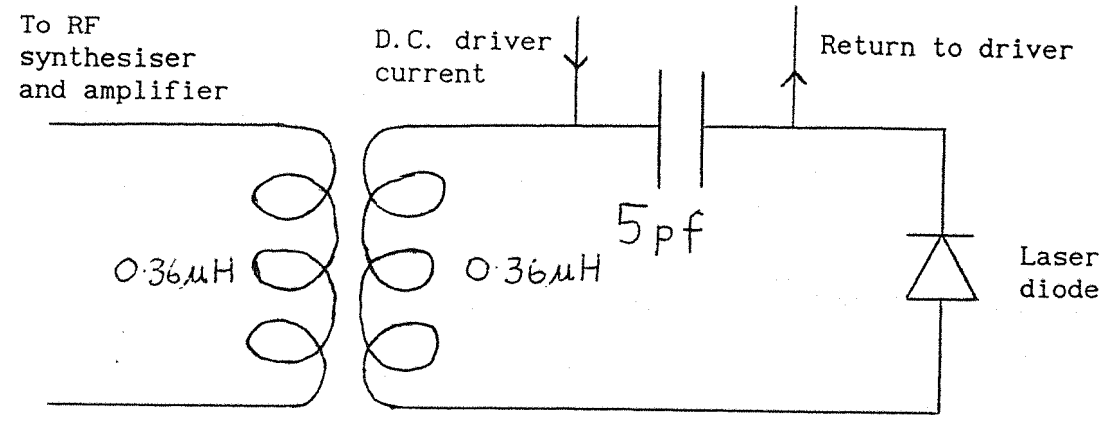

Fig. 4.1 The circuit for modulating the laser diode.

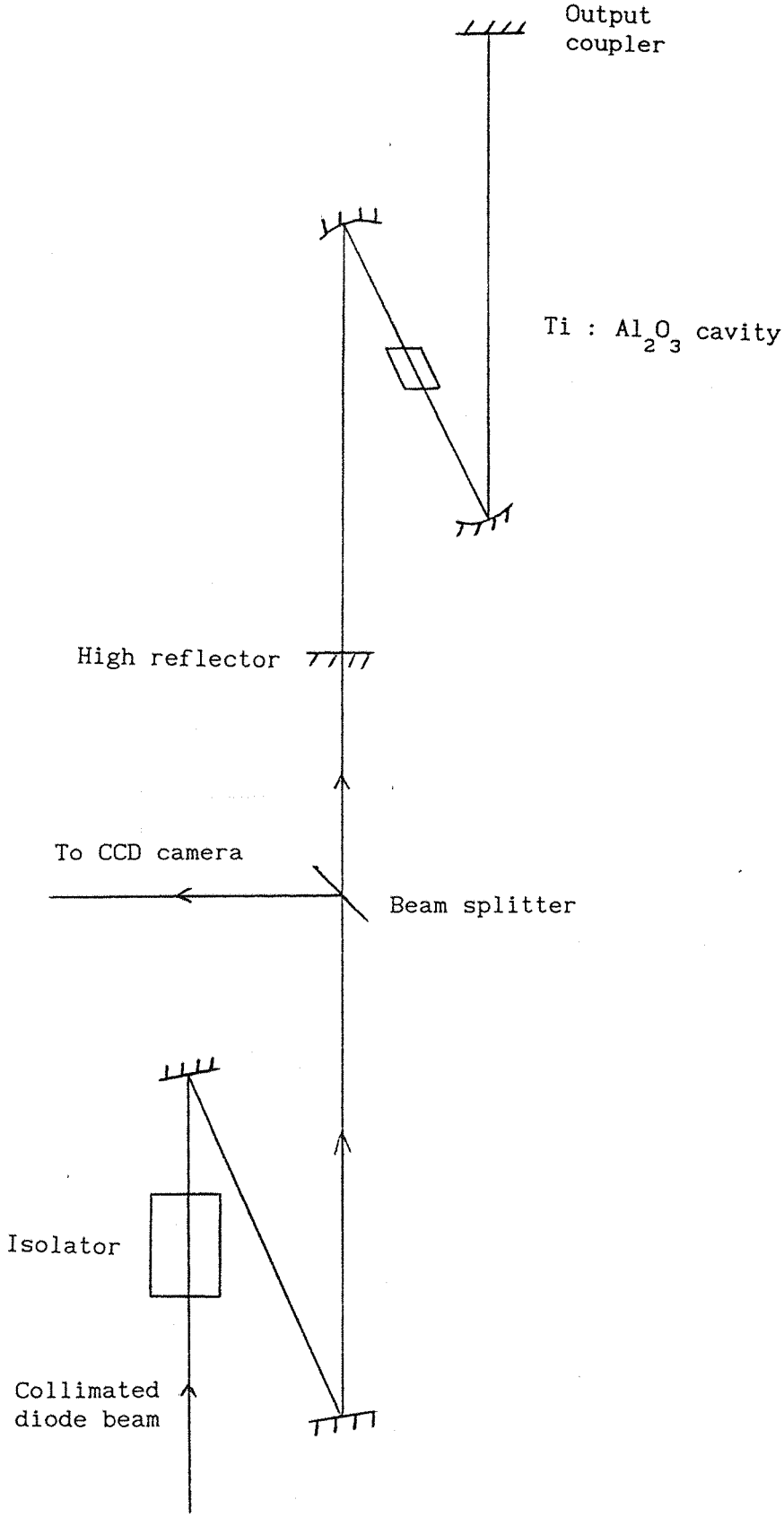

Fig. 4.2 A schematic diagram of the experimental arrangement for injection seeding.

detected so in order to increase the amount of diode power entering the $Ti:Al_2O_3$ laser the high reflector was replaced with another one which had a higher transmission at the diode wavelength. The original high reflector had a transmission of less than 0.1% and the replacement had a transmission of 1.7%.

Injection seeding was obtained and was indicated by unstable, shimmering fringes on the image observed with the CCD camera. It was very sensitive to the alignment of the beams, but was observable over a range of $Ti:Al_2O_3$ wavelengths of several tens of gigahertz, equivalent to scanning the bandwidth of the $Ti:Al_2O_3$ output across the diode frequency.

When a modulation signal was applied to the diode current, resonances were detected in the electrical circuit at intervals of about 45MHz. At these resonances the RF power being drawn from the amplifier reached a maximum. The output from the diode was reduced when the modulation frequency was on resonance.

A resonance at 213MHz, close to the intermode beat frequency of the laser, required 500mW of RF power to give 100% modulation of the diode output. The level of RF power required to give 100% modulation of the output varied with the drive frequency. When the RF power was applied, the diode output fell from its unmodulated value of 16mW to 11mW. The output was examined using a fast photodiode and a Tektronix 7104 oscilloscope and was seen to consist of pulses with a duration of 2.5ns.

3b. Results

Although the optical isolator provided 40dB of isolation, the small amount of $Ti:Al_2O_3$ output which was passing through it was sufficient to influence the behaviour of the laser diode. This transmitted signal, with a power of about 1μW, was sufficient to

determine the output frequency of the diode. With the Ti:Al_2O_3 beam blocked, the diode would lase on a certain longitudinal mode but under the influence of the Ti:Al_2O_3 light it could be made to lase either on this mode or on an adjacent mode. Tuning the Ti:Al_2O_3 output frequency from one mode to the other caused the diode output frequency to follow the Ti:Al_2O_3 frequency. Tuning the Ti:Al_2O_3 laser further from the diode wavelength would not cause the diode wavelength to change unless the isolation was deliberately reduced. Reduced isolation enabled the Ti:Al_2O_3 light to influence the diode over a wider range of frequencies.

The effect of the laser diode on the Ti:Al_2O_3 laser could be seen on the diode array signal which was used to measure the laser's bandwidth. When the Ti:Al_2O_3 output frequency was tuned sufficiently close to the diode frequency it moved to the same frequency as the diode. This occurred when the Ti:Al_2O_3 frequency was tuned to within about 10GHz of the diode frequency.

The injection locking ranges $\Delta\omega_{lock}$ for the two lasers may be calculated using Equation (4.9). For the Ti:Al_2O_3 laser with 3.6% output coupling and a cavity round trip time of 4.8ns the value of γ_e is $7.5 \times 10^6 s^{-1}$. A Ti:Al_2O_3 output of 200mW with 10mW of injected diode signal after allowing for beam splitter and mirror losses gives $\Delta\omega_{lock}$ = 540kHz.

For the laser diode the very short cavity gives a decay rate of $1.6 \times 10^{11} s^{-1}$. 1μW of injected Ti:$Al_2O_3$ power and 20mW of diode output power gives $\Delta\omega_{lock}$ = 370MHz.

The fringes seen on the CCD camera image were only visible when the diode was unmodulated, although the modulated diode output still influenced the Ti:Al_2O_3 laser. The diode signal caused fluctuations in the Ti:Al_2O_3 output with a period in the region of 1kHz, an effect which was observed whether or not the diode was modulated.

When the diode output was modulated it only interacted with the $Ti:Al_2O_3$ laser when the modulation frequency was closely matched to the intermode beat frequency of the laser. If the modulation frequency was detuned by more than 20kHz from the intermode beat frequency of the $Ti:Al_2O_3$ cavity the 1kHz fluctuation on the $Ti:Al_2O_3$ output was no longer seen. A detuning of 30kHz would stop the diode signal from controlling the $Ti:Al_2O_3$ output frequency.

The $Ti:Al_2O_3$ output was monitored using a fast photodiode and was seen to be modulated at the 206MHz round trip frequency of the laser cavity. This modulation had an amplitude which was about 30% of the average output power, and in common with the other injection seeding effects it was not observed when the diode modulation frequency and the $Ti:Al_2O_3$ intermode beat frequency were detuned by more than 30kHz. The $Ti:Al_2O_3$ modulation was not dependent on a modulated diode output and was observed when the diode was unmodulated. Switching off the laser diode often caused the $Ti:Al_2O_3$ laser to give an unmodulated output, but there were also occasions when the $Ti:Al_2O_3$ output was modulated at its intermode beat frequency without any diode signal being present. An oscilloscope trace of the modulated $Ti:Al_2O_3$ output with no diode light entering the laser is shown in Fig. 4.3. The trace was identical when the diode signal was present.

This type of modulated, continuous output has not previously been reported from a $Ti:Al_2O_3$ laser but Spence et al. [4.6] have reported self mode locking. Their laser was a modified version of the Spectra-Physics Model 3900 $Ti:Al_2O_3$ laser used in this work whose cavity length had been approximately doubled. The laser would switch from a free running to a mode locked output either spontaneously or as a result of a perturbation to the cavity or an adjustment to one of the cavity mirrors. Pulses with a duration of 2ps were observed.

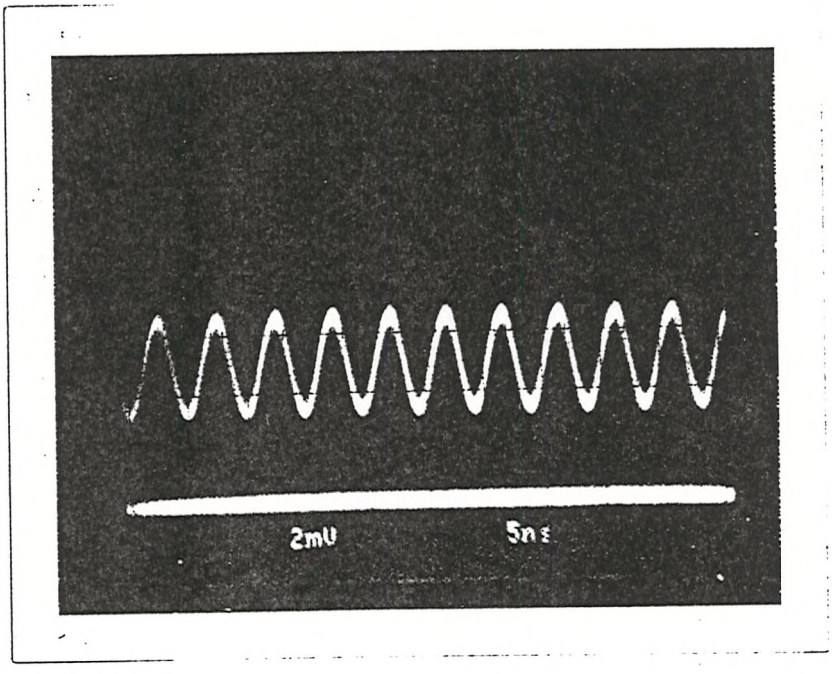

Fig. 4.3 Modulated Ti:Al_2O_3 output with no diode light entering the laser.

These pulses were frequency chirped and when an intracavity prism pair was used to compensate for this, the pulse duration was reduced to 60fs.

A scanning Fabry-Perot interfermeter was employed so that the bandwidth of the lasers could be studied with a greater resolution than was possible with the diode array. Its Free Spectral Range was 7.5GHz and it offered a resolution of 40MHz although the best resolution available from the oscilloscope screen on which the interferometer signal was observed was in the region of 200MHz. The bandwidth of the unmodulated diode was less than this and could therefore not be measured using the interferometer.

When modulated, the spectrum of the diode changed. Instead of consisting of a single narrow peak, it broadened and took on a form similar to that of an FM laser spectrum, i.e. with a peak at each end of the spectrum. The peak at the high frequency end of the diode spectrum was lower than the peak at the low frequency end. The width of the spectrum increased as the RF power used to modulate the diode was increased, until eventually the bandwidth of the diode covered the 7.5GHz Free Spectral Range of the interferometer. By this point the peak at the high frequency end of the diode spectrum had almost disappeared. As the RF power was reduced the height of the high frequency peak rose until it approached that of the low frequency peak.

This effect has been reported previously with modulated laser diodes [4.7]. The modulated current gives a modulated carrier concentration in the active layer of the diode which in turn modulates the refractive index. This modulates the output wavelength, giving rise to the broadened spectrum with a peak at each end.

Without injection seeding, the $Ti:Al_2O_3$ laser oscillated on half a dozen widely separated longitudinal modes over a frequency range of 4 - 7GHz. Injection seeding, both with the diode modulated

and unmodulated, reduced the $Ti:Al_2O_3$ bandwidth to 1GHz with lasing occurring on four or five modes which were now adjacent or next but one to each other. Good isolation of the diode from the $Ti:Al_2O_3$ laser was required for this to be observed as the $Ti:Al_2O_3$ output entering the diode caused it to give some output on the modes adjacent to its main output mode. This diode emission then passed back into the $Ti:Al_2O_3$ laser and caused it to lase at these frequencies as well as at the frequency of the main diode output mode.

The injection seeding behaviour of the titanium sapphire laser was investigated using an injected signal from a laser diode. The laser diode could be modulated to give a pulsed output but injection seeding effects were initially observed using an unmodulated diode signal. With the $Ti:Al_2O_3$ output wavelength matched to the 803nm wavelength of the diode and with the diode and $Ti:Al_2O_3$ beams properly aligned unstable, shimmering fringes were observed on an image formed from the combined beams of the two lasers. When the $Ti:Al_2O_3$ wavelength was tuned to within about 10GHz of the diode output frequency it moved to the same frequency as the diode output.

The current supply to the diode was modulated so that the diode produced a pulsed output with a repetition rate equal to the intermode beat frequency of the $Ti:Al_2O_3$ laser. The pulsed diode signal only influenced the $Ti:Al_2O_3$ laser when the modulation frequency applied to the diode current was within a few tens of KHz of the intermode beat frequency.

The injected diode signal, whether modulated or unmodulated, caused the $Ti:Al_2O_3$ laser to give an output which was modulated at its intermode beat frequency, an effect which was also observed sometimes with no injected signal present.

Under the influence of the diode signal the bandwidth of the $Ti:Al_2O_3$ output narrowed from 4-7GHz to 1GHz with lasing occurring on four or five longitudinal modes which were adjacent or next but one to each other. This could only be observed if the isolation of the diode from the $Ti:Al_2O_3$ laser was optimised since even very small amounts of

$Ti:Al_2O_3$ light entering the diode caused it to give a multimode output which would then cause the $Ti:Al_2O_3$ laser to lase at these other wavelenghts. In any future attempt to injection seed a $Ti:Al_2O_3$ laser using a laser diode it will therefore be essential to maximise the isolation of the diode from the $Ti:Al_2O_3$ laser. This may be done either by using optical isolators or by using a unidirectional ring cavity so that no light from the $Ti:Al_2O_3$ laser is directed back towards the diode.

4.4 References

4.1. H.L. Stover and W.H. Steier, Appl. Phys. Lett. 8 p.91 (1966).

4.2. A.E. Siegman, Lasers, University Science Books, Mill Valley, California (1980).

4.3. E.I. Moses, J.J. Turner and C.L. Tang, Appl. Phys. Lett. 28 p.258 (1976)

4.4. G. Reksten, T. Varghese and D.J. Bradley, Appl. Phys. Lett. 38 p. 513 (1981)

4.5. P. Brockman, C.H. Bair, J.C. Barnes, R.V. Hess and E.V. Browell, Opt Lett. 11. p. 712 (1986)

4.6. D.E. Spence, P.N. Kean and W. Sibbett, Opt. Lett. 16 p. 42 (1991).

4.7. B.W. Hakki, J. Appl. Phys. 51 p. 68 (1980).

CHAPTER 5

MEASUREMENT OF DOPANT CONCENTRATION IN FIBRES

5.1. Introduction

There is currently much interest in the incorporation of rare earth metal ions into the cores of glass fibres to form laser devices [5.1]. Such lasers have several useful properties. They are end pumped using another laser and the small diameter of the core, typically less than ten micrometres, leads to a high intensity when the pump beam is focused into the core. This in turn leads to a low threshold for laser action and a neodymium doped fibre has been observed to show laser action with a threshold of only 100μW absorbed pump power [5.2]. High slope efficiencies are also observed with many fibre lasers and a neodymium fibre laser has been demonstrated with a slope efficiency of 55% [5.3]. Long interaction lengths are available in a fibre which allows the use of weak absorptions not available in bulk glass devices.

Fibre lasers give a wide range of output wavelengths extending from 455nm in a thulium doped fluorozirconate upconversion laser [5.4] to 2.7μm in an erbium doped fluorozirconate glass fibre [5.5]. Laser action has been demonstrated from an erbium doped fibre at 1.55μm, the so-called "third window" for telecommunications [5.6]. This wavelength is of interest as the absorption of silica reaches a minimum around 1.5μm.

The amorphous structure of glass causes the transitions of the ions to show large linewidths which offers the possibility of tunable operation. Tunable operation has been obtained over a range of 80nm for the 1.08μm transition in a neodymium fibre and over a range of

25nm for an erbium fibre operating around the third telecommunications window [5.7].

The small size of the fibre eliminates the thermal effects which can be a problem with bulk glass lasers and the low threshold allows diode pumping for dopants which have a suitable absorption wavelength. Diode pumping has been demonstrated for neodymium [5.8], erbium [5.6], thulium [5.9], ytterbium [5.10] and ytterbium sensitised erbium [5.11].

Rare earth doped fibre amplifiers have been fabricated which exhibit gains of up to 20dB around 1.55μm [5.12], [5.13]. Doped fibre devices are thus particularly interesting for optical communications purposes since systems with an all-fibre geometry may be developed.

Doped fibres are fabricated mainly by variations of the Modified Chemical Vapour Deposition (MCVD) method [5.14] and by solution doping [5.15]. A problem arises in that the concentration of the dopant ions in the core is not accurately known. It cannot be controlled precisely and may vary by thirty per cent or more from the given concentration figure [5.14]. In order to characterise fibre devices, one wishes to know the concentration more precisely and the purpose of this work was to investigate the usefulness of a method for assessing the concentration.

5.2. Absorption Coefficient Measurements

a. Experimental Method

The method of quantifying the dopant concentration involves the use of the side fluorescence from the fibre. A length of the fibre to be tested is end pumped using a laser of appropriate wavelength to raise some of the dopant ions into an excited state. There is no feedback in the fibre except for that due to the Fresnel

reflections from the ends of the fibre so there is no stimulated emission and the ions decay back to the ground state by spontaneous emission. Most of this fluorescence exits from the side of the fibre, although some will be confined to the core and emitted as end fluorescence.

The dopant concentration is assumed to be constant along the fibre and consequently, for any unit length of the fibre, a fixed proportion of the pump power incident on that unit length will be absorbed by the ions within it. The side fluorescence observed from any point in the fibre is directly proportional to the amount of pump light absorbed in the core at that point. It follows from this that an exponential decay in the side fluorescence intensity should be observed with distance from the point at which the pump beam is launched into the fibre.

The pump power in the core is given by the following expression:-

$$P = P_o e^{-\alpha l} \qquad (5.1)$$

Where P is the power at a distance l beyond the point at which the power is P_o. The constant α is known as the absorption coefficient and has to be found in order to calculate the dopant concentration.

In order to measure the decay of the fluorescence signal strength with distance along the fibre, a piece of apparatus was built which would allow a length of approximately 40cm of fibre to be held perfectly straight. A diagram of the apparatus is given in Fig. 5.1. At one end of it was a micropositioner with a microscope objective on it which could be adjusted to obtain the optimum launch of the pump beam into the fibre core. Running parallel to the fibre was a sliding platform which could be driven along the length of the fibre by a stepper motor driven screw thread. The platform made a suitable base

Fig. 5.1 A schematic diagram of the apparatus used to record the sidelight intensity from the fibre.

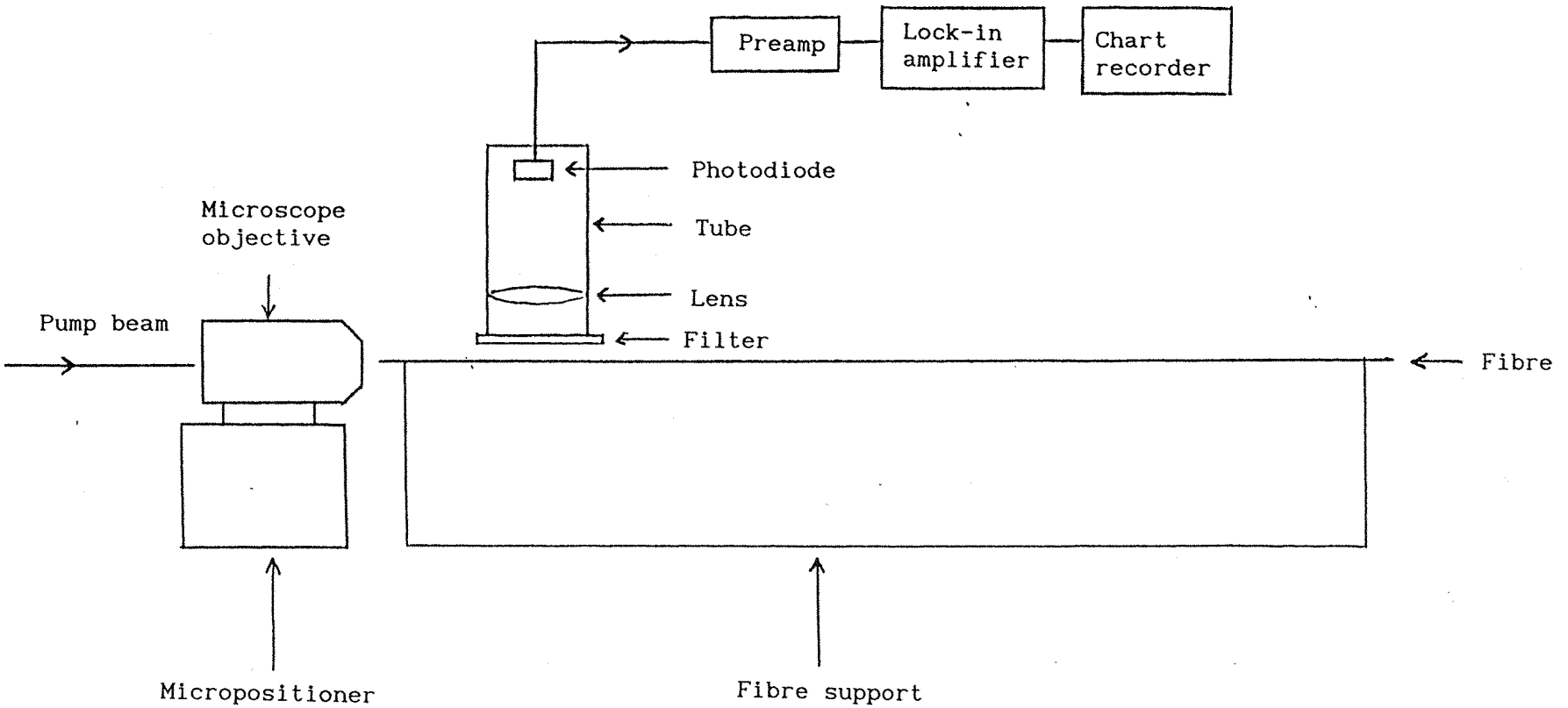

The lens and the photodiode are enclosed in a tube to exclude background light.

for fixing a detector which was clamped in position directly above the fibre.

The sliding platform unit was carefully positioned so that the detector would remain directly above the fibre all along its length as the stepper motor moved it along, and thus detect the maximum available signal strength at each point along the fibre's length. The detector consisted of a convex lens positioned several centimetres above the fibre which focused the light from it onto a photodiode appropriate for the fluorescence wavelength being emitted from the fibre under examination. Following suitable preamplification, the electrical signal from the photodiode was fed into a lock-in amplifier which displayed both a digital and a needle meter read-out indicating the relative strength of the signal being detected from the fibre. A filter of appropriate cut-off wavelength positioned below the convex lens ensured that only fluorescence from the fibre was detected by blocking out stray pump light from the fibre.

An electrical output from the lock-in amplifier was fed into a chart recorder so that a recording could be made on paper showing the variation of signal intensity with distance along the fibre. Starting with the detector close to the end of the fibre where the pump beam was launched into it, the stepper motor was used to move the detector slowly along the length of the fibre while the chart recorder made a recording of the varying signal strength.

The ends of the fibre were cleaved to obtain a good launch into the core and to enable observation of the profile of the beam of end light exiting from the far end of the fibre, which is of assistance when attempting to launch into the fibre.

b. Results

Initial work was carried out on neodymium doped fibres, using a pump wavelength of 514.4nm from an argon ion laser. Pumping at this wavelength causes excitation from the $^4I_{9/2}$ ground state to the $^4G_{9/2}$ level, with fluorescence being emitted at 1.08μm by a transition from the $^4F_{3/2}$ level to the $^4I_{11/2}$ level (Fig. 5.2).

The predicted exponential decay in the fluorescence strength along the length of the fibre was not observed. Instead, a series of peaks and troughs were observed in the signal giving variations amounting to as much as twenty or thirty per cent of the overall signal strength.

These variations are believed to be due to cladding modes - pump light which is propagating in the cladding of the fibre instead of in the core. This light will sometimes pass across the core, giving an increase in the pump intensity in the core at that point which causes a peak in the fluorescence intensity. Various attempts were made to minimise this effect. Index matching fluid was applied to the fibre near the launch end to remove light from the cladding and long fibres were employed where the pump light was made to propagate through as much as two metres of fibre before reaching the section which the detector was monitoring. It was hoped that in propagating through two metres of fibre which had its outer protective plastic coating still in place, most of the cladding light would be removed. The refractive index of the plastic is matched to that of the cladding glass so light which is incident on the boundary will tend to pass out of the cladding.

These attempts were unsuccessful as the peaks remained in the signal. Lengths of fibre with the plastic removed were bent and immersed in index matching fluid to encourage the removal of light from the cladding and sharp kinks were placed in the fibre to improve the coupling of cladding light into the plastic. The fluctuations in

Fig.5.2 Energy level diagram for Nd^{3+}.

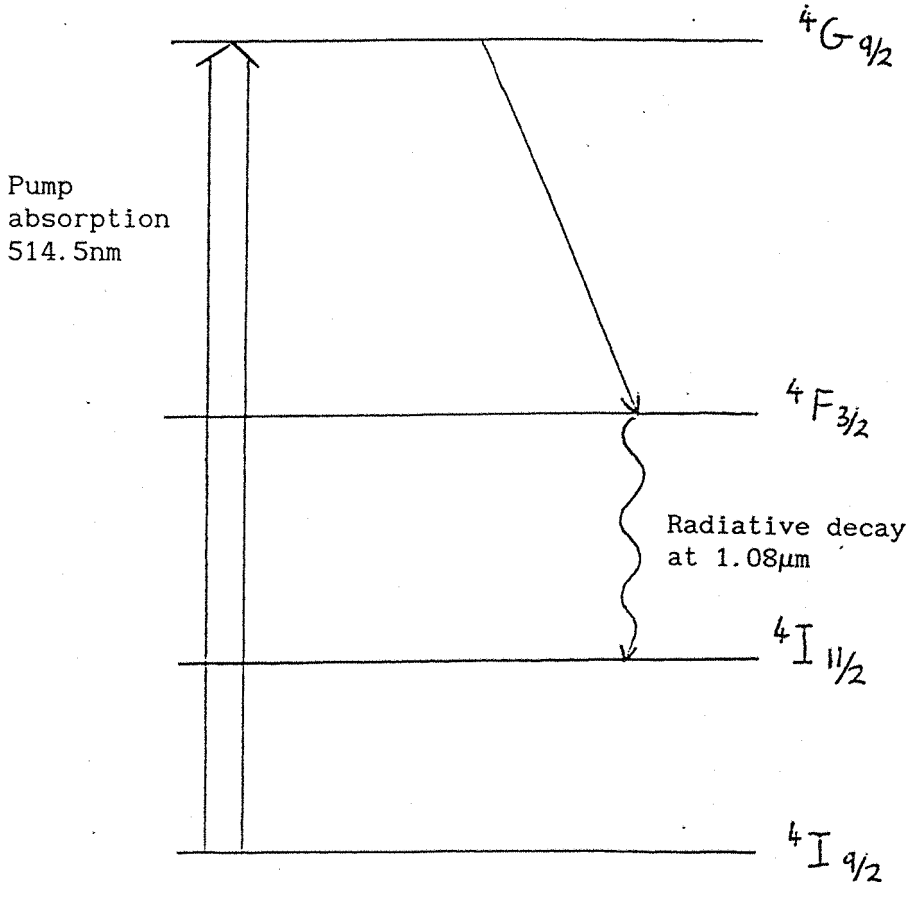

the signal remained in excess of ten per cent of the signal strength.

Different microscope objectives were used to launch the pump beam into the fibre, but this did not produce any improvement. Finally, a larger core neodymium fibre was used to reduce the proportion of the pump light launched into the cladding. An improvement was observed: the fluctuations were generally less than five per cent of the signal strength, but could not always be kept so small. It was desired to reduce them to no more than one per cent of the total signal strength in order to obtain data for calculating the absorption coefficient.

The next stage of the work involved thulium doped fibres, initially using a pump wavelength of 803nm from a Styryl 9 dye laser. This wavelength causes excitation of the thulium ion from the $^3H_6$ ground state to the $^3F_4$ level. Fluorescence is observed in a broad band between 1.7μm and 2.2μm due to a decay from the $^3H_4$ level back to the ground state (Fig.5.3a).

Initially, a fibre with a core radius of 4.5μm was used. This was about twice the radius of the larger of the two neodymium fibres used previously; it was hoped that the larger core would minimise the amount of pump light launched into the fibre cladding. The behaviour of the undesirable fluctuations in the signal strength was investigated in detail. They were still present and were more severe than those seen with larger core neodymium fibre.

The variation of the fluorescence signal was studied by launching into a fibre under varying conditions and recording the fluorescence signals parallel to each other so that direct comparisons could be made between them as the experimental conditions were varied. The signal was analysed both with and without index matching fluid and after variations in the launch conditions.

Fig.5.3 Energy level diagrams for Tm^{3+}.

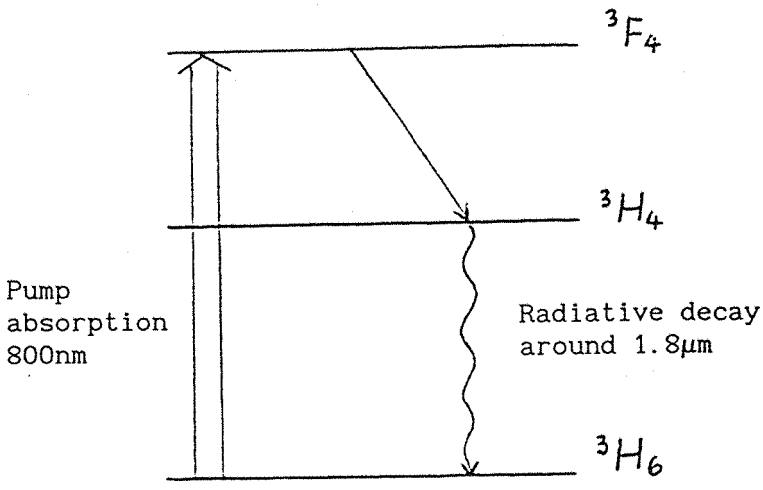

a) Under dye laser pumping

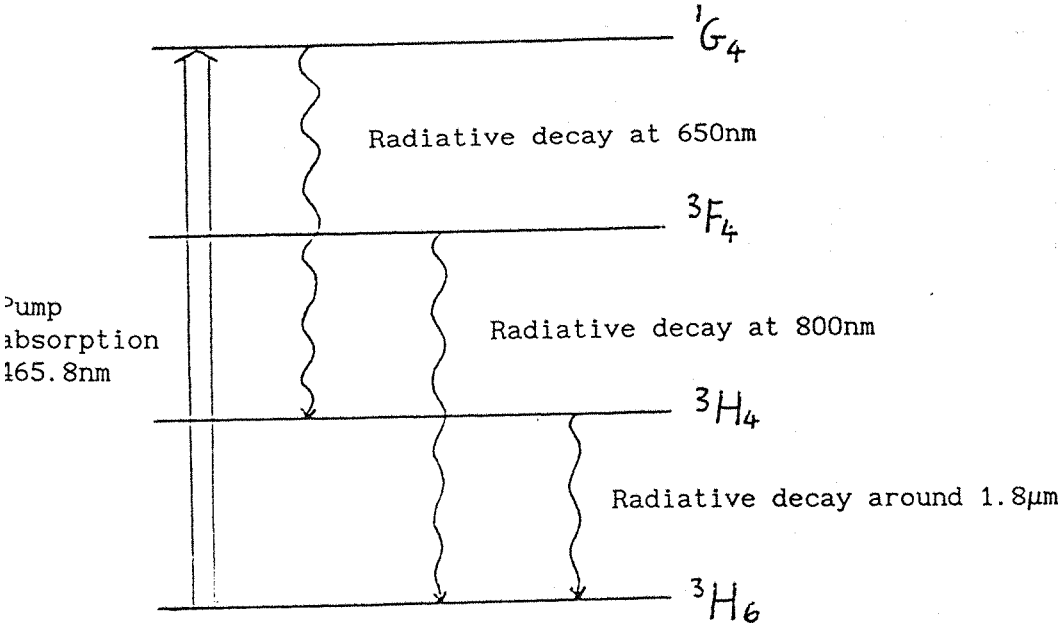

b) Under argon ion laser pumping

Signal fluctuations were found to reproducible; changes in the launch and the use of index matching fluid did not produce a different fluorescence signal. An example of the signals obtained is given in Fig. 5.4.

Fig. 5.4 consists of three recordings made along a 20cm length of thulium doped fibre. The large dips which occur at regular intervals are due to strips of card placed across the fibre. These serve as reference markers when comparing the different recordings.

Line 3 was recorded with the launch optimised to give maximum signal strength. After this, the micropositioner was adjusted so that the launch was completely lost and then re-optimised. The purpose of this was to investigate the effect of such a change in the launch on the sidelight signal obtained. Line 4 was recorded after this change and is identical to Line 3; altering the launch did not affect the signal obtained.

Lines 3 and 4 were both recorded with an optimised launch, so for comparison Line 5 was recorded with a non-optimised launch. The micropositioner was adjusted so that the signal strength was about half of that observed in Lines 3 and 4. Line 5 is the same as Lines 3 and 4 except that its overall magnitude and the magnitude of the fluctuations on it have been reduced.

The lines in Fig. 5.4 do not indicate an exponential decay in signal strength along the fibre and it has proved impossible to eliminate the fluctuations from the signal. These difficulties make the method inadequate for calculating the absorption coefficient. It is believed that light from the core gives rise to so-called "whispering gallery" modes [5.16] which propagate in the fibre cladding.

Fig.5.4 Sidelight fluorescence measurements along a 20cm length of Tm^{3+} doped fibre under varying launch conditions.

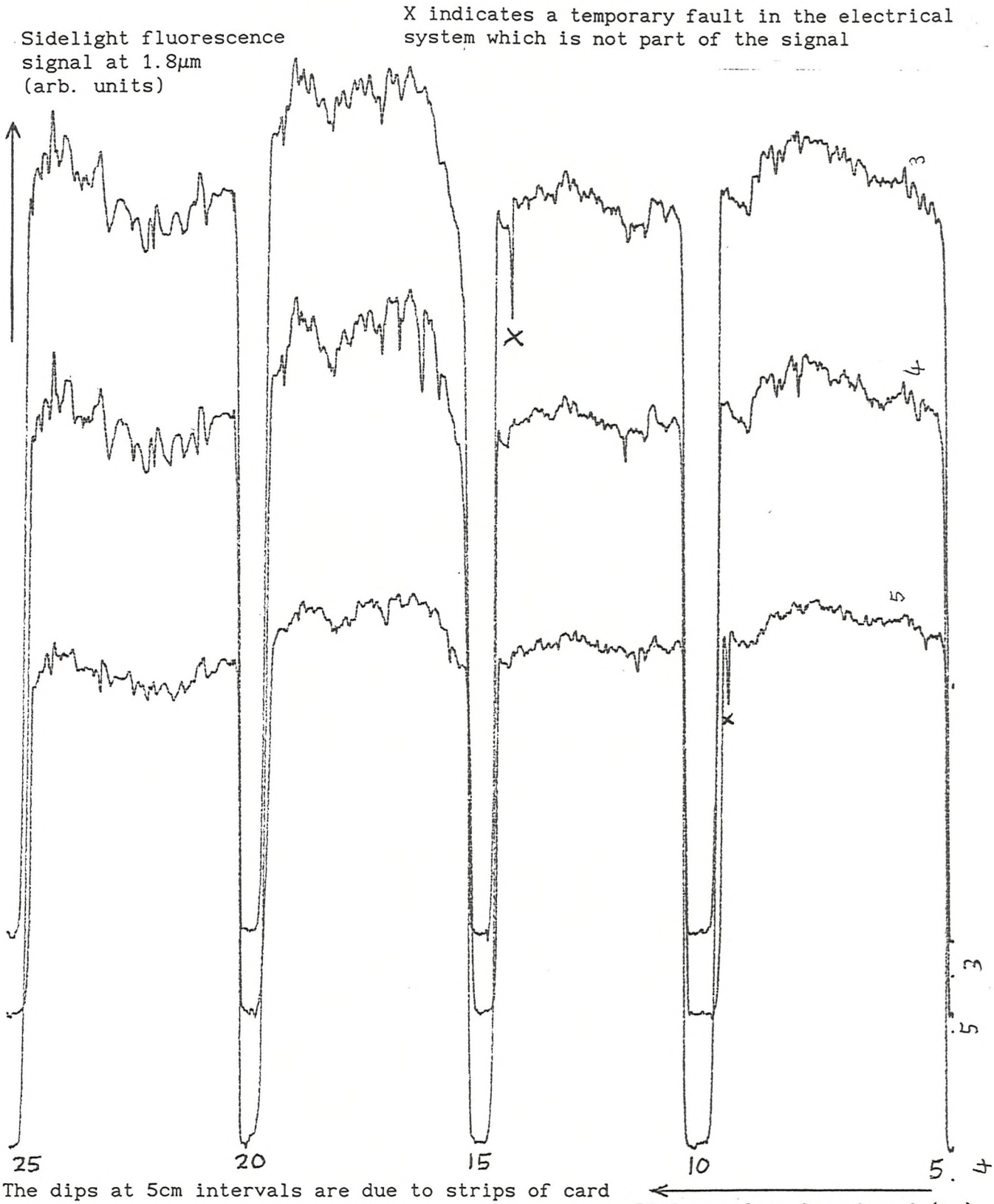

The dips at 5cm intervals are due to strips of card placed across the fibre as reference markers.

Line 3. A fluorescence measurement with the launch optimised.

Line 4. A fluorescence measurement made soon after Line 3 with the launch lost and then re-optimised.

Line 5. A measurement with a non-optimised launch.

5.3 Saturation Measurements

a. Theory and Experimental Method

Determination of the absorption coefficient, α, is not sufficient to calculate the dopant concentration in the fibre. It is also necessary to calculate the absorption cross-section of the dopant ions at the pump wavelength; the dopant concentration expressed in ions per cubic metre is given by the ratio of α to the cross section σ.

A possible method for the calculation of σ is to study saturation of the fluorescence by ground state depletion. As the pump power in the fibre is increased, the ground state of the dopant ions becomes depleted as more of the ions are in the excited state. At very high pump powers, the ions are mostly in the excited state and further increases in pump power have little effect on the number of ions in the upper level. The fluorescence intensity no longer increases with increasing pump power and the extra pump power propagates along the core without being absorbed. This is saturation and the number of ions N in the upper metastable state, which is proportional to the fluorescence signal is given by Equation (5.2).

$$N = \frac{N_o I/I_{sat}}{1+I/I_{sat}} \qquad (5.2)$$

Where N_o is the total number of ions in the fibre, I is the intensity of the pump light in the core expressed in watts per square metre and I_{sat} is the saturation intensity. I_{sat} is the pump intensity required to maintain 50% of the ions in the excited state and is the intensity at which photons pass through an area equivalent to the absorption cross section of an ion at an average rate of one photon per fluorescence lifetime. I_{sat} can be used to calculate the absorption cross section σ using Equation (5.3).

$$I_{sat} = \frac{h\nu}{\sigma\tau} \qquad (5.3)$$

where h is Planck's constant, ν is the frequency of the pump radiation and τ is the fluorescence lifetime. The value of τ has been measured to be 200 μs [5.17].

The saturation characteristics of the fluorescence were investigated by increasing the pump power launched into the fibre, while recording the fluorescence signal strength at a fixed point on the fibre and also measuring the pump power leaving the end of the fibre. By plotting the fluorescence signal strength against the pump power, a value for the saturation power in the core may be estimated and hence the saturation intensity, knowing the dimensions of the core. The dopant concentration may then be found from the ratio of α to σ.

Most of this work was undertaken using thulium doped fibres with the laser output maximised and an attenuator used to vary the power launched into the fibre. This arrangement eliminated the problems which would occur if the laser's output power were varied. The direction of the beam from an argon ion laser is liable to change slightly when the output power is varied and this would alter the launch conditions and give false results. The data obtained was processed on a computer in order to obtain accurate values for the saturation power.

To enable calculations of the dopant concentration to be made, the absorption coefficient for each fibre was found by employing the "cut back" technique. The pump power from the end of the fibre is measured and the fibre is repeatedly shortened by cutting pieces off the end. The power from the end rises exponentially as the fibre is shortened, allowing an estimate for the absorption coefficient to be made. It can be seen from Equation (5.1) that plotting $\ln P$ where

P is the power detected at the end of the fibre against the fibre length l gives a line of gradient - α.

In order to obtain reliable results from the saturation measurements it was necessary to have a detector whose response was linear over the range of signal strengths which it was detecting. The detector response was tested by passing light through two pieces of polaroid glass onto the photodiode. One piece was rotated relative to the other and the photodiode response was compared with the transmission expected as the polaroid was rotated. The photodiode response was found to be linear.

The values obtained for the dopant concentrations were much lower than expected and this effect was investigated in detail. Fibres having widely varying dopant concentrations and different core sizes were studied and pump wavelengths of 803nm from the Styryl 9 dye laser and 465.8nm from an argon ion laser were used. Pumping at 465.8nm causes excitation from the $^3H_6$ ground state to the $^1G_4$ level, with fluorescence emitted at three different wavelengths. Most of the fluorescence is observed at 650nm and 1.8μm (Fig. 5.3b).

The values of α, I_{sat}, and dopant concentration obtained for the thulium doped fibres are given in Table 1. The values of I_{sat} were obtained from Graphs 1 - 8 in which the fluorescence signal from the fibre is plotted against the pump power exiting from the end of the fibre. The number of the graph corresponding to each I_{sat} value is indicated after the calculated thulium concentration in the table.

b. Results and Discussion

Table 1 gives the value of α for each fibre obtained from the cut back and the value of I_{sat} obtained from the saturation measurement. The value of the absorption cross section σ implied by the value of I_{sat} is also given followed by the thulium ion concentration $[Tm^{3+}]$ implied by the values of α and σ. The Fibre Specification column gives the fabricator's figure for the dopant concentration in parts per million and also the radius of the fibre core.

Table 1

Fibre Specification	Pump Wavelength 803nm	Pump Wavelength 465.8nm
300ppm Core radius 4.5μm	$\alpha = 0.83\pm0.02 m^{-1}$ $I_{sat} = (2.6\pm0.1)\times10^{8} Wm^{-2}$ $\sigma = (4.7\pm0.2)\times10^{-24} m^{2}$ $[Tm^{3+}] = 8.8\pm0.3$ppm (1)	$\alpha = 2.86\pm0.13 m^{-1}$ $I_{sat} = (1.52\pm0.06)\times10^{8} Wm^{-2}$ $\sigma = (1.36\pm0.05)\times10^{-23} m^{2}$ $[Tm^{3+}] = 9.7\pm0.6$ppm (2)
57ppm Core radius 2.9μm	$\alpha = 0.265\pm0.003 m^{-1}$ $I_{sat} = (3.7\pm0.1)\times10^{8} Wm^{-2}$ $\sigma = (3.2\pm0.1)\times10^{-24} m^{2}$ $[Tm^{3+}] = 3.6\pm0.1$ppm (3)	$\alpha = 0.68\pm0.15 m^{-1}$ $I_{sat} = (2.65\pm0.13)\times10^{8} Wm^{-2}$ $\sigma = (8.0\pm0.4)\times10^{-24} m^{2}$ $[Tm^{3+}] = 3.9\pm0.9$ppm (4)
1700ppm Core radius 2.3μm	$\alpha = 115\pm0.3 m^{-1}$ $I_{sat} = (8.5\pm0.2)\times10^{8} Wm^{-2}$ $\sigma = (1.40\pm0.04)\times10^{-24} m^{2}$ $[Tm^{3+}] = 380\pm14$ppm (7)	$\alpha = 7.4\pm0.2 m^{-1}$ $I_{sat} = (2.2\pm0.4)\times10^{9} Wm^{-2}$ $\sigma = (9.4\pm1.8)\times10^{-25} m^{2}$ $[Tm^{3+}] = 370\pm72$ppm (8)

GRAPH 1

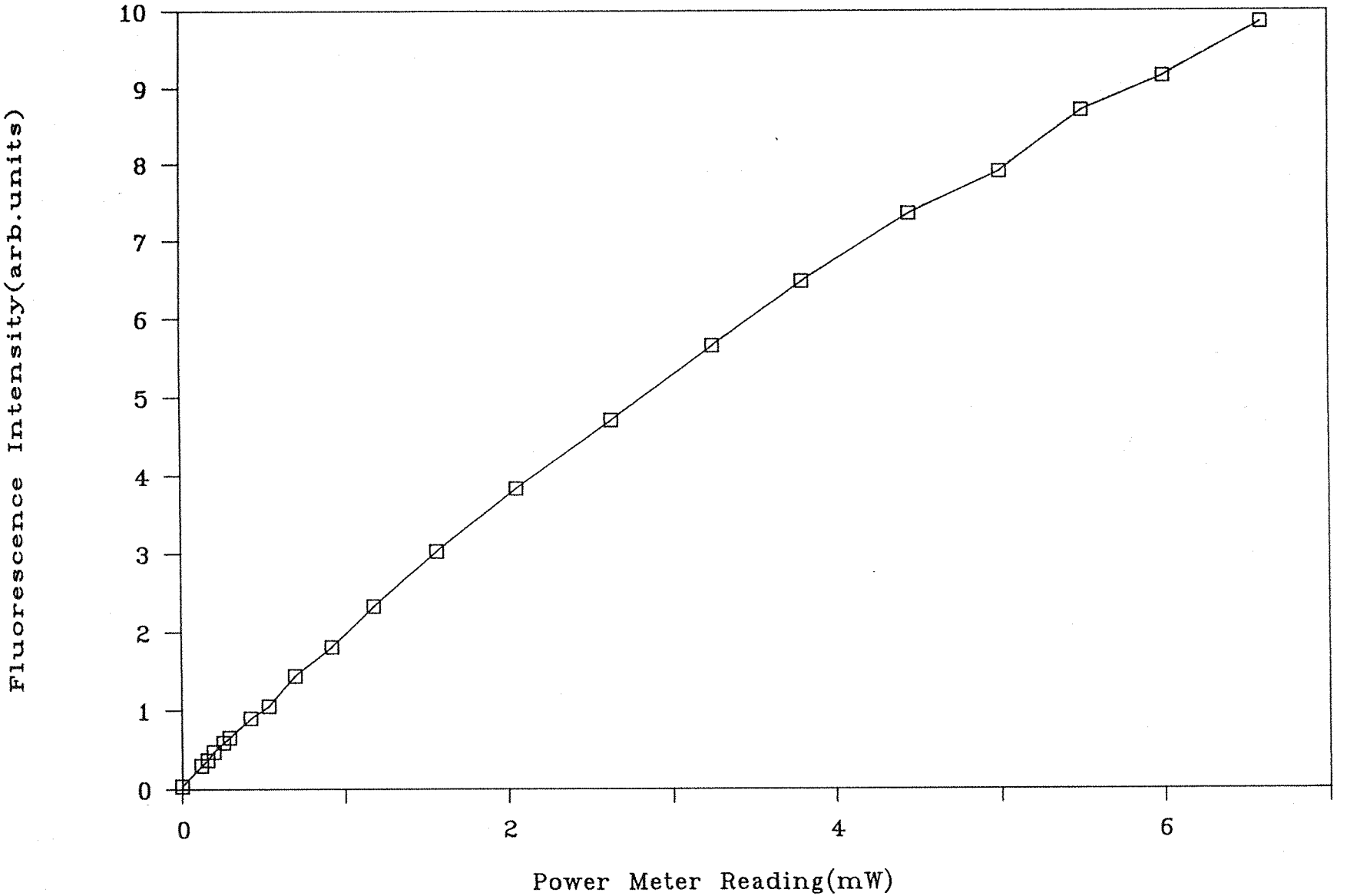
Fluorescence Intensity(arb.units)
10
9
8
7
6
5
4
3
2
1
0
0
2
4
6
Power Meter Reading(mW)

GRAPH 2

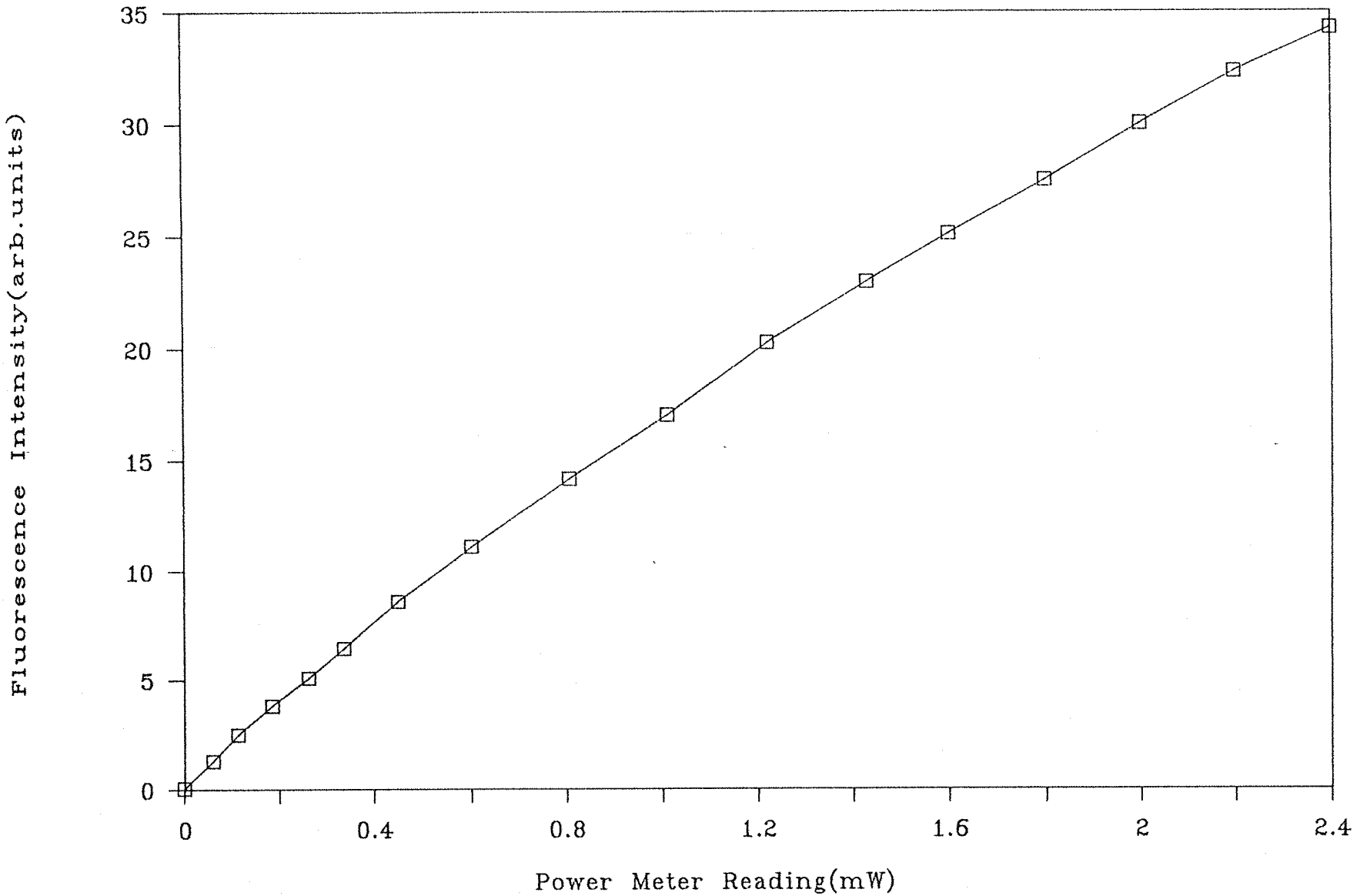
Fluorescence Intensity(arb.units)
35
30
25
20
15
10
5
0
0
0.4
0.8
1.2
1.6
2
2.4
Power Meter Reading(mW)

GRAPH 3

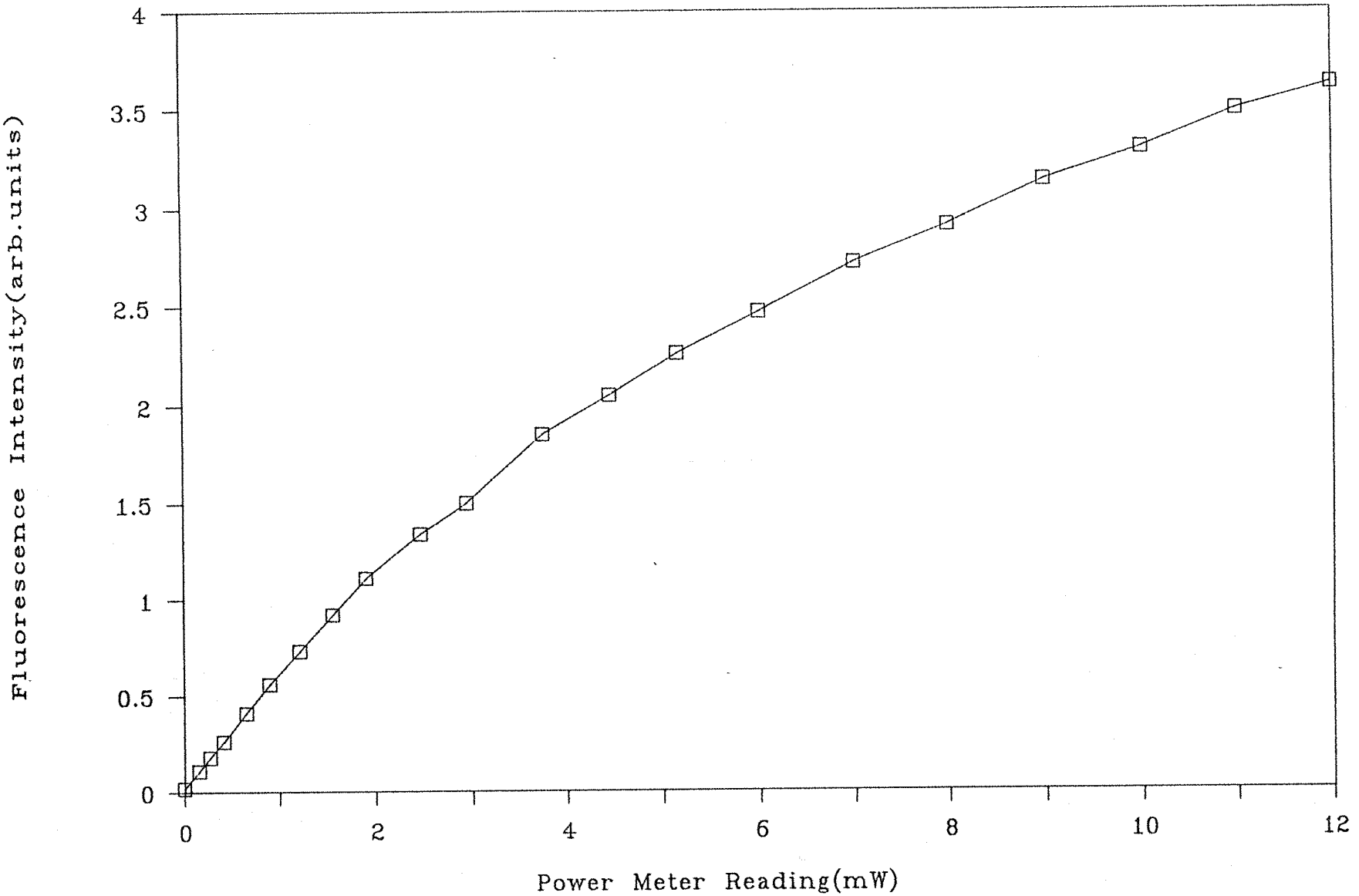
Fluorescence Intensity(arb.units)
4
3.5
3
2.5
2
1.5
1
0.5
0
0
2
4
6
8
10
12
Power Meter Reading(mW)

GRAPH 4

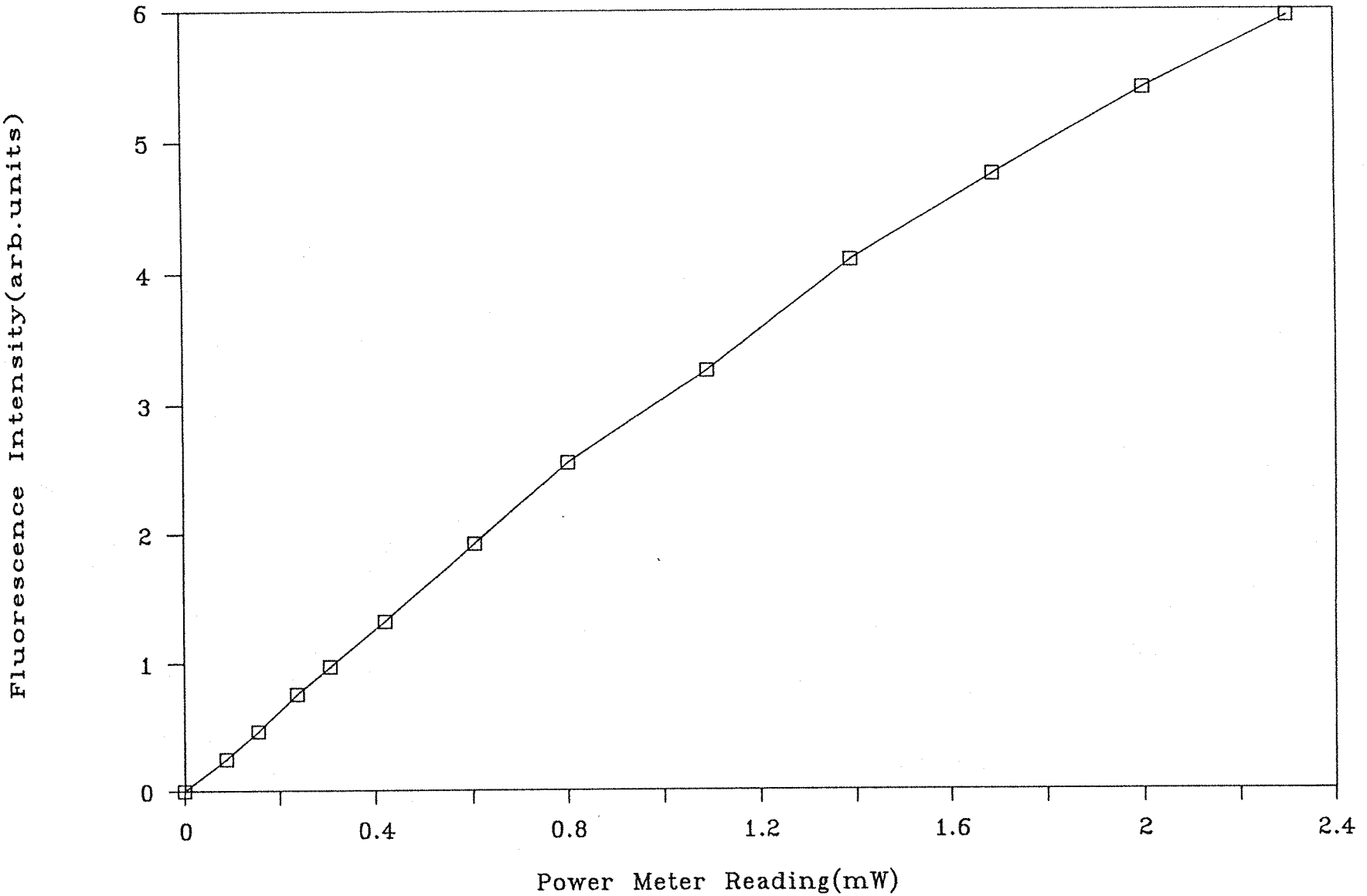
Fluorescence Intensity(arb.units)
0
1
2
3
4
5
6
0
0.4
0.8
1.2
1.6
2
2.4
Power Meter Reading(mW)

GRAPH 7

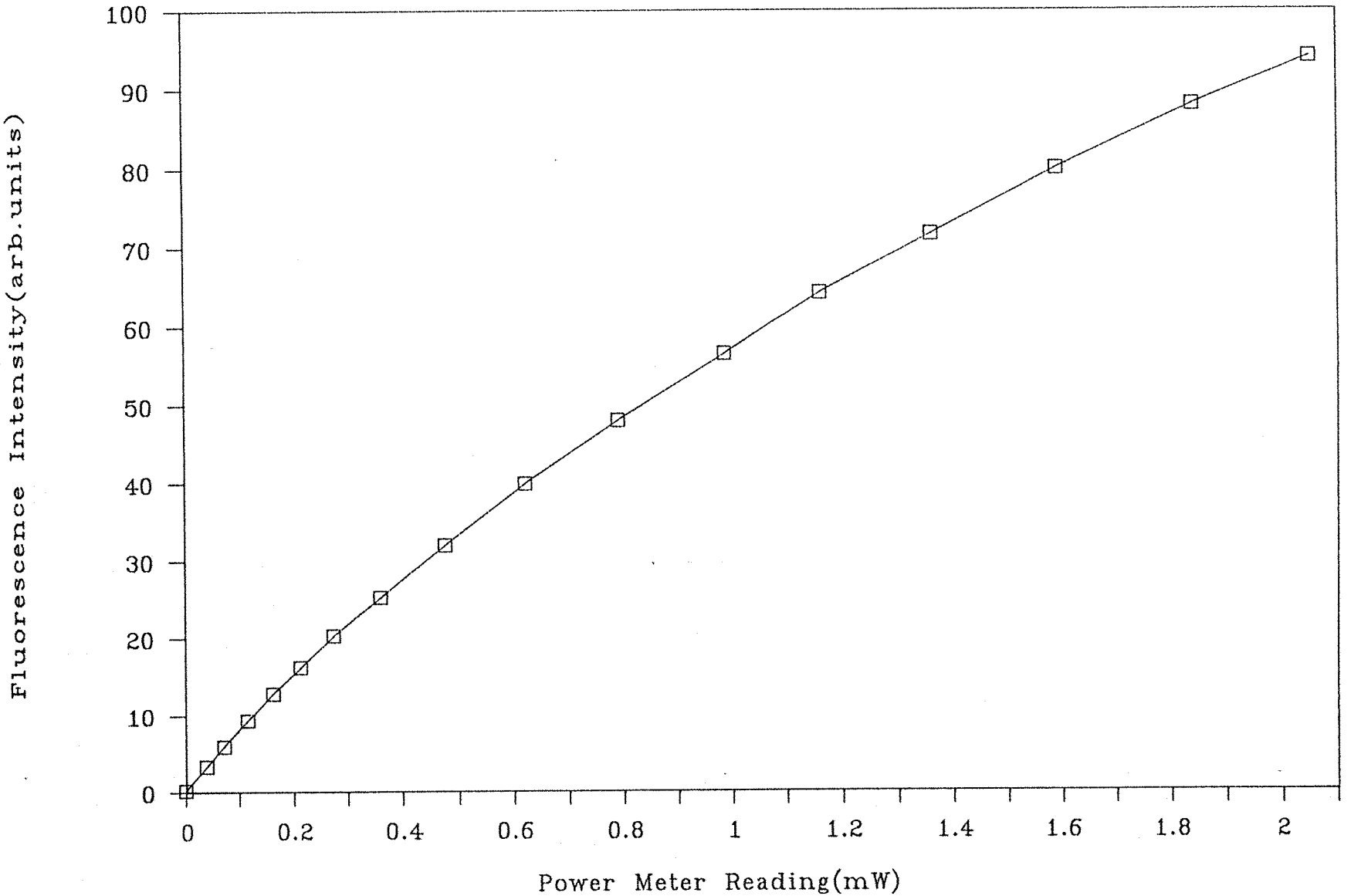
Fluorescence Intensity(arb.units)
100
90
80
70
60
50
40
30
20
10
0
0
0.2
0.4
0.6
0.8
1
1.2
1.4
1.6
1.8
2
Power Meter Reading(mW)

GRAPH 8

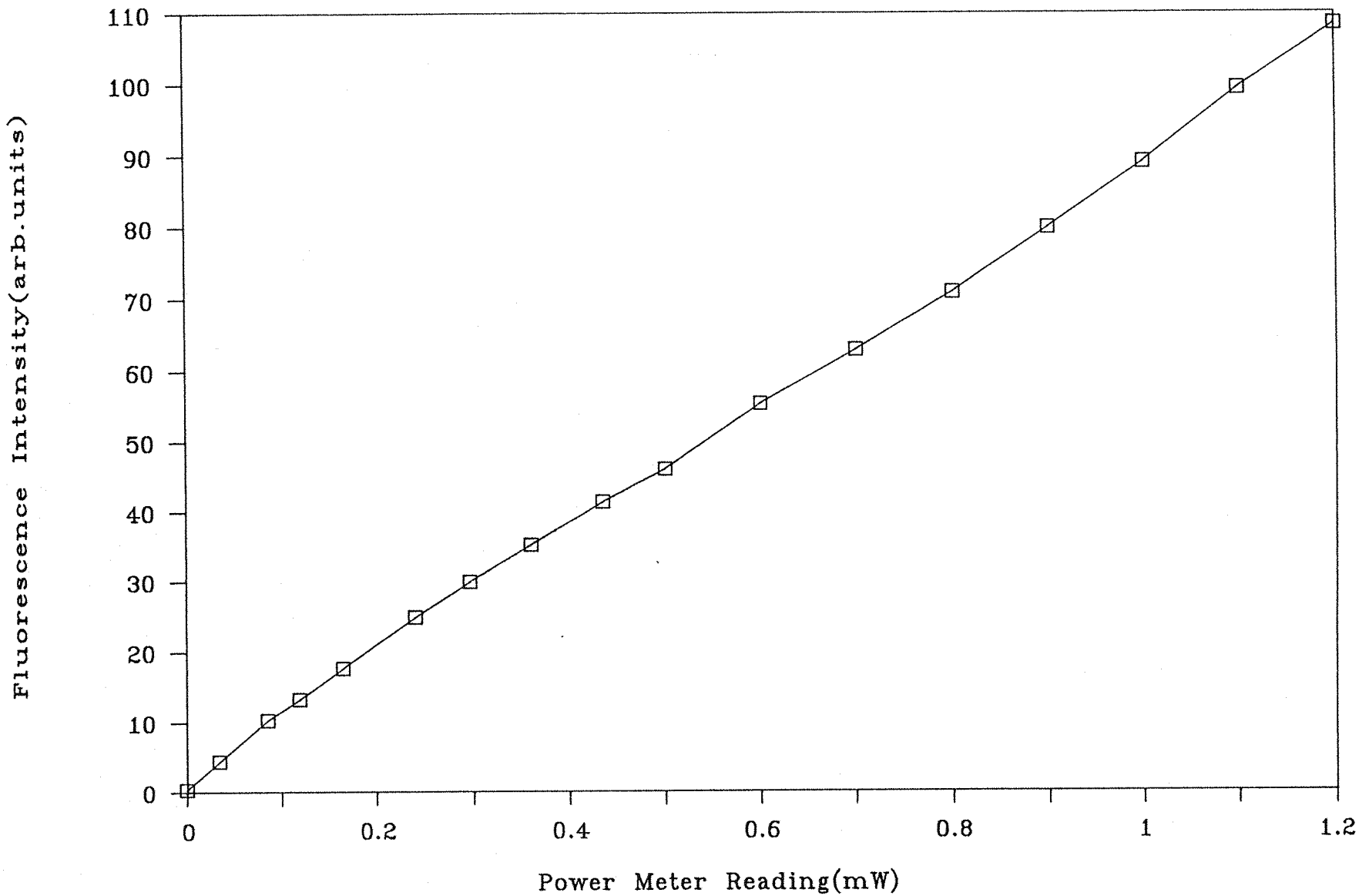
Fluorescence Intensity(arb.units)
110
100
90
80
70
60
50
40
30
20
10
0
0
0.2
0.4
0.6
0.8
1
1.2
Power Meter Reading(mW)

GRAPH 9

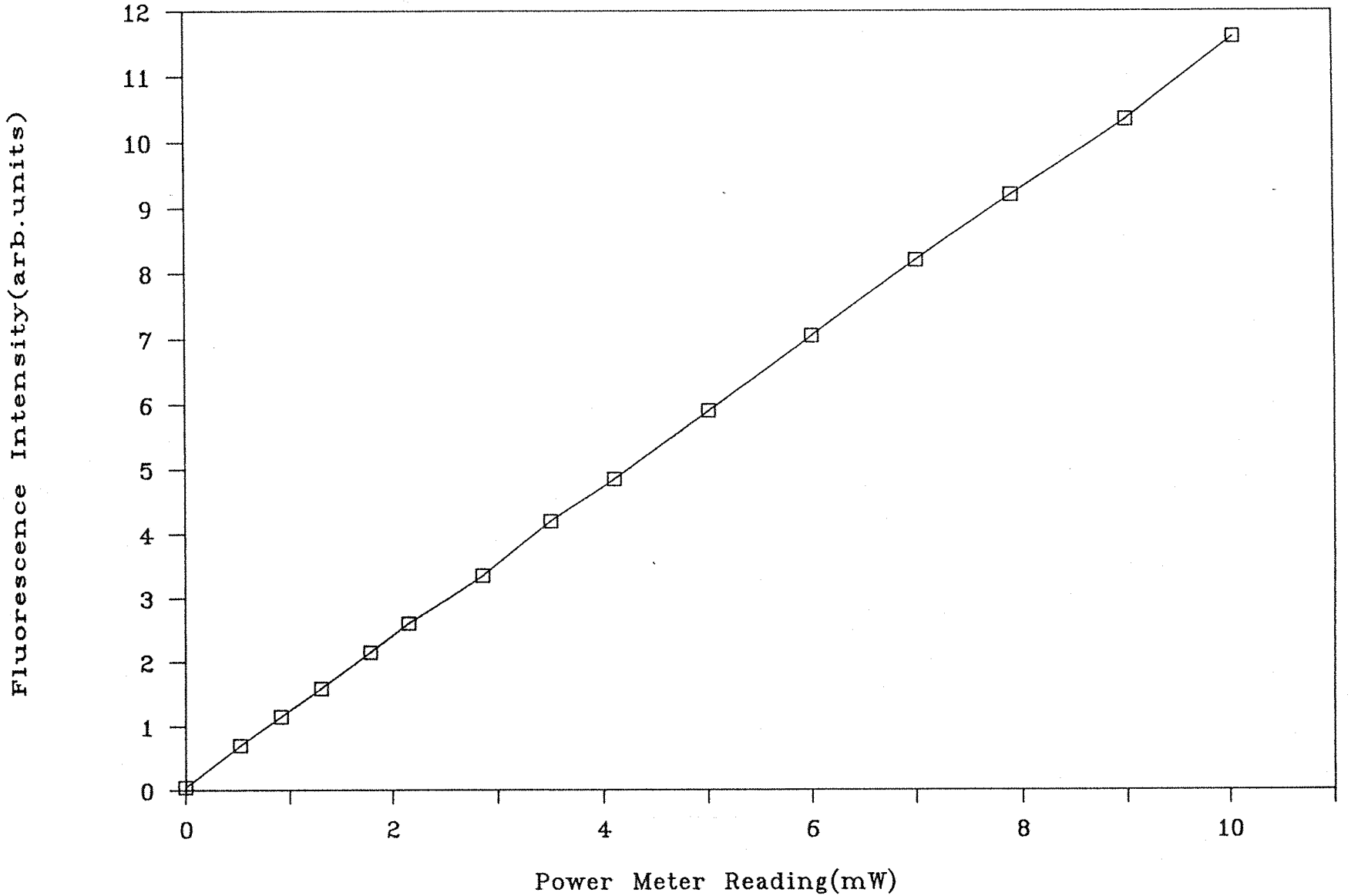
Fluorescence Intensity(arb.units)
0
1
2
3
4
5
6
7
8
9
10
11
12
0
2
4
6
8
10
Power Meter Reading(mW)

A 57ppm fibre with a smaller core radius was also tested but the results obtained with a pump wavelength of 803nm were unreliable due to an experimental mistake. The core was saturated during the cut back, causing an incorrect value for α to be obtained. This error was avoided when performing the other cut backs by ensuring that the power in the core was kept below the saturation power.

A saturation measurement similar to those performed on the fibres was carried out on a thulium doped preform - a glass rod with dopant in its centre from which a fibre is fabricated. The dopant concentration was 800ppm and a pump wavelength of 465.8nm was used. The results are plotted in Graph 9 from which it is evident that the fluorescence intensity rises linearly with the pump power and no saturation behaviour is observed. This confirms that the saturation effects are only observed at the much higher intensities obtained when launching into a fibre core.

The values obtained for the dopant concentration at different pump wavelengths agree closely and lie within the limits of their errors for each fibre. The 300ppm fibre and the 57ppm fibre absorb the shorter wavelength pump light more strongly than the longer wavelength, as indicated by the larger values for σ and α. The 1700ppm fibre is observed to show the opposite effect and is more strongly absorbing at the longer wavelength. It is a highly doped fibre and clustering effects-interactions between closely spread ions - may influence its behaviour.

Although the agreement between the concentration values obtained at the two different pump wavelengths is encouraging, the large difference between these values and the values established by the fabricator are a cause of concern. The values given by the fabricator are believed to be approximately correct.

No values for the absorption cross sections of the thulium ion in silica have been published, but recent work by Brocklesby and

Lincoln suggests a value between $5 \times 10^{-26} m^2$ and $5 \times 10^{-24} m^2$ at a wavelength of 785nm on the $^3H_6 \rightarrow {}^3F_4$ transition [5.18]. This is compatible with the values obtained for the cross section at the peak absorption at 803nm in this work.

The analysis used here assumes that the observed saturation of the fluorescence is due to depopulation of the ground state, but it is possible that some other mechanism may be responsible. Mechanisms which could be responsible for the observed saturation behaviour are excited state absorption of either the pump or the fluorescence photons. Excited state absorption occurs when an ion in the metastable level absorbs another photon and is raised to a higher energy level. This reduces the number of ions able to undergo radiative decay from the metastable level and would therefore reduce the intensity of the fluorescence signal seen from the fibre.

A possible method for measuring the dopant concentration in the cores of rare earth doped fibres has been investigated. The method involved measuring the absorption coefficient of the fibre and the saturation intensity of the ions within it. Attempting to measure the expected exponential decay in the sidelight intensity with distance along the fibre proved unsuccessful since pump light in the cladding crossed the core at frequent intervals along the fibre giving an irregular signal intensity. Due to this problem the absorption coefficient was found by the cut back method instead.

It was also necessary to measure the saturation intensity in order to find the dopant concentration. The saturation intensity was found by measuring the levelling off in the intensity of the fluorescence which is observed when the pump signal is sufficiently strong to raise a large proportion of the ions into the metastable level.

The values for the dopant concentration which were obtained from these measurements were consistently lower than the values which were quoted by the fibre manufacturer. Fibres with widely varying dopant concentrations and different core diameters were tested using two

different pump wavelengths. The concentration values obtained at the two different wavelengths for each fibre agreed within the limits of the errors, suggesting that a concentration related phenomenon is involved. If this phenomenon could be identified through further work, then this method for measuring the concentration could yield useful information.

83a

5.4. References

5.1 P. Urquart, Proc. IEE, Pt. J. p.385 (1988)

5.2 R.J. Mears, L. Reekie, S.B. Poole and D.N. Payne, Electron. Lett. 21 p.738 (1985).

5.3 M. Shimitzu, H. Suda and M. Horiguchi, Electron. Lett. 23 p.768 (1987).

5.4 J.Y. Allain, M. Monerie and H. Poignant, Electron. Lett. 26 p.166 (1990).

5.5 M.C. Brierley and P.W. France, Electron. Lett. 24 p.935 (1988).

5.6 L. Reekie, I.M. Jauncey, S.B. Poole and D.N. Payne, Electron. Lett. 23 p.1076 (1987).

5.7 L. Reekie, R.J. Mears, S.B. Poole and D.N. Payne, J. Lightwave Technol. 4 p.956. (1986).

5.8 L. Reekie, I.M. Jauncey, S.B. Poole and D.N. Payne, Electron. Lett. 23 p.884 (1987).

5.9 R. Allen and L. Esterowitz, Appl. Phys. Lett. 55 p.721 (1989).

5.10 D.C. Hanna, R.M. Percival, I.R. Perry, R.G. Smart, P.J. Suni, J.E. Townsend and A.C. Tropper, Electron. Lett. 24 p.1111 (1988).

5.11 W.L. Barnes, S.B. Poole, J.E. Townsend, L. Reekie, D.J. Taylor and D.N. Payne, J. Lightwave Technol. 7 p.1461 (1989).

5.12 T.J. Whitley, Electron. Lett. 24 p.1537 (1988).

5.13 K. Inoue, H. Toba, N. Shibata, K.Iwalsuki and A. Takada, Electron Lett. 25 p.594 (1989)

5.14 S.B. Poole, D.N. Payne and M.E. Ferman, Electron. Lett. 21 p.737 (1985).

5.15 J.E. Townsend, S.B. Poole and D.N. Payne, Electron. Lett. 23 p.329 (1987).

5.16 A.S. Sudbo and E. Nesset, J. Lightwave Tech. 7 p.785 (1989).

5.17 D.C. Hanna, I.M. Jauncey, R.M. Percival, I.R. Perry, R.G. Smart, P.J. Suni, J.E. Townsend and A.C. Tropper, Electron. Lett. 24 p.1223 (1988).

5.17 W.S. Brocklesby and J. Lincoln, private communication.